Master's thesis

NTNU
Norwegian University of Science and Technology
Faculty of Engineering
Department of Civil and Environmental Engineering

Saroj Sapkota

Overtopping and breaching of rockfill dams with and without a central core

Master's thesis in Hydropower Development
Supervisor: Fjóla Guðrún Sigtryggsdóttir
Co-supervisor: Geir Helge Kiplesund
June 2022

NTNU
Norwegian University of
Science and Technology

Saroj Sapkota

Overtopping and breaching of rockfill dams with and without a central core

Master's thesis in Hydropower Development
Supervisor: Fjóla Guðrún Sigtryggsdóttir
Co-supervisor: Geir Helge Kiplesund
June 2022

Norwegian University of Science and Technology
Faculty of Engineering
Department of Civil and Environmental Engineering

NTNU
Norwegian University of
Science and Technology

Abstract

Embankment dams are vulnerable to excessive through flow and overtopping due to erodible and pervious nature of materials used such as rockfill and earthfill. Majority of dams in the world are embankment type which pose serious risks and possible hazards in the downstream areas in case of failure. The seriousness of this topic has created a huge demand for dam safety and regulation. It is therefore very important to have a reliable consequence classification of dam. Implementation of the regulations and the proper design requirements demand full knowledge and understanding of dam behaviour during failure and in extreme load situation. So this study has become a step forward in the direction of defining and evaluating breach process and parameters. Eight different physical models are presented here which include dams with central core and without core. All of these are rockfill dams and subjected to excess through flow and overtopping, and the results are observed for both the types. It was noted that dams without central core see excess throughflow while dams with core failed mostly with overtopping. Unlike dams with additional protection layers, there is no sudden breakout and collapse giving huge downstream flood. However the peak discharge associated with the dam breaching is significant and should be addressed in the floodzone mapping. Some already existed parametric models are also employed to compare results with the physical modelling. Softwares like SFM (Agisoft), GIS, R programming script help to handle big data files and extract quality result from the analysis.

Preface

This master thesis project is submitted as a part of two year master of Science program, Hydropower development. The study includes physical model tests in Hydraulic laboratory at NTNU which are planned in relaton to the project WP1.2 on dam construction and safety within the research center HydroCen. The physical model tests were carried out with the guidance of main supervisor Associate Professor Fjóla Gudrun Sigtryggsdóttir, and co-supervisor Geir Helge Kiplesund. This work mainly focuses on an embankment dam breaching process and parameters analyzed in both the parametric and the physical model.

Table of Contents

List of Figures

List of Tables

Acknowledgement

Foremost, I would like to express my sincere gratitude and warmest thanks to my main supervisor, Associate Professor Fjóla G.Sigtryggsdóttir for her best advice and guidance all the time throughout this project work. I would also like to thank her for allowing me to direct this study in the way I wanted. In addition to being very enthusiastic about the thesis and project work, she also constantly checked on my health and safety in the laboratory, which I very much appreciated.

Alongside, I would like to give special thanks to my co-supervisor Geir Helge Kiplesund for helping me to unravel the confusion and assisting with working on data and analysis. I always appreciated that he took the time to check on my progress in the laboratory and was always there to offer advice.

I cannot thank enough my friend Raj KC for his valuable work support during the physical model construction in hydraulic lab. Without him dam model tests would not have been completed on time.

Furthermore, my wife and my family deserve my gratitude as well for all of their encouragement and support during this period of study. Also, I am thankful to my classmates for the memories and the friendships I have made here. NTNU has been a wonderful place for me for the past two years.

1 Introduction

The purpose of dams has been to irrigate agricultural land since ancient times, and it remains an important tool for this purpose until today. The dam usage has been expanded to different applications like flood control, hydropower, recreation, navigation, and several human purposes. In the last few decades, dam safety hazards have significantly increased, resulting from dam failures and the large losses downstream due to increasing population and land use (Adamo et al., 2020).

The worldwide association, ICOLD assists nations in developing and managing the world's water and hydropower resources to meet the challenges of the 21st century. It sets standards and guidelines to ensure that dams are constructed and operated safely, efficiently, economically, and in an environmentally sustainable and socially just manner. ICOLD defines large dam as “A dam with a height of 15 meters or greater from lowest foundation to crest or a dam between 5 meters and 15 meters impounding more than 3 million cubic meters.” (ICOLD, 2011).

Dams are classified based on different characteristics such as material used for construction, dam usage, shape, and size etc. Amongst them, an embankment dam, particularly a rockfill is made of materials which are erodible and pervious. These are vulnerable to the overtopping and excess through flow which causes damage to the structural stability leading to dam breaching. Once the loading on the dam exceeds the resistance against failure, there is possibility of several failure mechanisms acting together as it is always difficult to find out a single failure mechanism for the breaching process (Zhang et al., 2009).

When the dam is overtopped, the degree of severity depends on the breach opening, width, height and rate of erosion (D. C. Froehlich, 1995b). The breaching formation is estimated based upon the material properties, mean erosion rate and acceleration due to gravity (Walder & O’Connor, 1997). The breaching mechanisms have not been investigated to the fullest. The current practice to determine breaching parameter is with the help of statistically derived parametric equation based on historical dam failure and physically based breach models. These equations do not describe dam type, configuration and material used very well which gives significant room for uncertainties while doing dam breaching assessment. So, it is interesting to see in more detail about the breaching mechanism and available methods to estimate the breaching parameters of rock fill embankment dams.

1.1 Objective

It is intended that this work helps to reduce dam hazards by improving the safety of embankment dams. Having safer dams is an objective that is being pursued continuously as more dams are needed in the future while existing dams continue to meet their objectives. More precisely, an important aspect of the thesis is assessing relevant literature, preparing, and running an experimental study in NTNU's Hydraulic Laboratory, and analyzing both the data and results. This is to create the experimental data on the breaching of rockfill dams and

use of the Agisoft program (Structure from motion) to evaluate the breaching parameters, and qualitative and quantitative analysis of breaching process.

1.2 Thesis outline

There are total of six main chapters in this thesis which are divided according to the overview of the content inside. This is a first chapter where brief description of how the thesis has been organized is presented. Second chapter is about the background study of the related literature review where it looks into dam definitions, breach process and parameters, parametric models, and physically based breach model is shortly described. The third chapter explains all the physical model tests conducted in the hydraulic laboratory and presents how they were done with what materials and configuration. Chapter four is all about the result of parametric and physical modelling which are based on theories explained in earlier chapters. Result from the softwares like side veiw tracking of failure, breaching parameter analysis in Agisoft, failure discharge observed in the sensors are all presented with proper diagrams. Chapter five is a discussion section for the model comparision which in the end also gives some of the limitations of the laboratory physical model tests of this study. Finally, the last chapter is about the conclusion with some future recommendation at the end.

2 Background

In this section, some of the basic features of rockfill Embankment dam is presented. An overview of embankment dam failure, breaching process and the breach parameters caused by the overtopping are also described. In the end of this section, breaching parameters estimated from parametric equation and simplified physically based breach model are presented.

2.1 Rockfill dam features

Dams constructed from rockfill can be constructed at sites where suitable rock can be quarried at or near the dam site, and where the foundations will not be affected by material settlement due to the weight of the load or by erosion caused by any water seeping through or under the dam. With modern methods of compaction, a wide variety of rocks can be used, including relatively weak ones such as sandstones, siltstones, schists, and argillites. Laboratory tests are usually performed on samples of material, pilot fills are tested in situ and the results of such tests are used to guide construction procedures and zones for the use of materials (Alonso & Cardoso, 2010).

A watertight membrane must be incorporated, either centrally within the dam or as an upstream facing. The central core for waterproofing is usually a core of clay, silt asphalt or concrete. Central core of clay or silt are thicker than the asphalt or concrete for stability and better performance. An earth core is protected by a transitional layer in between the clay and rockfill section. The centrally installed core is protected against weathering, extreme temperature and ultra violet radiation which is less vulnerable to the damage and permit the cutoff to be constructed along the center line of the dam (Ratnayaka et al., 2009).

A typical cross-section of a rockfill dam is shown in the Figure 2.1 below.

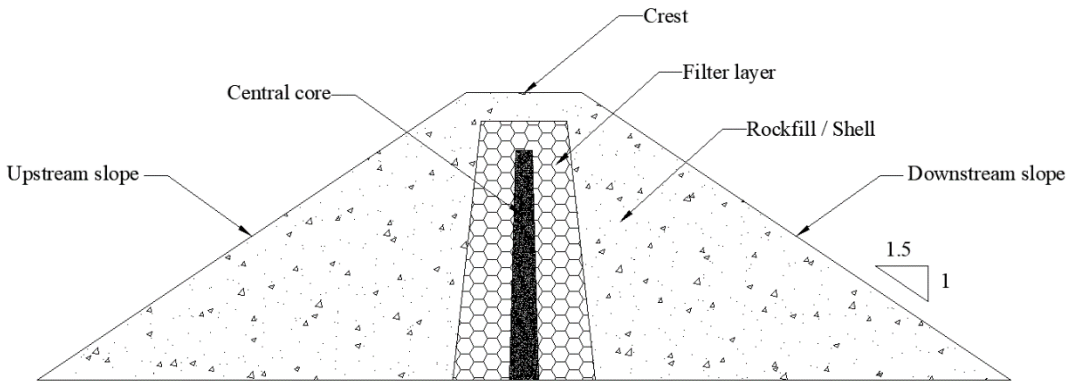

Figure 2.1 Sketch of a rockfill embankment dam with a central core (erosion protection on dam slopes not shown)

2.2 Embankment dam failure modes

Overtopping a dam is often a precursor to a dam failure. Overtopping can be caused by inadequate spillway design, debris blocking spillways, or settlement of dam crests. Another cause of dam failure is foundation defects, such as settlement and slope instability. "Piping", also known as seepage erosion, is the third most common cause of failure. The most common places for seepage to occur are around hydraulic structures, such as pipes and spillways, in animal burrows, around the roots of woody vegetation, and in cracks in dams, dam appurtenances, and dam foundations (D. C. Froehlich & Asce, 2008; ICOLD, 2011). In addition, dam failures can be caused by structural failures of the materials used in construction as well as insufficient maintenance.

2.3 Overtopping failure

Embankment dams are generally not designed as overflow ones and their resistance against surface erosion is limited. Dam overtopping is due to insufficient spillway capacity, improper manipulation, a landslide in the reservoir or when the design discharge is exceeded (Jandora et al., 2008). Moraine dams generally fail by overtopping and incision. The triggering event may be a heavy rainstorm, or an avalanche or rockfall that generates waves that overtop the dam (Clague & Evans, 2000).

Each time a reservoir inflow exceeds its outflow rate, headwater accumulates upstream of the structures within the reservoir. In this case the headwater level reaches the danger zone and even go over the crest level. Consequently, failure due to overtopping is more likely because several degradation mechanisms work together to undermine the embankment, resulting in its collapse. According to data released by the International Commission on Large Dams (ICOLD), earth and rockfill embankments are among those most vulnerable to problems arising from flood management, which may cause the watertight core or crest level to overtop and lead to erosion and failure. Overtopping is the most prevalent cause of dam failure worldwide, accounting for more than half of all known failures (Marche, 2005).

2.4 Embankment dams breach parameters

On the basis of several selected embankment dam failures and on experience gained, basic parameters that characterize the progression of embankment dam failure have been determined. These are as follows:

- Time related parameter of a failure
- The shape and the size of a breach
- The progress of a dam failure
- The maximum breach discharge

In the case of dam overtopping, the characteristics presented will depend on the dam type, the properties of the sub-base, the erodibility of the dam body and sub-base, and the riverbed (floodplain) discharge capacity downstream of the dam. The failure parameters are

calculated based on the historical dam failure events or by means of calculations (D. C. Froehlich & Asce, 2008; Jandora et al., 2008).

2.4.1 Time related parameters

The following parameters describe the course of failure progression over time.

Time of danger identification

Time of danger identificaton t_i is the moment when water begins to overflow its allowable limit which does not necessarily a signal of danger or dam failure but moment to increase the awareness, warning, and evacuation. For instance Mostiste dam which initiated temporary emergency activities like lowering reservoir water level, partial demolition of spillway and extensive dam reconstruction in 2005/2006 due to concentrated leakage (Říha, 2006).

Time of breach initiation

Time of breach initiation t_s begins with the danger identification and ends at the start of the beginning of the failure (Jandora et al., 2008).

Time of the beginning of the failure

Time of the beginning of the failure t_b is the moment when the water overflowing the dam crest starts doing significant destruction on the downstream face or the total failure of the dam crest. From this moment, there is a real danger of dam failure and work on evacuation and warning to the downstream area is important (Jandora et al., 2008).

Time of failure duration

Time of failure duration t_f is a breach formation phase starting from the point of failure to the point when the maximum size of the breach and the maximum breach discharge are attained.

Time of attaining maximum breach discharge

Time of attaining the maximum breach discharge t_k is the moment when the maximum discharge flow through the breached dam profile which corresponds to the maximum size of breach is attained in the case of large reservoir storage volume (Jandora et al., 2008).

The time related parameter can easily be described in the chart in Figure 2.2 below.

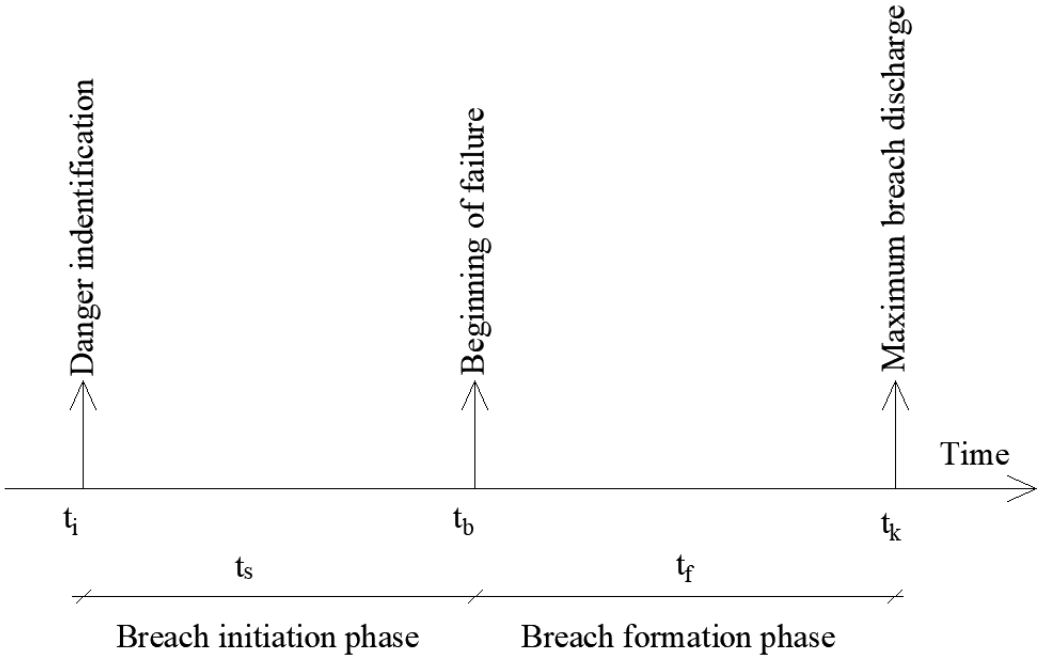

Figure 2.2 Time related parameter

2.4.2 Dimensional parameter

Another significant parameter of an embankment failure is the dimensional characteristic which often is a function of time and described in the Figure 2.3 (Jandora et al., 2008).

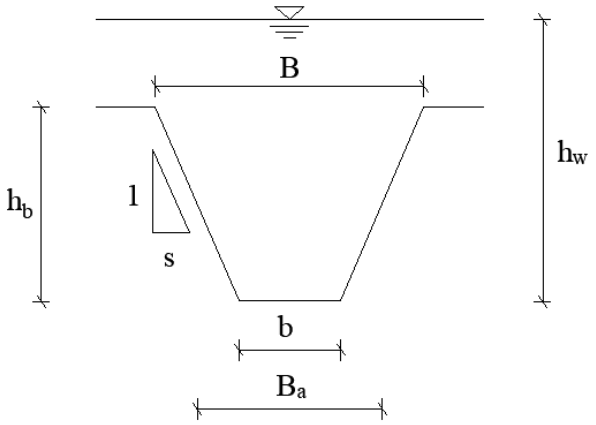

Figure 2.3 Breach opening cross-section

Hydraulic depth

Hydraulic depth of water at time of dam failure h_w is a vertical distance measured from the bottom of the final breach to the reservoir water level at this time.

Average breach width B_a

Average breach width is the average of top to bottom width of the breach.

Breach width at top of breach B

Width at the top level of the breach and generally the maximum width.

Breach width at breach bottom b

Average breach side slope factor S (experiments carried out has shown that the breach slopes in the beginning are almost vertical and the slope sliding occurs later on after the breaching.

Breach cross-sectional area A_b is the flow area perpendicular to the velocity vector and located at the place with the highest breaching.

2.4.3 Discharge

Breach discharge

Q_b is the water volume flowing per unit time in the breach cross-sectional area.

Maximum breach discharge

Q_{max} is the maximum discharge through the breach opening.

Reservoir inflow

Q_{in} is the water coming into the reservoir

Reservoir outflow through appurtenant structure

Q_f (Spillway, outlets, intakes)

2.5 Parametric modelling

Parametric modeling uses statistically derived regression equations for estimating embankment breach characteristics. On the basis of historical data from dozens of dam failures, such equations for dam breaching have been developed. As far as dependent parameters are concerned, they include breach width, shape, side slope, peak outflow, and failure time, while independent variables include reservoir volume, initial water level, dam height, dam type, configuration, failure mode, and material erodibility (ASCE/EWRI, 2011). The parametric model simply gives a single value as a result and does not describe the internal process and the breach development over time which the user should be aware of while doing the analysis, and extracting the result, conclusion etc. Empiric equations are powerful due to their simplicity since they do not require any computer simulations or physical models to be implemented. The simplicity, however, may also be its weakness, as breach parameter prediction uncertainty has been observed to be quite large for these models (Wahl, 2004).

2.5.1 Parametric breach models

MacDonald & Langridge-Monopolis (1984), performed a study of 42 dam failures composed of earth fill and non-earth fill dams out of which 30 were earth fill and remaining 12 were rockfills and combinations of others. The three main categories of the variables were studied which are flow characteristics, embankment characteristic and breach characteristics. This study noted that the volume of material removed during breaching earth fill dams is generally higher than that removed during breaching non-earth fill dams because the latter dams are more erosion resistant. They also got a factor called breach formation factor which helps to find out the relation for breach volume eroded and failure time of breaching. The breach formation factor (BFF) is the product of outflow volume of water and elevation difference between peak reservoir level and base of breach. Depending on whether the breach reached the base of the dam, they found that the breach shape was either triangular or trapezoidal, and the side slope was most often 2V:1H. The relation they thus found between the breach volume eroded and breach formation factor was as given below.

$$V_{er} = 0.0261(V_w h_w)^{0.796} \text{ (earth fill dams)}$$

$$V_{er} = 0.00348(V_w h_w)^{0.852} \text{ (non-earth fill dams)}$$

Where:

V_{er} = Volume of material removed during the breach

V_w = Water volume above the base of breach

h_w = Height of water above base of breach

The breach development time t_f and the erosion rate for the earth fill dam is found to be consistent during the breach. However, for non-earth fill dams, the relation between them is not same because of the different breach formation and structural instabilities. Hence there is a relation between the failure time and volume of breach material eroded for earth fill dam alone as shown below.

$$t_f = 0.0179(V_{er})^{0.364} \text{ (earth fill dams)}$$

Where:

V_{er} = Volume of material removed during the breach

t_f = Failure time

The relationship between the peak discharge outflow Q_p and breach formation factor was established for both the dam types of earth fill and non-earth fill. It was found that the peak discharge for the latter case is larger due to the combination of progressive breach erosion

and sudden collapse due to structural instabilities. The peak discharge equation is presented below.

$$Q_p = 1.154(V_w h_w)^{0.412} \text{ (earth fill dams)}$$

$$Q_p = 3.85(V_w h_w)^{0.411} \text{ (non-earth fill dams)}$$

Froehlich (1995a), assembles data for study from 63 embankment dam failures from a variety of sources and made relations to find out the breach parameters mainly the average width, height of breach, side slopes and breach formation time.

$$B_{avg} = 0.1803 k_o (V_w)^{0.32} (h_b)^{0.19}$$

Where, k_o accounts for overtopping cases whose value becomes 1.4 for this case and 1.0 for other than overtopping failure. V_w is the volume of water above the invert of breach and h_b is the height of breach. The average side slope Z was estimated to be 1.4 for the overtopping case and 0.9 for others. Froehlich (1995a), also presents that the breach development time t_f and volume of water above the invert of breach V_w has the following relation to estimate the failure time.

$$t_f = 0.00254(V_w)^{0.53}(h_b)^{-0.9}$$

Froehlich, (1995b) based on the 22 embankment dam failures presents the peak outflow Q_p built on the multilinear regression analysis. The logarithmic transformation of all variables was used to obtain the best linear relation for estimating the peak discharge through the breach. The peak discharge thus calculated is made to be a function of water volume store above the breach invert and the water level in the reservoir above base at the time of failure. This estimation of peak flow also incorporates a factor of safety as it offers the upper and lower boundary values which gives a range of data to be on the safe side.

$$Q_p = 0.607(V_w)^{0.295}(h_w)^{1.24}$$

Where:

V_w = Water volume above the base of breach

h_w = Height of water above base of breach

Froehlich (2008), performed further study with 74 embankment dams in order to develop and redefine the breach parameters like average width, side slopes for trapezoidal section and the breach development time. The overtopping factor has been reduced to 30% from 40% from Froehlich (1995a) study and the newly proposed average breach width is shown below.

$$B_{avg} = 0.27k_o (V_w)^{0.32}(h_b)^{0.04}$$

Where, k_o accounts for overtopping cases whose value becomes 1.3 for this case and 1.0 for other than overtopping failure. V_w is the volume of water above the invert of breach and h_b is the height of breach.

The side slope was also defined in more simple form as S = 1.0 for overtopping and 0.7 for the other cases.

He estimated the time of failure as shown below.

$$t_f = 63.2\sqrt{\frac{V_w}{gh_b^2}}$$

Xu et al. (2009), studied 182 embankment dam failures out of which half were more than 15 meters height. They applied both the addictive and multiplicative regression analysis to get the best regression model which was necessary due to the nonlinear relation between the breaching parameters and the five control variables. Unlike other models, this model was able to account the effect of degree of erodibility of materials such as low, medium, or high and, also considered the type of failure as overtopping or piping. The expression proposed for the top width (B_t) of breach opening is as follows:

$$\frac{B_t}{h_b} = 1.062\left(\frac{h_d}{h_r}\right)^{0.092}\left(\frac{V_w^{1/3}}{h_w}\right)^{0.508} e^{B_2}$$

Where, B_t top width of breach opening

h_b height of breach

h_d height of dam

h_r referential dam height (15 m)

V_w Volume of water above breach bottom

h_w height of water above breach bottom

$B_2 = b_3 + b_4 + b_5$ in which b_3 is 0.061, 0.088 and -0.089 for dams with corewalls, concrete faced dams, and homogeneous/zoned-fill dams, b_4 = 0.299 and -0.239 for overtopping and seepage erosion/piping, b_5 = 0.411, -0.062, and -0.289 for high, medium, and low dam erodibility.

The expression for the average width is as shown below.

$$\frac{B_{avg}}{h_b} = 0.787 \left(\frac{h_d}{h_r}\right)^{0.133} \left(\frac{V_w^{1/3}}{h_w}\right)^{0.652} e^{B_3}$$

Here, $B_3 = b_3 + b_4 + b_5$ in which b_3 is -0.041, 0.026 and -0.226 for dams with corewalls, concrete faced dams, and homogeneous/zoned-fill dams, b_4 = 0.149 and -0.389 for overtopping and seepage erosion/piping, b_5 = 0.291, -0.140, and -0.391 for high, medium, and low dam erodibility, respectively.

The expression for the peak discharge is as follows:

$$\frac{Q_p}{\sqrt{gV_w^{5/3}}} = 0.175 \left(\frac{h_d}{h_r}\right)^{0.199} \left(\frac{V_w^{1/3}}{h_w}\right)^{-1.274} e^{B_4}$$

Here, $B_4 = b_3 + b_4 + b_5$ in which b_3 is -0.503, -0.591 and -0.649 for dams with corewalls, concrete faced dams, and homogeneous/zoned-fill dams, b_4 = -0.705 and -1.039 for overtopping and seepage erosion/piping, b_5 = -0.007, -0.375, and -1.362 for high, medium, and low dam erodibility respectively.

The expression for the failure time is as shown below:

$$\frac{t_f}{t_r} = 0.304 \left(\frac{h_d}{h_r}\right)^{0.707} \left(\frac{V_w^{1/3}}{h_w}\right)^{1.228} e^{B_5}$$

Here, $B_5 = b_3 + b_4 + b_5$ in which b_3 is -0.327, -0.674 and -0.189 for dams with corewalls, concrete faced dams, and homogeneous/zoned-fill dams, b_4 = -0.579 and -0.611 for overtopping and seepage erosion/piping, b_5 = -1.205, -0.564, and 0.579 for high, medium, and low dam erodibility respectively. t_r is set as 1 hour.

It was found out that the erodibility of a dam material has a greater effect in the breach parameters and their consideration has improved the predictive ability of parametric model equations. Also, the multiplicative regression analysis was found to be effective over addictive except for the breach depth. The geometrical breach parameters by this study are more accurate than the hydraulic one due to the availability of more reliable data. Overall, the predictive errors associated with these equations are less than those purposed by other similar studies.

Froehlich (2016a) studied data from 111 embankment dam failures to obtain expressions for expected values of the average width, side slope, and formation time of the breach, along with expressions to calculate variances and prediction intervals of the parameters. The expression for the average width is as shown below:

$$B_{avg} = 0.23 k_o V_w^{1/3}$$

Where, k_o is 1.5 for overtopping and 1.0 for piping failures.

V_w is volume of water above breach bottom

The time for breach development which is time of failure is estimated with the following formula.

$$t_f = 60 \text{ x } \sqrt{\frac{V_w}{g h_b^2}}$$

He gave different side slopes than from the previous studies as S = 1.0 for overtopping and 0.6 for the piping failures. He also concluded that these empirical relations do not provide the physical processes involved. Rather they make the calculation and procedures simple to find out the breaching parameters.

Froehlich (2016b), based on the 41 embankment dam failures and looking at their peak discharge has proposed a new peak discharge expression which gives most accurate estimation.

$$Q_p = 0.0175 \text{ x } k_M \text{ x } k_H \text{ x } \sqrt{\frac{g V_w h_w h_b^2}{W_{avg}}}$$

Where, k_M is 1.85 for overtopping and 1.0 for other failures mode which accounts for failure mode. k_H is a factor accounting for embankment height and estimated as follows:

$$k_H = 1 \; for \; h_b \leq h_s$$

$$k_H = \left(\frac{h_b}{h_s}\right)^{1/8} \; for \; h_b > h_s$$

Where h_b is height of breach and h_s is height of small embankment dam. It was noted that the mode of failure largely determines the outflow peak discharge as overtopping creates 85% more discharge than the rest.

2.6 Physically based model

The parametric models presented in the previous chapter 2.5 do not consider the physical processes involved and just come up with a single value which has a higher degree of uncertainty associated with the output results. Many of these empirical models are developed from limited statistical analysis of data collected from historic dam failures where the prediction uncertainties of these methods are widely recognized to be very large, but have never been specifically quantified (D. C. Froehlich & Asce, 2008). The various ways in which breaches can form in embankment dams, and the large number of factors that influence the speed and extent of embankment erosion, are difficult to describe with rigorously precise mathematical formula. Hence, physically based breach formation models,

consisting of coupled simulations of the hydrodynamic and material aspects of embankment erosion, are being used more often to evaluate dam failures as the physical processes are understood better, and as increased computational capabilities enable complicated mathematical calculations to be carried out in acceptably short amounts of time (Wahl, 2004). Since the empirical models do not consider the physical breaching processes and the detail breach models are computationally expensive, physically based models simplify the assumptions on hydrodynamic, morpho dynamic processes to find out the breach related parameters (Zhong et al., 2016).

There are numerous physically based earthen embankment dam breach models. Zhong et al. (2016) described three such models which are: NWS BREACH, HR BREACH and DLBreach. He stated that in the results of 12 dam breach analysis NWS BREACH has large errors for cohesive embankments since it uses noncohesive sediment transport model and does not consider headcut erosion as a typical mode of cohesive dam breach. In HR BREACH, headcut and surface erosion modes are taken into account as well as various surface erosion equations for cohesive and noncohesive soils. The DLB Breach model employs a nonequilibrium total-load sediment transport model and headcut erosion model, respectively, for noncohesive and cohesive embankment breaching. He found out that all the three models can well address the overtopping as well as piping failure very nicely.

Morris et al. (2018) in a guide to breach prediction states different physically based breach models. One of the refined methods is EMBREA which is primarily for the embankment dam beaching and the program was developed at HR Wallingford, UK. The program can model overtopping failures of homogeneous, composite, and layered embankments, as well as internal erosion failures of homogeneous and layered embankments. In addition, it can simulate the failure of surface protection layers, such as grass cover, resulting in dam breaches. EMBREA has several unique features which should be of interest to the reader. During the breach growth process, EMBREA can model both macro and micro failure of banks due to soil slope instability. Furthermore, it does not assume predefined geometry (typically a trapezoidal, triangular, or rectangular shape in other simplified models) when predicting breach growth. It is possible to model materials with different erodibilities, allowing for the analysis of even the most complex of modern dam constructions without any need for simplifications. DSIG (Dam Safety Interest Group) selected it as one of three most promising breach models for a closer evaluation and concluded that the model, along with SIMBA (now incorporated into WinDAM), performed the best, offering the greatest opportunity for future industry use (DSIG, 2017) (Morris, 2011).

3 Physical modelling

This section includes the physical model tests conducted in hydraulic laboratory at NTNU. Several tests were performed in different configuration and out of which eight tests are taken for this study which are on homogeneous rock fill dams with and without the core. This section presents previous tests experiments, material used, flume setup, construction procedure and testing.

3.1 Laboratory experiments

There were various dam break experimental studies carried out in the past. Majority of them concentrated to the investigation of failure mechanism and breaching parameters. Most of them are carried out in the flume setup. Tinney and Hsu (1961) first conducted laboratory and field experiments on the erodible fuse plug washout and described the side erosion characteristics. On the laws of sedeiment transport they explained the sediment wash out mechanisms (Schmocker, 2011). Majority of those laboratory tests were conducted to estimate the geometrical breach opening, breach development time and peak outflow discharge.

In this study, only the relavant tests are described as the same flume were used to conduct a total of 19 dam model tests within the Hydrocen project WP1.2.2. Out of this total number, only 8 tests are related to the topic in this study which is breaching of rockfill dams with and with out a core. The model tests 3, 4, 5, 6, 15 are with core and model tests 17, 18, 19 are with out core.

3.2 Flume setup

The flume setup is in hydraulic laboratory at the Norwegian University of Science and Technology (NTNU) which is of 25 meters length, 1 meter width and 2 meters height. One side of the flume is partially made of glass to make the test visible to the cameras and for observation. The highest discharge that the flume can reach is 500 litre per second from two intake pipes. To avoid the backwater effect, the flume is equipped with 0.35 m height aluminium boxes which are made more frictional with geotextile clothes on top to avoid easy sliding of the dam material.

The flume is facilitated with the pressure measuring 11 metal pipes with several holes in each to get the average value of pressure across the width at dam base. The metal pipes are then connected to the rubber pipes which go into the pressure transducer producing voltages corresponding to the water columns. The spacing between the pressure pipes are made roughly 0.2 meter except for the most upstream one. The pore pressure development was compared to previous models of a half dam (no toe) reported on by Kiplesund et al. (2021).

The reservoir created in the upstream is relatively small when compared to the real case scenarios which is because of the limited space available and other laboratory limitations. In order to reduce the effect of water coming into the upstream pond, the peripherial circumference near the outlet of the intake pipe is designed with several holes to spread water. The water level in the upstream of flume is measured to find out the volume of water

collected with the help of stage-volume curve. This is further verified with the data collected from acoustic sensor which measures the water level. For the core of the dam, a flexible rubber membrane is used which is fixed on the wall to both sides with the help of self-adhesive transparent tape. The core height is 0.8 meter and throughout across the width which is 1 meter.

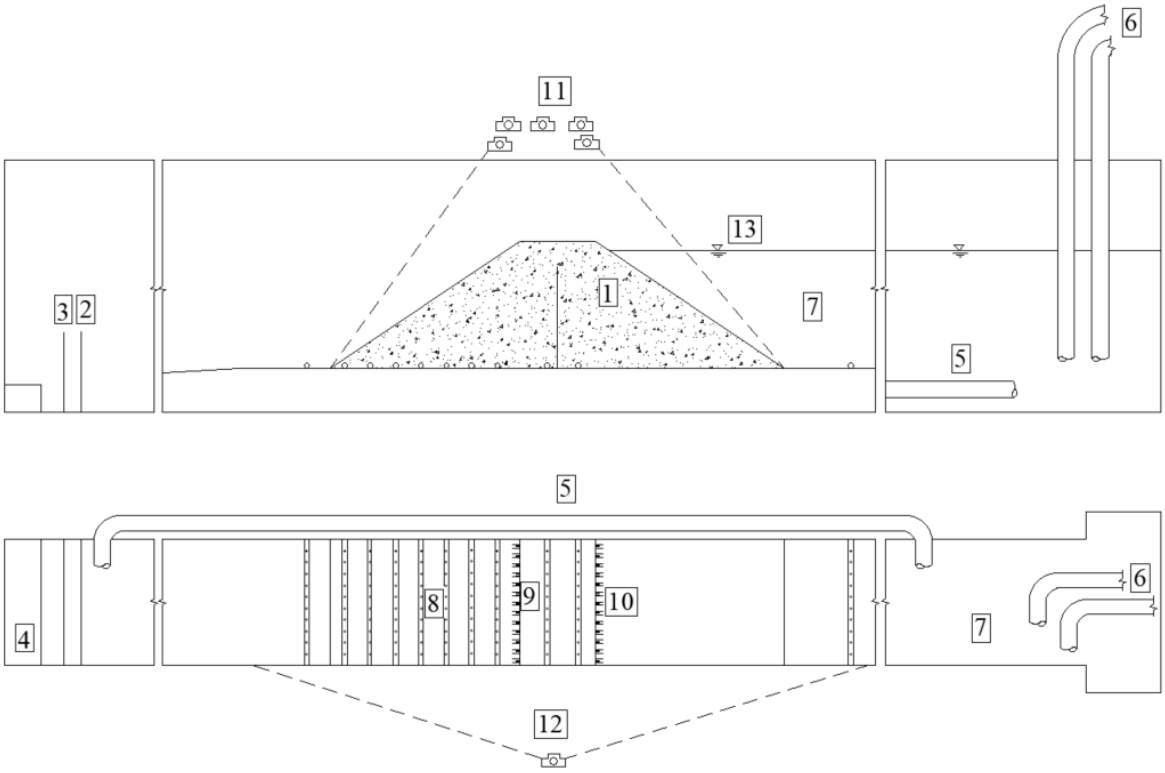

Figure 3.1: Hydraulic flume setup in the laboratory at NTNU

In the Figure 3.1 above, the numbering is done to describe different parts of the flume setup and their relative position in the space. They are described below:

1- Main dam body
2- Coarse mesh trash rack
3- Fine mesh trash rack
4- Flume outlet
5- Bypass pipe
6- Intake pipes
7- Upstream reservoir
8- Pressure measuring pipes
9- Downstream slope
10- Upstream slope
11- Top view cameras
12- Side view cameras
13- Reservoir water level

The model and the tests are carried out under the surveillance of several cameras around the flume. For the tests in this study a total of 9 cameras were used out of which seven are on the top and two from the side. At the end of the flume there is a fine mesh trashrack to stop outflow of small size particles that helps to retain the fine materials in the flume otherwise the material will lose some of the fine portion and becomes more coarser.

Figure 3.2 below shows the top view and section view with pressure pipes as well as dimension of the dam body.

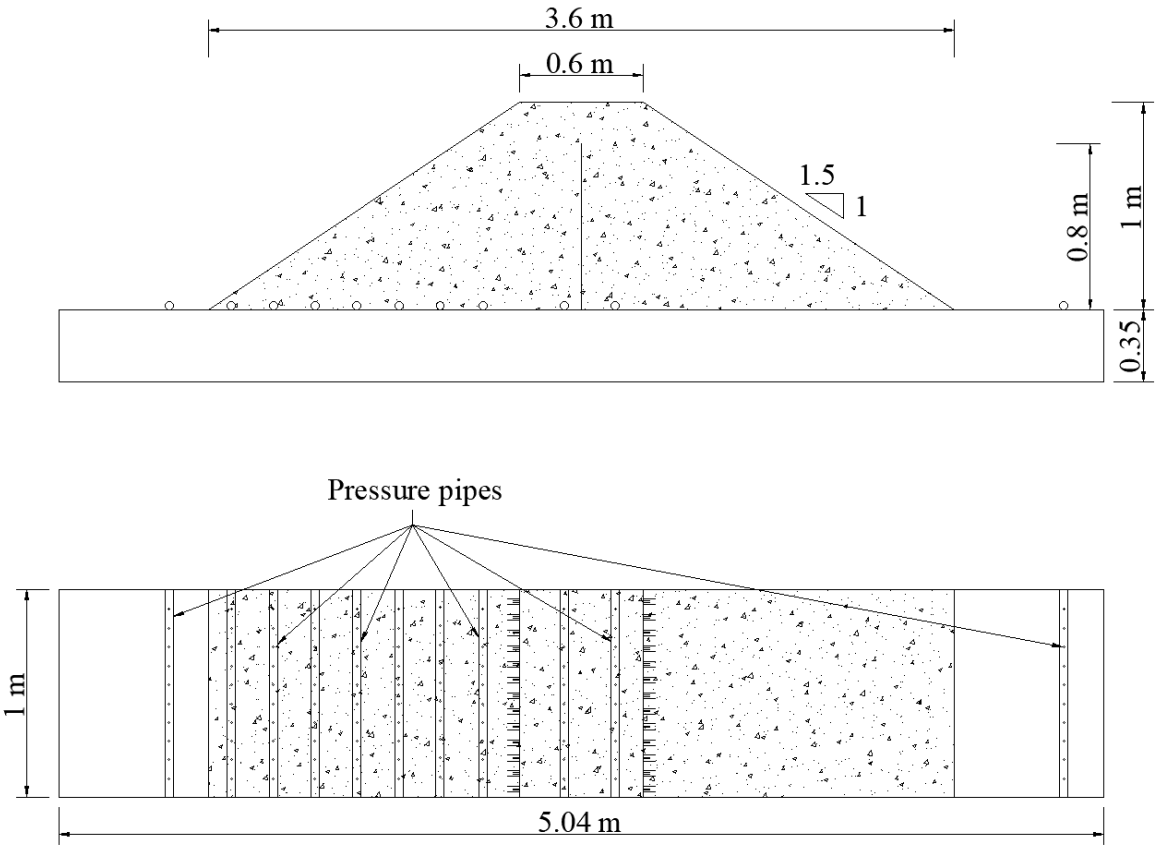

Figure 3.2: (Top) Sectional view of dam body and pressure sensor pipe: (Second figure) Planar view of dam body and pressure sensors

3.3 Materials used

The main materials used are shell material which is a mixture of fine to coarse grain size, rubber membrane for a core and water from the storage tank. Since this study only focuses on the homogenour rockfill dam with out protection, no filter material and riprap were used for the dam model construction. The dam material was taken from the local quarry which has significant portion of fine material. If mixed with water with out removal of fine particles

would increase the sedimentation in the water storage tank. Also, the pumping system has the limitation that the most fine size that can go into the pumping is 0.5 mm which mandate to filter out the fines before placing into the flume which was a time consuming task as the material volume was huge almost 4.5 tons.

The washing of fine material was done in the concrete mixer for larger particle size and seive table for fine materials. The material taken was made of Gabbro, Greenschist and crushed granite. The material and the grain size distribution for the dam model was referenced from the existing dam data in Norway by the Norwegian Water Resources and Energy Directorate (NVE, 2012). To get the correct grain size for the model, it was scale down in 1:10 and the grain size distribution is as shown in the Figure 3.3 below. The grain size distribution shows the largest dimension of the gravel is around 60 mm while smallest is 0.5 mm. It has been noticed that the material had been becoming coarser for the later tests as some of the finest particles could not be stopped with in the flume with fine mesh trash rack.

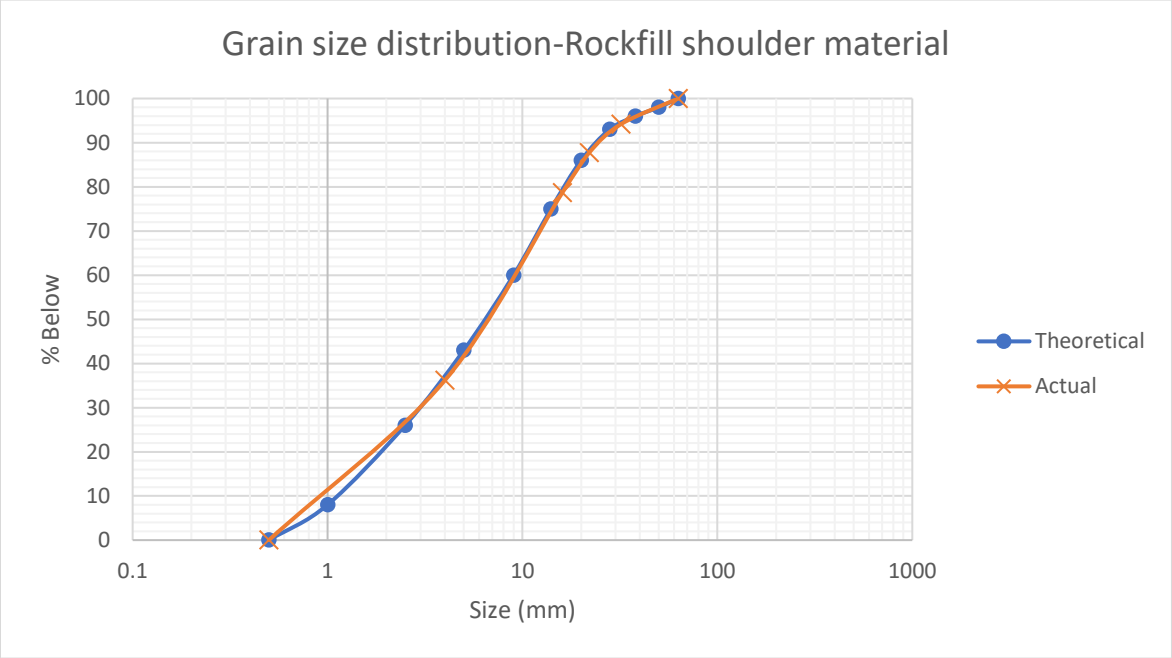

Figure 3.3: Particle size distribution curve for dam material

For the central core of the dam a flexible rubber membrane is used which is impervious and sealed against the wall with self adhesive tape. To create proper resistance on the dam bottom, geotextile is used which makes the contact between dam material and bottom surface frictionial and provide good stability.

3.4 Construction procedure

The first step in construction was making the outline of the dimension of the dam body on the wall of the flume. As the dam height was 1 meter every 0.1 m increment in height was marked with horizontal lines which help to maintain the same level and compaction during construction phase. After that materials kept in bags were taken into the flume with the help

of crane in the downstream position of flume so that the material can be carried in the desired quantity during the building phase. Just before the model was started to build, the pressure sensors pipes were cleaned thoroughly to take all the ingressed sands and fine grains out to get an accurate measurement of water column pressure.

Figure 3.4 below shows the dam with central core under construction and a wooden plank being used to make a ramp for easy dumping of material once the dam gained its height during building phase.

Figure 3.4: Dam with central core under construction

Once the cleaning work finished, the building tools namely wheel barrow, shovel, tamper rod were taken down into the flume. The shell material was loaded into the wheel barrow with shovel and drove onto the dam builing position and dumped down. Then tamper rod was used to compact the material with each drop from 10 cm height and 10 times across the layer surface to ensure the consistency of compaction for each 10 cm height increment. The tamper used was 4.5 kilogram with square base at the bottom. For each 10 cm increment in height, the level was checked with the horizontally aligned laser light which was kept by the side of flume. After the dam reached around 20 cm height, it was time to set the core membrane at the centre across the flume with the help of transparent self adhesive tape for

dam with internal core. When the core was installed properly, the same procedure of filling the dam following the outline dimension was repeated until it reached the crest level. Every time the dam gained it‘s height, it had to be ensured that the compaction was consistent and level was same throughout. In many of the tests, pilot channel has been designed and this has to be built at given dimension at left side of the dam crest in the direction of water flow. The dam was not so complex to build and only took three days in average to finish everything for a testing day.

Once the test is completed, and when necessary photos and measurements are taken, next step is to take all the material to downstream end of flume and a thorough cleaning and getting the dam ready for the next test. After every test the material becomes unevenly mixed which adds extra work for mixing it again to get well graded grain mixture for next model setup. Figure 3.5 below shows the empty flume ready for building next model after the cleaning and moving material down to the end. This picture is for the reference purpose for the understanding of relative size of the flume as person standing inside is of 175 cm in height.

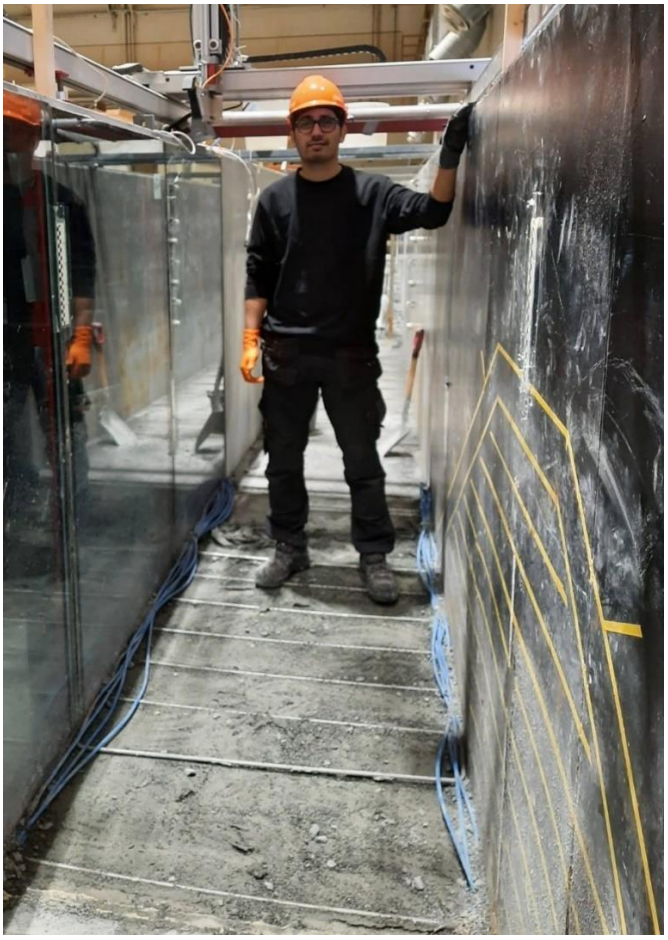

Figure 3.5: Inside the flume showing the dam location, dimension outline and pressure sensor pipes

3.5 Experiments conducted

There are altogether 4 experimental tests have been done for this study but the previous similar tests which are relevant are also taken for the analysis and result part. The model test 15 is with a rockfill dam with a core while model tests 17, 18 and 19 are homogeneous rockfill dams without core.

3.5.1 Rockfill dam with a central core

The dam model 15 is a breaching test with a central core and pilot channel at top left corner along water flow direction. This test was done with a rubber membrane core at center to see how the through flow and breach development change with installation of core membrane. On the testing day, the first step was to clean the pressure sensor pipes with water placed on the bucket just above the flume to make sure there is no water bubble in pipe and the pressure reading is correct. The next step was to set the cameras in their respective position on top and at side, and to supply power to each of them. Seperate DSLR camera was used to take photo of dam body by hand which was useful for structure for motion (SFM) software for their start and end 3D modelling.

Before the test started, the dam body was made wet with water spray just to make sure that it was not dry and uniformly wet all around the dam structure. The bypass valve was then closed and intake valve opened allowing water to accumulate in the upstream reservoir until it reached the core height (0.8 m). As soon as water reached the core top, intake valve was shut down to check the amount of water drop and leakage through the dam body. Once this was done, intake valves were opened again and set to the specified discharge value, for example 15 liter per second for this test.

Figure 3.6 Water just overtopped on rockfill core dam

In the Figure 3.6, it could be seen that water has just started overtopping in the pilot channel made on the dam crest which is with dimension of top width 20 cm, bottom width 10 cm and height 10 cm. The breach development and details alongside breaching progresses has been noted down for further analysis later. All the cameras and sensors are confirmed activated in the middle of the test so that all the data are captured and available. Once the breaching reaches to the end, the intake valves are closed and bypass valve is opened to drain all the stored water in upstream pond. The images are taken again with the DSLR camera and manual measurement of breach opening is done just incase if measuerment is needed later for further verification. The dam material after test spreads over the downstream side of the flume which needed to be cleaned and collected to the end of flume. Same steps are repeated to build and start the another dam model.

Figure 3.7 Homogeneous rockfill core dam at the end of breaching (View from upstream)

3.5.2 Rockfill dam without a core

There are three tests (model 17, 18 and 19) conducted for a dam without central core membrane while the rest of the dimensions and building procedure are same as before for dam model 15. The building procedure for this dam was even simpler as the dam just possess shell material and would not need any installation of rubber core membrane which saved time of construction. Pilot channel of same dimension as in model 15 was built on dam crest to initiate the breach on the cameras side so that the breach progress view was captured and

observed well. The testing time for this type of model is very short as there is no leakage test and dam fails in short period of time with excessive through flow. In the Figure 3.8 it is seen that there is excessive throughflow and water reaches almost to the dam crest.

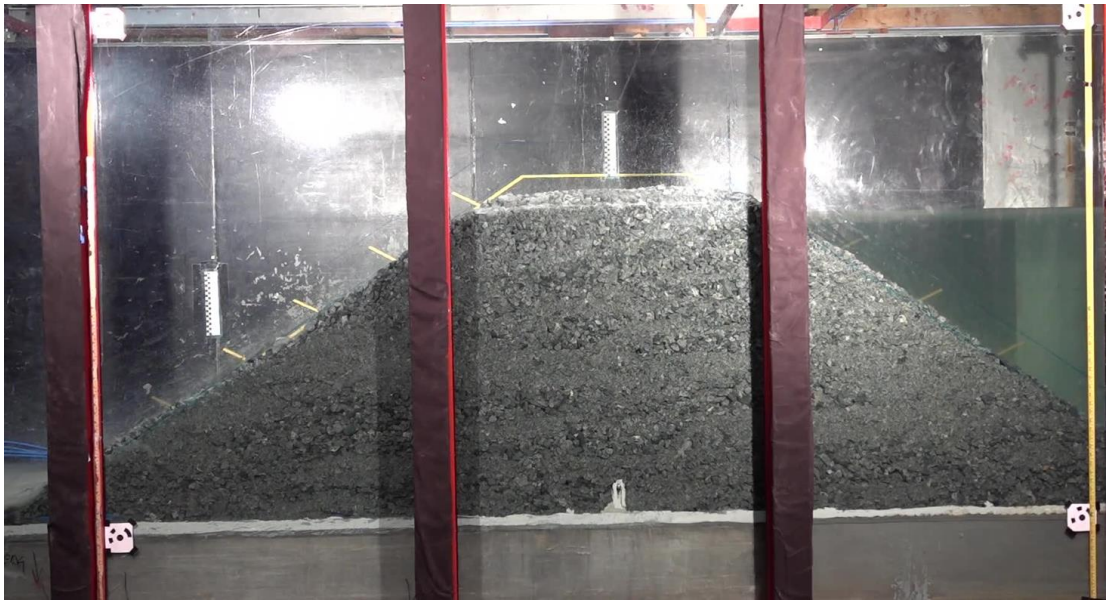

Figure 3.8 Rockfill dam without core with excess throughflow

In case of dam without core, there is less obstruction inside dam body to the flow of water and hence the failure surface pattern in the end becomes more regular and smooth as shown in the Figure 3.9.

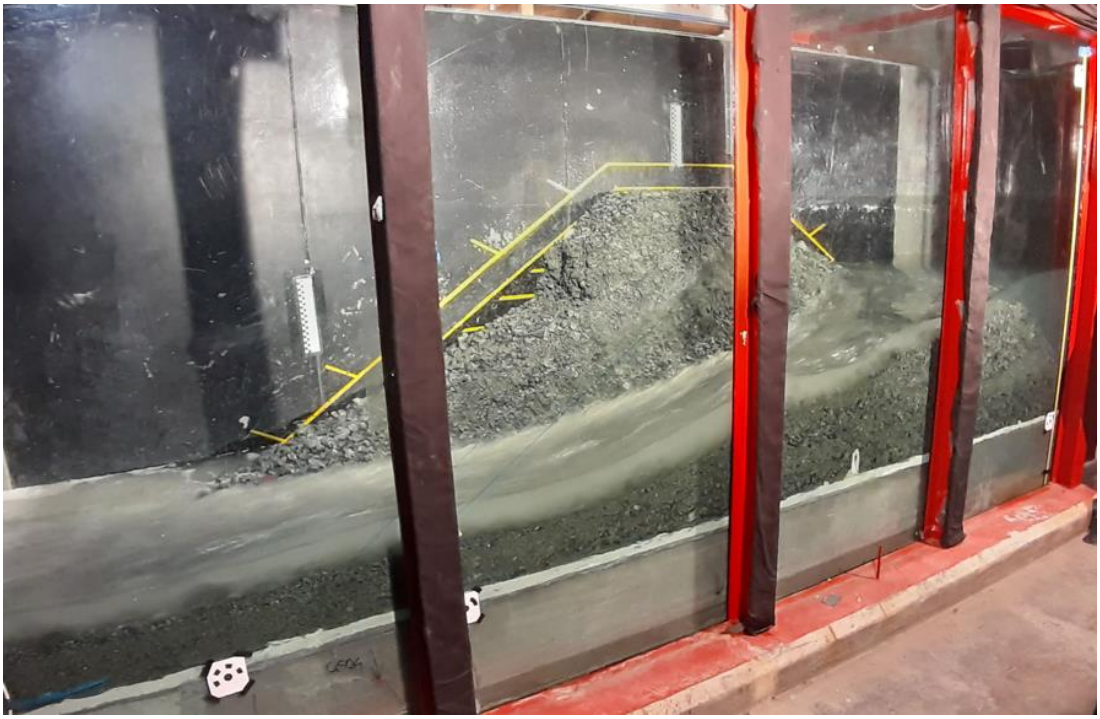

Figure 3.9: Rockfill dam without core final breaching view

4 Analysis and Results

This section presents the physical model test results and the parametric model output. A summary of breach development and progress, side view tracking, breaching paramters, 3D modelling in SFM, Agisoft and failure discharge etc are included here. The figures, calculation tables, and charts are not all presented here, rather they are presented in detail in the appendix section at the end of the thesis.

4.1 Dam model tests conducted

A total of eight tests (five with a core and three without core) are used for this study. All the model were run with pilot channel on dam crest with dimension of 20 cm top width, 10 cm bottom width and 10 cm height. The first four models were run previously in October 2020 while the remaining tests were conducted in february 2022.

The Table 4.1 below briefly describes all the models, their features and configuration.

Table 4.1: Summary table for dam model tests

Model No.	Description	Core material	Maximum discharge	Camera No.
M3	Rockfill dam with core	XPS foam	8	6
M4	Rockfill dam with core	Rubber membrane	5.5	6
M5	Rockfill dam with core	Rubber membrane	5	6
M6	Rockfill dam with core	Rubber membrane	10	6
M15	Rockfill dam with core	Rubber membrane	15	9
M17	Rockfill dam without core	None	15	9
M18	Rockfill dam without core	None	20	9
M19	Rockfill dam without core	None	15	9

4.2 Breach formation

In order to understand the breach development process and the progress it makes once the breach starts, the side view cameras were used to capture the videos and utilize it to process in GIS softwares to extract useful information about the breaching parameters and data for further analysis. For this study, images every 30 seconds were extracted covering all the start and end breaching period. These images were georeferenced in QGIS with the local coordinate system which was assigned manually with know coordinates fixed on the wall of the flume. Once one of the images is assigned with the local coordinate system, the rest of all the images extraced every 30 seconds are also assigned coordinates in R programming script which takes reference from pixel coordinate to assign the local coordiante values. When all the images are georeferenced and converted into .tif file format, they are added to the QGIS software as a raster layer for digitizing the side view of breach opening.

In QGIS, there are different tools to digitize the image. The polyline option was better to draw the side view breach progress for every 30 seconds. The software offers different color code for different time interval so it becomes easy to observe how the breach development changes over time. Some of the interesting side view digitized images are shown here for model 15 and model 17 while the rest of the models are presented in the appendix section.

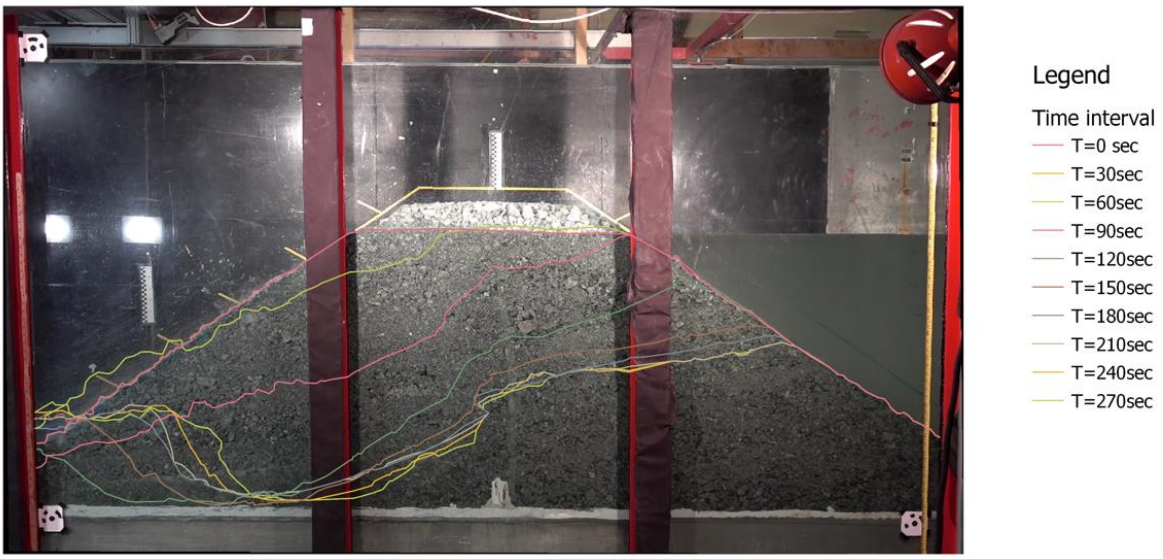

Figure 4.1 Temporal evolution of breach surface for M15

Figure 4.1 shows the model 15 dam with internal core which has breach formation progress over time period of 270 seconds once the breaching starts at T = 30 seconds. The different color lines take different time interval as shown in the legend section and their corresponding breach surface shows the breach progress until that period of time. This clears that the breach development for the first few minutes is so rapid and slows down later when time reaches around 150 seconds.

It was also observed that the breach progress towards toe side was faster than it was on the crest which is further explained by the data noted in

Table ***4.2*** and the corresponding chart plotted.

Table 4.2: Breach progress at crest and 40 cm downstream from core (M15)

Time interval	Level at crest (cm)	At 40 cm downstream (cm)
0	90	90
30	90	90
60	90	77
90	79	47
120	54	22
150	44	14
180	39	13
210	37	13
240	37	9
270	36	6

When the same data in

Table ***4.2*** is plotted in the chart, it becomes easier to visualize the breach development over time in the respective position which is shown in the Figure 4.2 below.

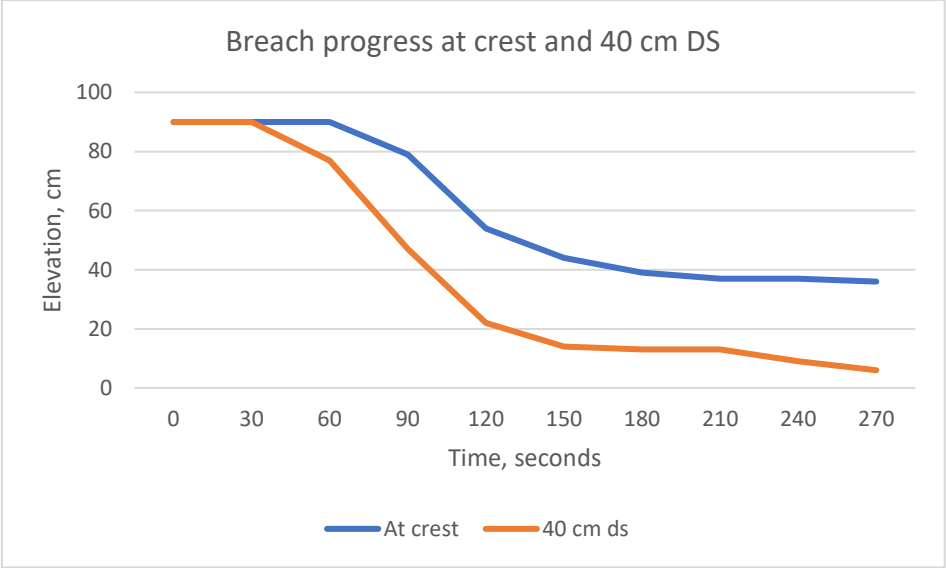

Figure 4.2: Breach progress over time for M15

The temporal evolution of dam breaching is presented in a single frame for all the images captured in 30 seconds interval which is presented in the Figure 4.3 below. The line follows the breach surface from the side view and gives the breach development progress for each 30 seconds time interval.

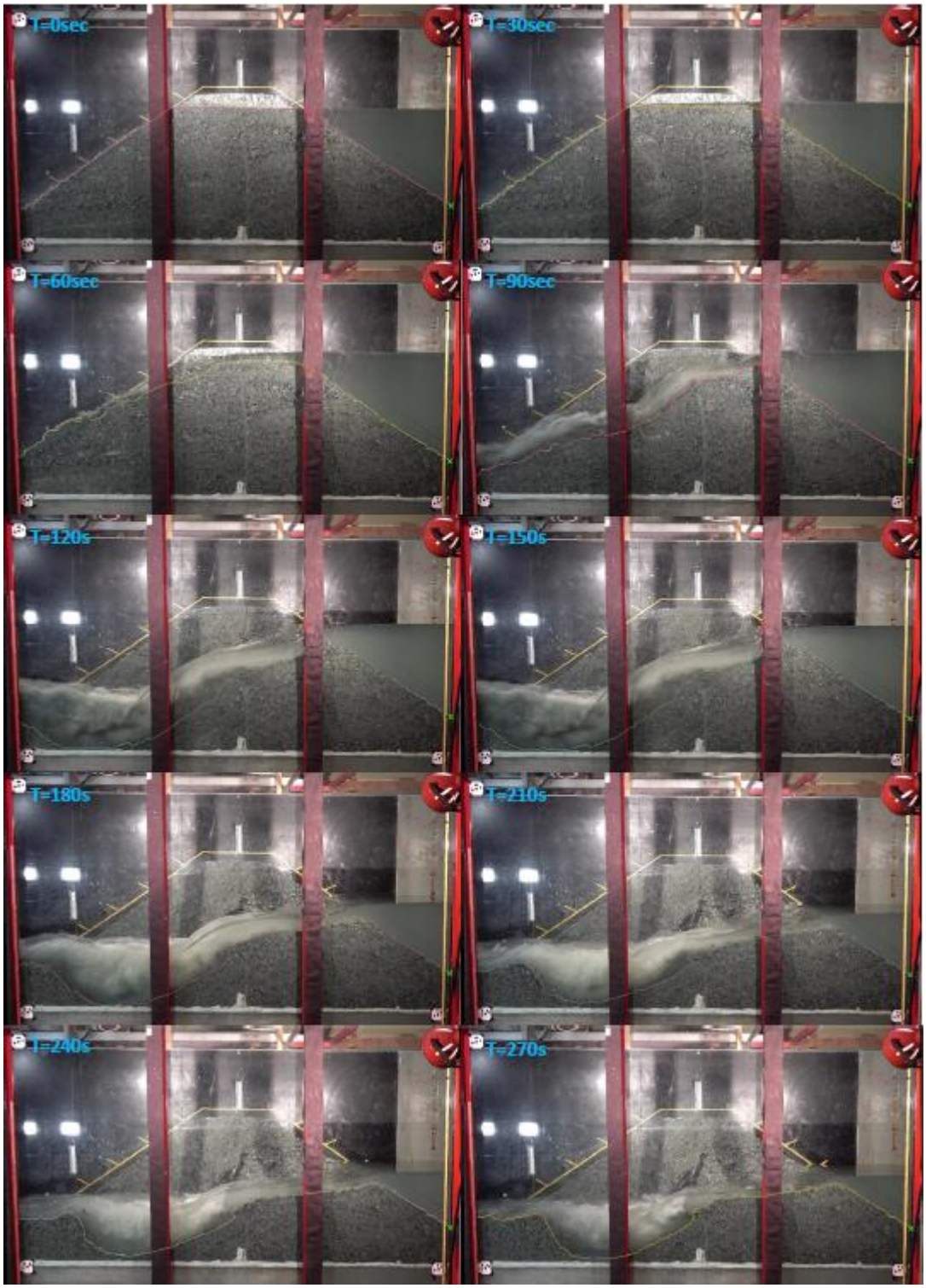

Figure 4.3: Temporal evolution of dam breaching of model 15 in 30 seconds time interval

The same procedure is repeated for the rest of the models and breach formation along with side view tracking is done for all of them. Model 17 as an example of dam without core is presented here to show the breach progress and changes seen when the configuration is changed to without core type. For this model too, 30 seconds images were extracted and georeferenced all images in QGIS with the help of R programming script. When the breach

progress development for every 30 seconds is digitized, the following Figure 4.4 is obtained which has different color lines representing different time intervals.

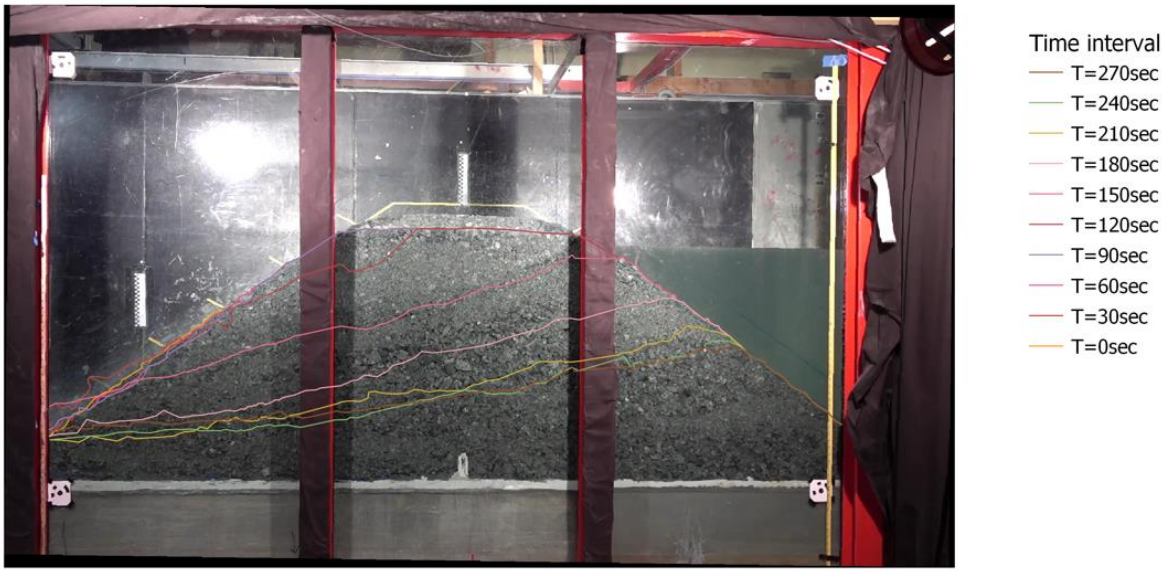

Figure 4.4: Temporal evolution for breach surface for M17

As similar to M15, the breach progress at downstream side is faster than in the upstream part which is shown by the data in Table 4.3 and chart here as well.

Table 4.3: Breach progress at crest and 40 cm downstream from core (M17)

Time interval	Level at crest (cm)	At 40 cm downstream (cm)
0	90	90
30	90	90
60	90	90
90	90	90
120	90	77
150	68	57
180	49	37
210	34	30
240	33	24
270	32	26

When the same data in Table 4.3 is plotted in the chart, it becomes easier to visualize the breach development over time in the respective position which is shown in the Figure 4.5 below. This graphs draw the conclusion that the breach progress to the downstream side happens sooner and progress towards the upstream side.

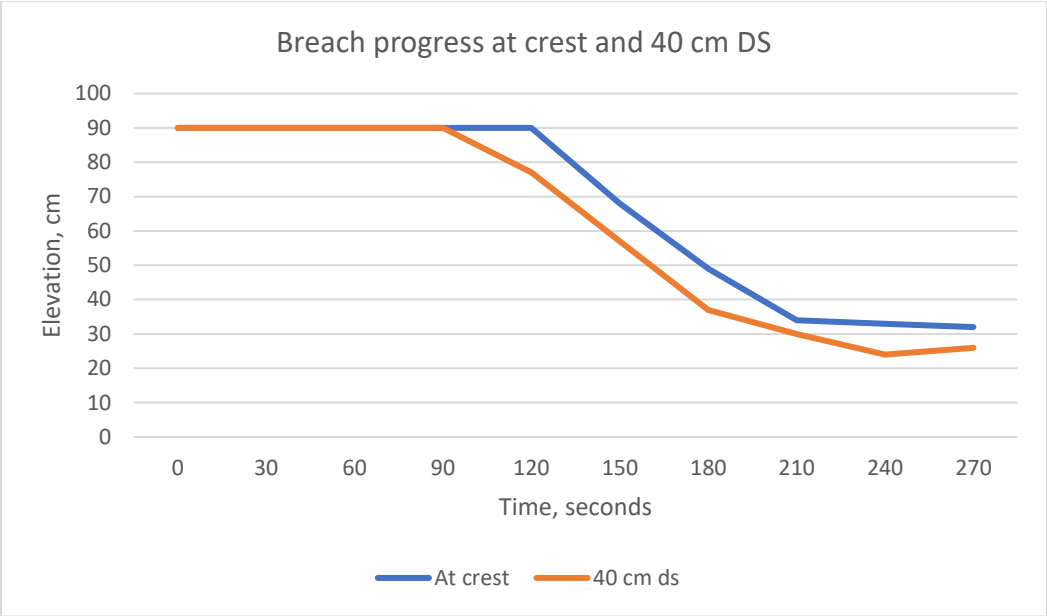

Figure 4.5: Breach progress over time for M17

Similarly for the model 17, the side view tracking for every 30 seconds time interval is shown below in Figure 4.6. This is a rockfill homogeneous dam and there is no rubber membrane core in the center. When the breach starts to develop, it progresses rather smooth and silent with no sudden failure and peak flow as seen in the previous tests with additional protecton layer conducted by Senarathna (2021) in his master thesis study.

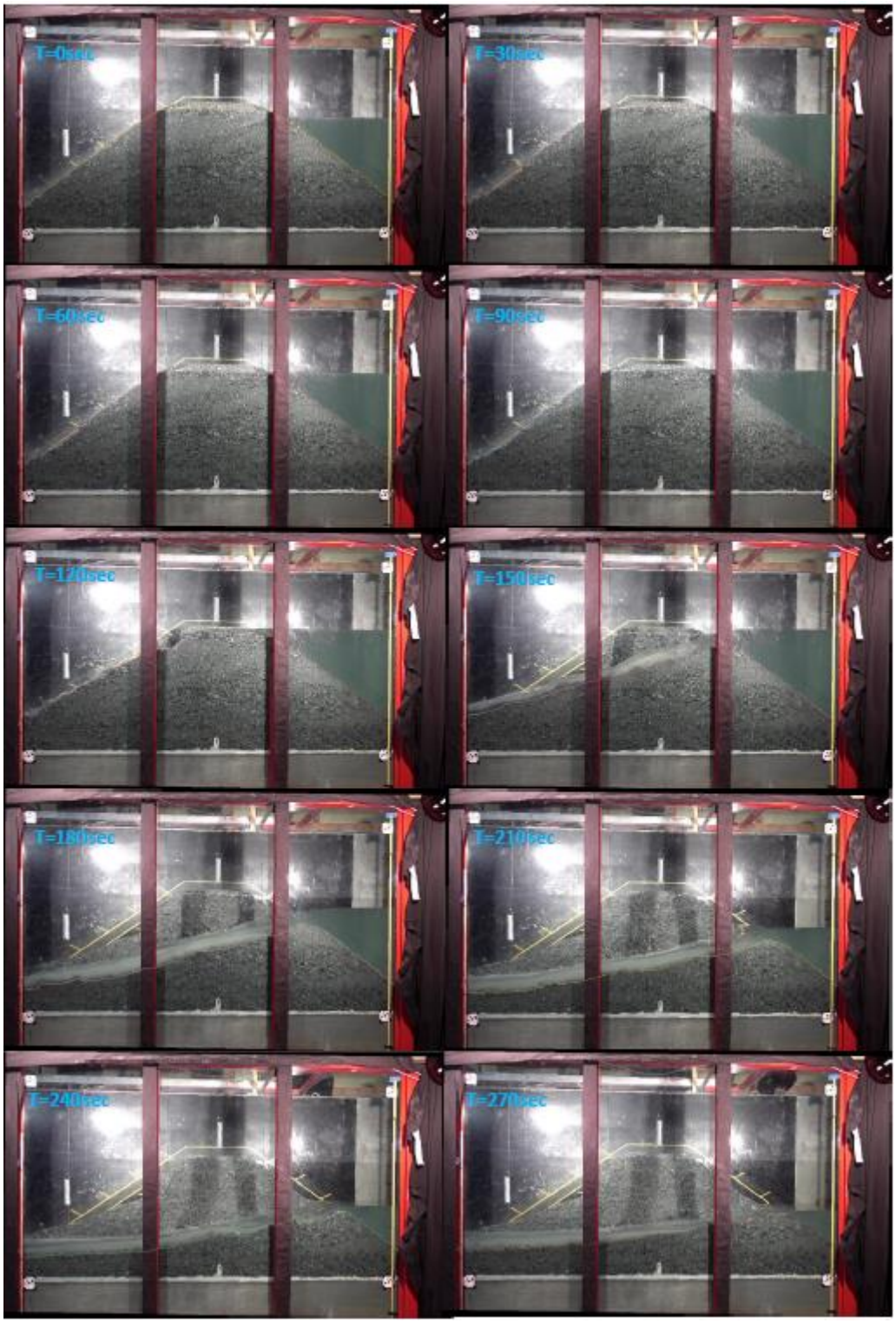

Figure 4.6: Temporal evolution of dam breaching of model 17 in 30 seconds time interval

4.3 Structure from motion, Agisoft

In Structure from Motion (SfM), overlapping two-dimensional photographs are taken from numerous locations and angles to create three-dimensional models of the scene being photographed. Various versions of this technology have been around since 1979, but applications were uncommon until the early 2000's. SFM has many applications in many subfields of geosciences (geomorphology, tectonics, structural geology, geodesy, mining) as well as in archaeology, architecture, and agriculture (Shervais & Dietrich, 2016).

In this study Agisoft Metashape Professional 1.7.5 version was used for processing images and 3D modelling. The first step was to collect data in the laboratory flume and from the dam model setup which was mainly capturing the images, videos, and reference points on flume's wall to generate the local coordinate system. As the dam surface before and after breaching are interesting to look at, images were taken at start and end, and while videos running throughout the testing period provide the images needed for dynamic breach analysis. It is important to note that the camera should be positioned such that the overlapping between images is sufficient, for example around 40 % of overlapping.

To get the 3D modelling of the dam model in Agisoft the first thing to carry out is to upload the images and align it which is very simple steps in the software. Here the software tries its best to refines the camera position for each photo finding out the relative position of the cameras that generates point cloud model. The next step is building the dense point cloud where the software based on the camera position calculates the depth information for each camera and combine into a single dense point cloud. In this step unnecessary points and data can be removed to make the working space clean and look nice. Once the dense point cloud is built up, the next step is to make polygonal mesh model based on the dense cloud data. Here the program defines the dam model as a polyhedral object by a combination of edges, faces and point vertices. Finally, the texture of the model is improved in the build texture step to obtain the realistic view of model but can be skipped if untextured model is sufficient for the final result. Furthermore, there are more steps, if necessary, can be proceeded for example building tiled model and building DEM to get the elevation model and data to abstract the profile and cross-section from the model setup (Agisoft, 2018).

This study carries out 3D modelling in SFM for the model tests M15 and M17 which covers both the dam with core and without core types. Handheld DLSR camera was used to take the photos at the start and end surface of the dam model which has been utilized in this software to extract the 3D model at start and end surface condition. Figure 4.7 shows the three dimensional model of dam model 15 before breach which is model test of rockfill homogeneous dam with a central core. The image is cropped to show only the main part of the dam which is being affected by the breaching action. The left side of the dam in picture is downstream and right side of the dam is upstream which is also clued by the flow direction of dam material towards left side which was due to the erosion of material during breaching.

Figure 4.7: Three dimensional model of M15 before breach

Figure 4.8: Three dimensional model of M15 after breach

Figure 4.8 shows that the breach happened to the side where pilot channel was build which is left side of dam in the flow direction.

When the breach happens, it is interesting to see the breach profile, cross-section and analyse the breach dimensions. To do so, it is first necessary to get the DEM of the dam model surface. Figure 4.9 and Figure 4.10 show the DEM of dam models M15 at start and at end.

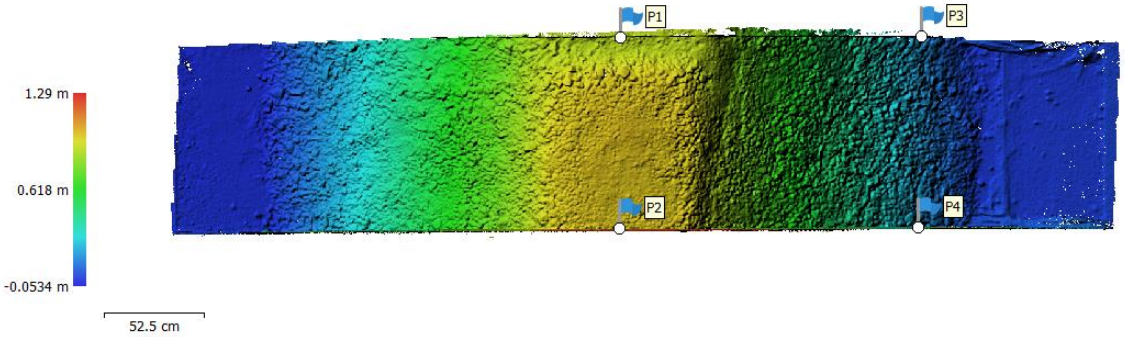

Figure 4.9: DEM of model M15 at start before breach (Upstream: left end)

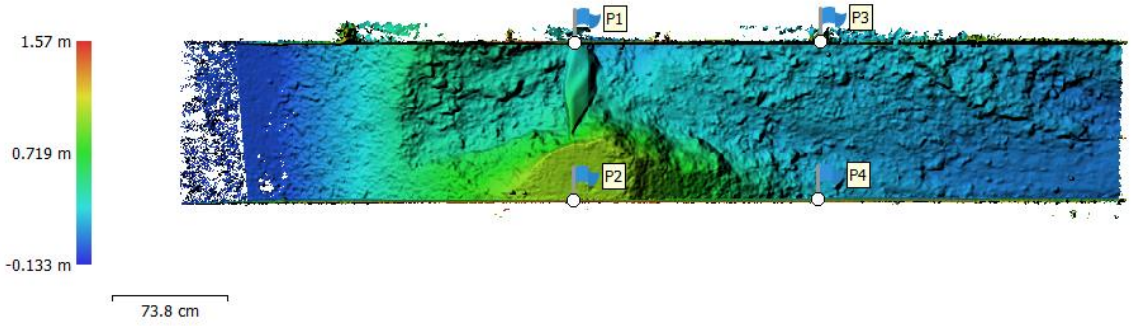

Figure 4.10: DEM of model M15 after breach (upstream: left end)

The DEM models are processed in GIS software to get the elevation data and output results such as cross-sections, profile etc. Some important sections and profiles of some sensitive areas of dam are presented here so that the before and after breach situation can be analysed.

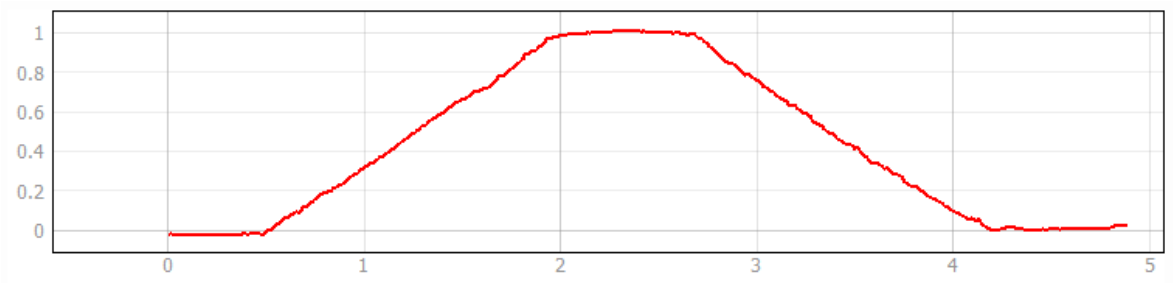

Figure 4.11: Dam profile before breach of model M15 (upstream: left end)

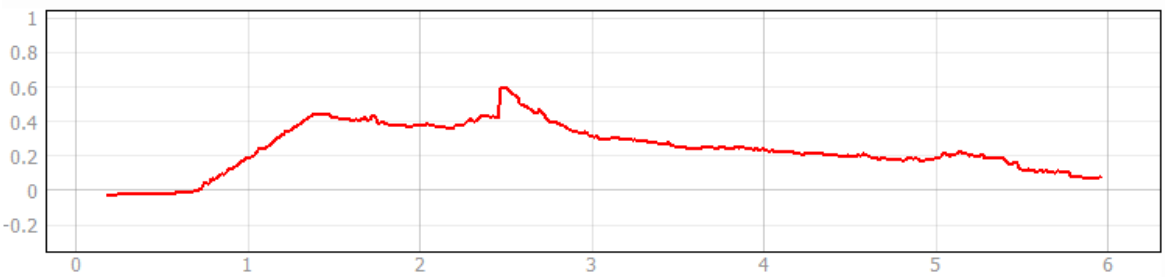

Figure 4.12: Dam profile after breach of model M15 (upstream: left end)

Figure 4.11 and Figure 4.12 are the dam profile before and after the breaching for model 15. The first profile gives the unaffected surface profile of dam model while second profile shows the breached surface gradually loosing elevation to the downstream side. At the center of the dam, there is small upside projection of the rubber membrane core which is on the way of water flow and obstructing material to move downstream. Similar profiles are drawn at different positon of the dam to see how breach changes in dam body which are placed in the appendix section of this report.

Likewise cross-sections at core are also plotted from the DEM model in QGIS and presented here. In Figure 4.13 it can be seen that the pilot channel at the left side has the invert level of 0.9 meter for 0.1 meter bottom width which increases to 1.0 meter when attains the full top width of 0.2 meter. Once the breach happens, Figure 4.14 shows the cross-section in the same positon along core and the changes happened after the breaching can be seen. The lowest level of breach is at the far left corner where the invert level has gone upto 0.1 meter elevation depth. From the deepest point to the right side elevation starts gradually increase and reach the original level of 1.0 meter at a distance of 0.6 meter from the left end.

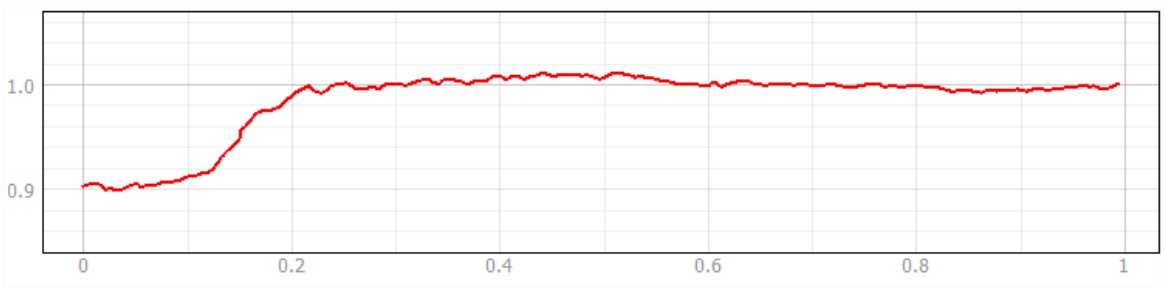

Figure 4.13: Cross-section at core of dam model M15 before breach (View from upstream)

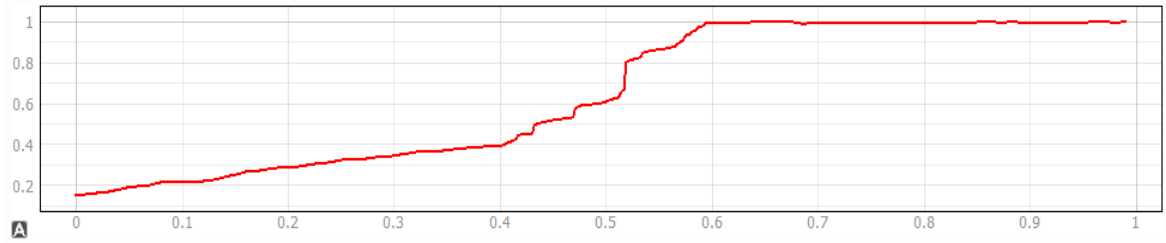

Figure 4.14: Cross-section at core of dam model M15 after breach (View form upstream)

For the rest of the model tests the same procedure was carried out to get the DEM, and profiles, cross-sections at different dam locations. The details for one more model M17 which is rockfill dam without core is presented here in Figure 4.15 and Figure 4.16 to describe in detail atleast one with core and one without core type.

Figure 4.15: Three dimensional model of M17 before breach

Figure 4.16: Three dimensional model of M17 after breach

The diffeence between the previous model test M15 and this model M17 is that the later test has smooth fall of breach surface level which is due to the absence of core material in the middle and the breach becomes more consistent throughout from top to bottom leaving no abrupt elevation difference along flow direction. The DEM models are built here as well to see the dam surface before and after the breach for without core case.

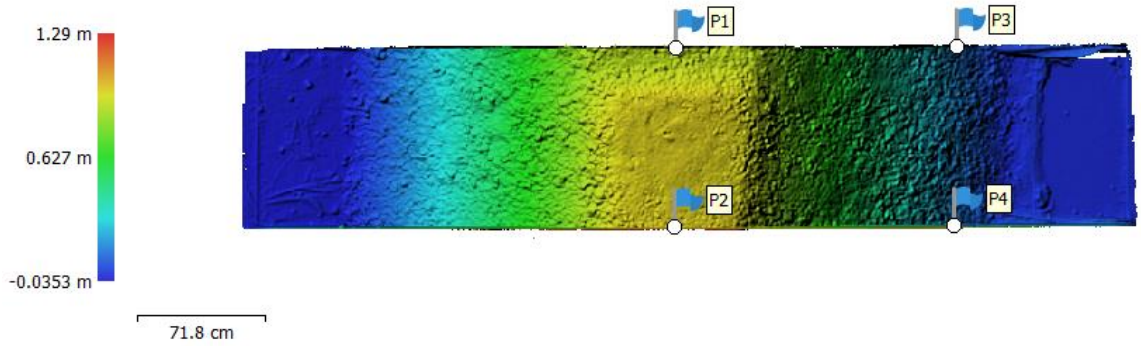

Figure 4.17: DEM of model M17 at start before breach (upstream: left end)

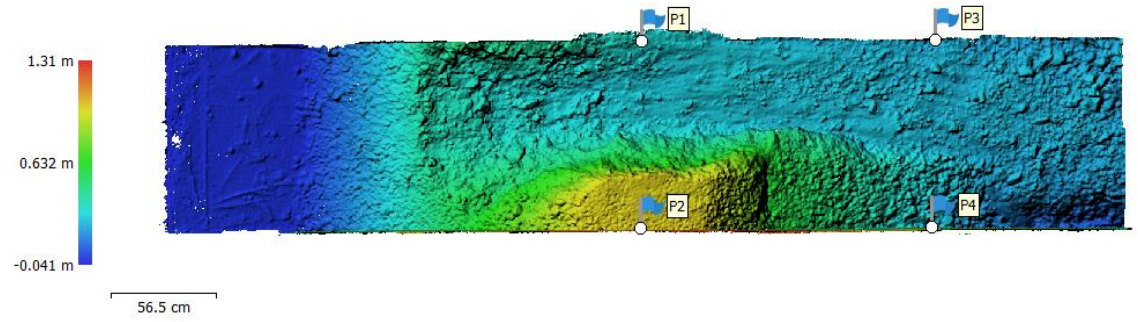

Figure 4.18: DEM of model M17 at start after breach (upstream: left end)

DEM models shown in Figure 4.17 and Figure 4.18 give a very clear hint that the pilot channel to the left of the flume on dam crest helps to develop the breach in its side and the final breaching has happened entirely on the left side of flume. The elevation difference after the breach is shown with different color code as mentioned in the legend. Several profiles and cross-sections are drawn in different dam location but the most significant ones are presented here in the Figure 4.19 and Figure 4.20.

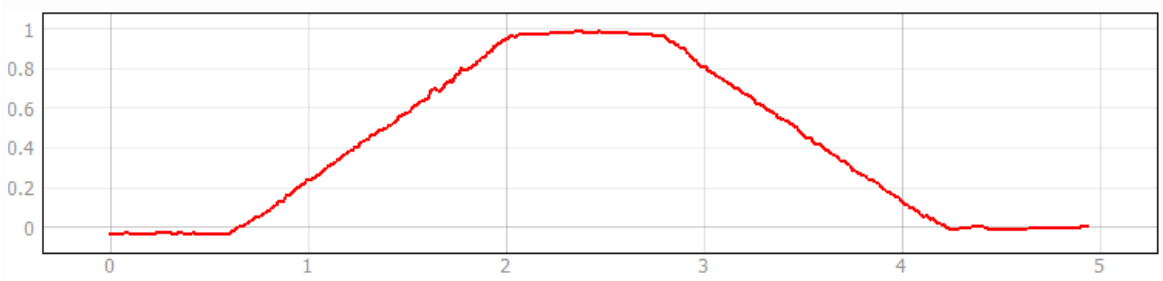

Figure 4.19: Dam profile before breach of model M17 (upstream: left end)

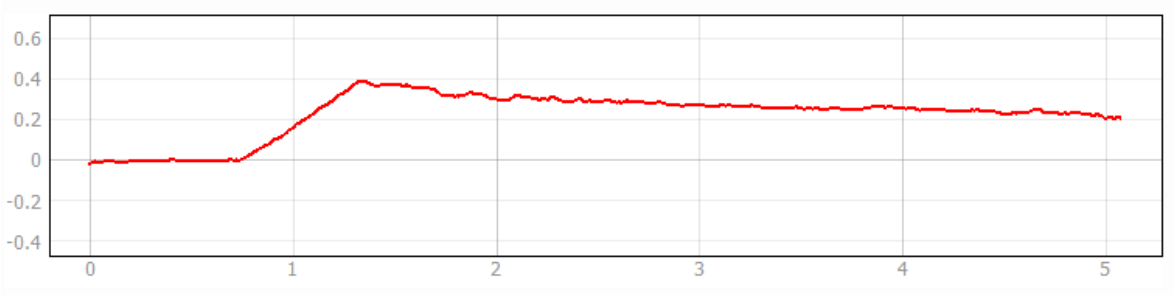

Figure 4.20: Dam profile after breach of model M17 (upstream: left end)

Cross-section at core of the dam is drawn to see the before and after breach situation which is shown in the Figure 4.21 and Figure 4.22. It clearly shows that the breach takes place along the pilot channel and develops to the full size as shown in the figures. From the Figure 4.21 the dimension of the pilot channel seems not regular but roughly correct to the designed dimension of bottom width 0.1 meter, top width 0.2 meter and depth 0.1 meter. At the end of the breaching in the Figure 4.22 the pilot channel has expanded to very large opening as bottom width increased to almost 0.5 meter, top width to 0.73 meter and depth to 0.7 meter. The right side of the dam crest is remained undisturbed with the dam breaching which is due to the limited size of breach opening.

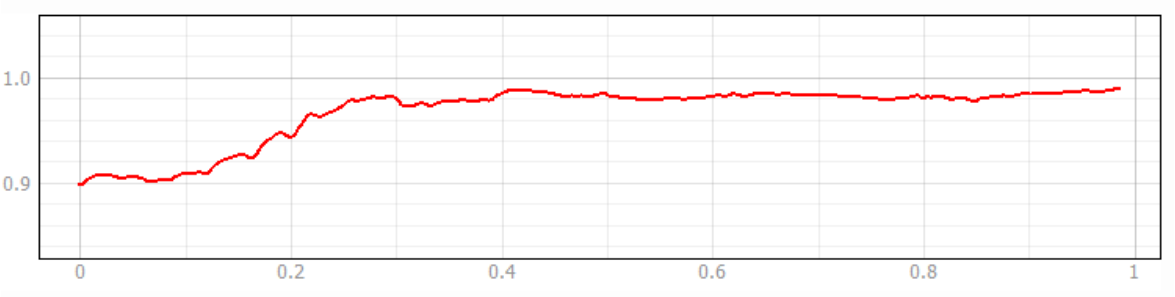

Figure 4.21: Cross-section at core of dam model M17 before breach (view from upstream)

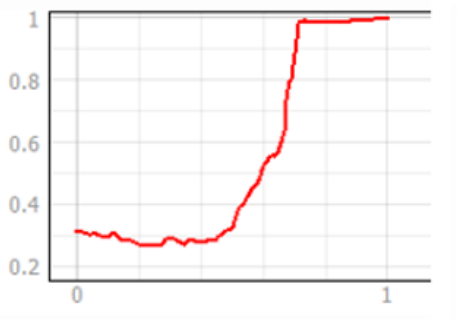

Figure 4.22: Cross-section at core of dam model M17 after breach (view from upstream)

4.4 Inflow and failure discharge

Inflow discharge and water level in the upstream reservoir was measured and obtained from the sensor data. As incoming flow and water level data in the storage pond in the flume is known over the time, the outgoing water through or over the dam is calculated with the help of stage-volume reservoir curve. Reservoir volume curve gives the information about volume change for each unit increment in water level in the reservoir which is shown in the Figure 4.23. The volume curve shows the water storage capacity when the dam is filled up to the crest level of 1.0 meter is nearly 9500 liters which is for rockfill dam without any protection layers. An equation is obtained with the best R^2 value of 1 which is shown in the same chart and is used to calculate the volume in the reservoir for any elevation increase or decrease during the breaching test and water level fluctuations.

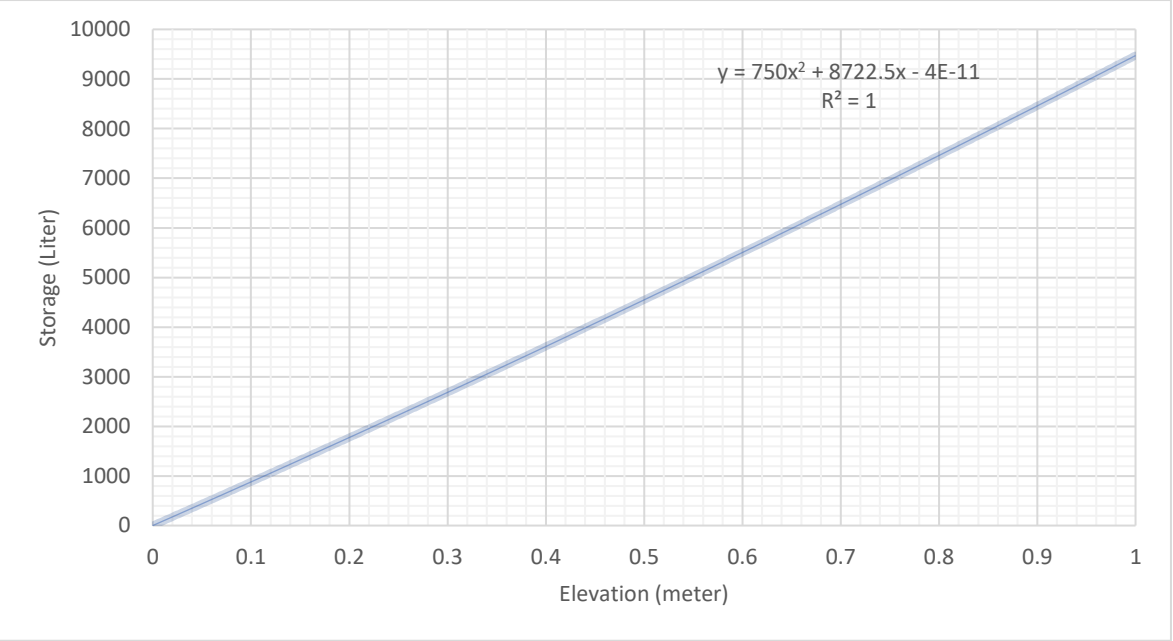

Figure 4.23: Reservoir volume curve for the dam model

A simple water balance equation is employed to calculate the outflow water from the upstream reservoir which is as shown below.

Change in storage = inflow – outflow

Using the reservoir curve above in conjuction with water level reading, the volume of the reservoir for the given time can be calculated. Then the inflow data are used in the above water balance equation to calculate the outflow and each time step is proceeded likewise till the end. Figure 4.24 shows the inflow, outflow and storage data for the whole period of test that lasts for 7000 seconds which is roughly 2 hours. However the dam breached almost in the middle at 4000 seconds which can be seen with the rapid fall of storage and outflow discharge. It is also noted from the chart that the leakage test was performed by shutting the inlet valve down and there is gradual decrease of water volume in the time period from T = 1200 seconds to T = 3500 seconds. Thereafter the inlet valve was opened again allowing rapid increase of water volume which becomes stable for short time afterwhich the dam was overtopped and failure is seen with sudden decline of both the storage and outflow. At the

end, it is seen that the storage comes to almost zero and there is no inflow as well as all valves were closed.

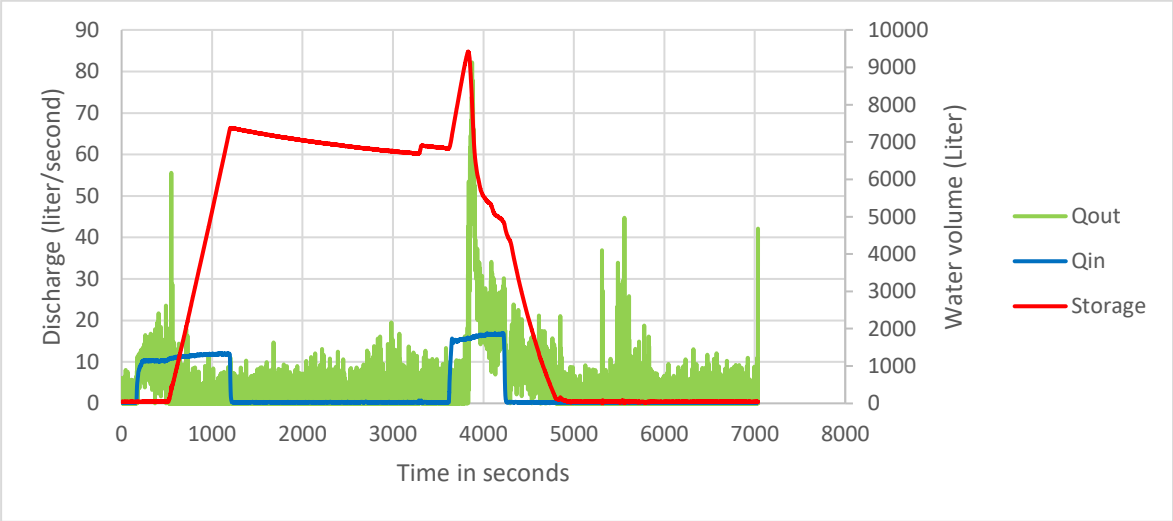

Figure 4.24: Out flow, inflow and storage variation in upstream reservoir for model M15

Same procedures were followed to find out the out flow discharge for model 17 and the chart is shown in Figure 4.25. In this case there is no core membrane which results excessive through flow from the beginning and no leakage test was performed. For that reason there is no flat portion in the storage curve as in the previous model M15 during the leakage test. Here in this case as well, the failure is shown by the rapid fall of storage and outflow discharge while inflow valve was closed right after the breach which can also be seen in the chart.

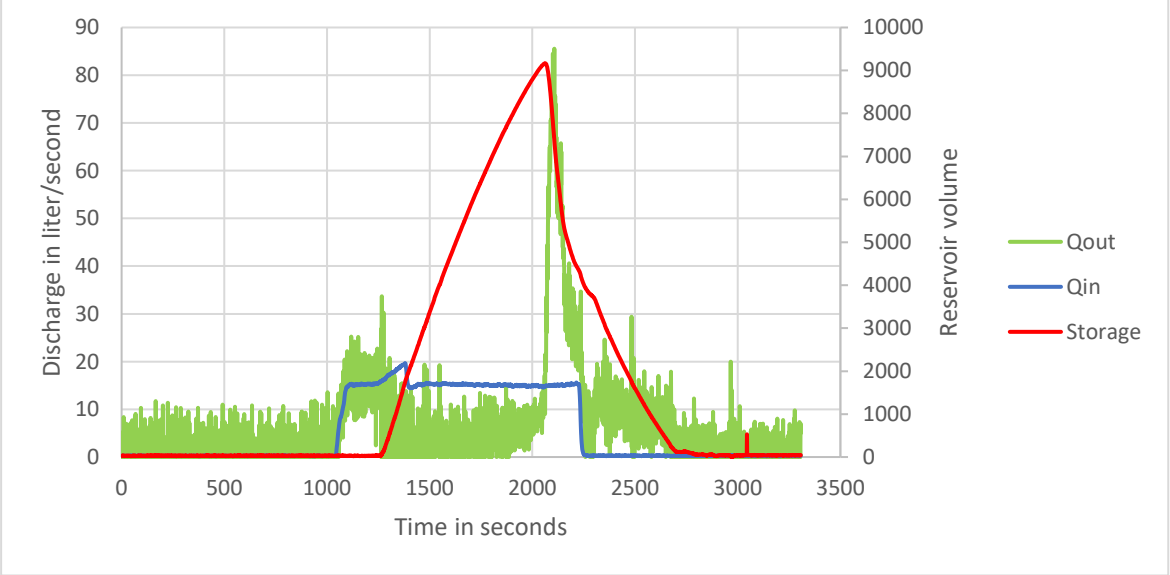

Figure 4.25: Out flow, inflow and storage variation in upstream reservoir for model M17

4.5 Comparison to parametric models

The models are compared based on the breach parameters such as peak discharge, average width and failure time which are major parameters in dam breaching process. Several different parametric model equations were employed to get the variety of results and to compare one another with the physical modelling. So as to compare them in detail, results are taken from different calculation and methods applied previously such as side view tracking of breach development, Structure of motion analysis in AGISOFT, profile and cross-section made in GIS softwares, charts, tables etc plotted from the result extracted from those all. Table 4.4 below describes the peak discharge for model 15 measured in physical test conducted in lab, and values obtained from different parametric model equations. It is noted that Zhang et al., (2009) gives the closest value to the measured one in the physical modelling.

Table 4.4: Peak discharge from physical model and different parametric equations

Model 15	Peak discharge, Q_p	Unit
Measured	0.08	m^3/s
MacDonald 1984	0.36	m^3/s
Froehlich 1995b	1.02	m^3/s
Xu Zang 2009	0.11	m^3/s
Froehlich 2016b	0.31	m^3/s

Similarly, failure time for model 15 is also noted from the physical model test and compared to the one obtained from emperical equations which is shown in the Table 4.5 below.

Table 4.5: Failure time from physical and parametric models

Model 15	Failure time, t_f	Unit
Measured	0.04	hour
Froehlich 1995a	0.01	hour
Froehlich 2008	0.07	hour
Xu Zang 2009	0.01	hour
Froehlich 2016a	0.06	hour

Another important breaching parameter is average width which is the average of top and bottom width and summarized in the Table 4.6 below. Here it is clearly seen that the average width from measured values and from different parametric models are not so differed with greater values as all of them are within the range from 0.44 to 0.65 meter.

Table 4.6: Average width measured in physical model and parametric models

Model 15	Average width, Bavg	Unit
Measured	0.6	m
Froehlich 1995a	0.48	m
Froehlich 2008	0.68	m
Xu Zang 2009	0.63	m

Similarly for the model 17 which is a rockfill dam without a central core, breach parameters are found out and presented in the tables below. Table 4.7 presents peak discharge measured in physical model conducted and values obtained from different parametric equations.

Table 4.7: Peak discharge from physical model and different parametric equations

Model 17	Peak discharge, Q_p	Unit
Measured	0.09	m^3/s
MacDonald, 1984	0.32	m^3/s
Froehlich, 1995b	0.75	m^3/s
Xu Zang, 2009	0.09	m^3/s
Froehlich, 2016b	0.22	m^3/s

Table 4.8 shows the failure time for model 17 measured in model tests and calculated different values from parametric equation which is in hours.

Table 4.8: Failure time from physical and parametric models

Model 17	Failure time, t_f	Unit
Measured	0.05	hour
Froehlich, 1995a	0.01	hour
Froehlich, 2008	0.08	hour
Xu Zang, 2009	0.01	hour
Froehlich, 2016a	0.07	hour

Table 4.9 presents average width for model 17 measured in physical model test and from different parametric model equations which is average of top and bottom width.

Table 4.9: Average width measured in physical model and parametric models

Model 17	Average width, Bavg	Unit
Measured	0.65	m
Froehlich, 1995a	0.44	m
Froehlich, 2008	0.64	m
Xu Zang, 2009	0.52	m

From the measured values and parametric equation employed, it is noted that some models for some breach parameters give closest measured values while some has little deviation. So, it is always a good practice to check with several existing and reliable methods and giving a range of values instead of getting single result to avoid possible error and misinterpretation.

5 Discussion

This section discusses the result from the previous sections and compare parametric models with physical models conducted. This section also includes charts and tables to simplify the findings and for easy understanding. At the end of this chapter, there is limitation of the setup which explains things that limit the laboratory experiments and results.

5.1 Breaching process and parameters

In previous chapter 4, breaching parameters such as peak discharge, failure time and average width are presented based on the observation of physical model tests in hydraulic laboratory, NTNU and also with the parametric modelling. The result from different models are not so consistent and is interesting to see the percentage deviation of resulting values to one another. The divergence in breaching parameter values between parametric models and the observed values in physical models are discussed for both the dam models M15 and M17.

Table 5.1: Percentage deviation from observed peak discharge values (M15)

Model 15	Peak discharge, Q_p	% deviation	Unit
Measured	0.085		m^3/s
MacDonald 1984	0.36	324	m^3/s
Froehlich 1995b	1.02	1100	m^3/s
Xu Zang 2009	0.11	29	m^3/s
Froehlich 2016b	0.31	265	m^3/s

Table 5.2: Percentage deviation from observed failure time values (M15)

Model 15	Failure time, t_f	% deviation	Unit
Measured	0.04		hour
Froehlich 1995a	0.01	75	hour
Froehlich 2008	0.07	75	hour
Xu Zang 2009	0.01	75	hour
Froehlich 2016a	0.06	50	hour

Table 5.3: Percentage deviation from observed average width values (M15)

Model 15	Average width, Bavg	% deviation	Unit
Measured	0.6		m
Froehlich 1995a	0.48	20	m
Froehlich 2008	0.68	13	m
Xu Zang 2009	0.63	5	m

Table 5.1, Table 5.2 and Table 5.3 respectively compares percentage deviation of values in parametric model than from the values in physical model for peak discharge, failure time and average width. For peak discharge values, Zhang et al. (2009) gives the least error which is just 29 % more than the measured one. D. C. Froehlich (1995b) has the maximum percentage of diverged value which is 1100 % but the model introduced later in 2016 by the same person has improved the model and gives the closer value.

For failure time, all the parametric models are equally capable as all of them giving similar result and none of them varied by more than 75 %. Amongst them, D. Froehlich (2016a) is a bit more accurate which has little deviation of just 50 %. Similarly for average width, all the parametric models look satisfying with similar result to physical model and if one is picked as a best, Xu et al. (2009) gives the least percentage deviation of just 5 %. So, some of the models are good at one parameter while some other gives best result for another. This hints that no single model is fully confident to give the breaching parameter values, and suggests utilizing number of possible methods to check and verify the output result before coming into the conclusion.

The similar discussion is done for model test M17 where comparison for peak discharge, failure time and average width are presented in the Table 5.4, Table 5.5 and Table 5.6 respectively. For peak discharge value for model 17, Xu et al. (2009) gives the least diverted value from the observed one. For failure time in this case, only two parametric models look satisfactory: D. C. Froehlich, (1995a) and Zhang et al. (2009). For average width values, all the models are equally good, D. C. Froehlich & Asce (2008) being the best.

Table 5.4: Percentage deviation from observed peak discharge values (M17)

Model 17	Peak discharge, Q_p	% deviation	Unit
Measured	0.09		m^3/s
MacDonald 1984	0.32	256	m^3/s
Froehlich 1995b	0.75	733	m^3/s
Xu Zang 2009	0.09	0	m^3/s
Froehlich 2016b	0.22	144	m^3/s

Table 5.5: Percentage deviation from observed failure time (M17)

Model 17	Failure time, t_f	% deviation	Unit
Measured	0.05		hour
Froehlich, 1995a	0.01	80	hour
Froehlich, 2008	0.08	700	hour
Xu Zang, 2009	0.01	88	hour
Froehlich, 2016a	0.07	600	hour

Table 5.6: Percentage deviation from observed average width (M17)

Model 17	Average width, Bavg	% deviation	Unit
Measured	0.65		m
Froehlich, 1995a	0.44	32	m
Froehlich, 2008	0.64	2	m
Xu Zang, 2009	0.52	20	m

All these results from this comparison conclude that some models are so good to estimate some specific breaching parameters while others are good at some others. It means one who work on this type of study should go under number of different models' study before coming into any conclusion which otherwise would lead to false or wrong information.

5.2 Breaching rate

The breaching rate for all the test models is calculated as shown in the Table 5.7 so that comparison can be made to see how different dams go under different breaching rates. To simplify this table for good understanding, a chart is presented in Figure 5.1 below. In the chart of breaching rate, the blue columns are breaching rate for dam with central core and green columns without core. The breaching rates for the dams with central core are lower in values with range from 0.35 to 0.4 cm per second. While for the dams without core, the breaching rate is higher with range from 0.5 to 0.6 cm per second. It is seen from the chart that the result is consistent for their dam types and configuration which enhance the reliability of the test results. Another interesting finding which the Table 5.7 explains is the time of failure for dam with core are higher than dam without core. In average dam with central core takes 150 second for full breaching while dam without core takes 90 seconds in average for the same process. This result shows that dam with core is more resistant to failure and erosion than the dam without core.

Table 5.7: Comparision of breaching rate at core for different dam models

Dam model	Breach initiation time (sec)	Maximum breach time (sec)	Time interval (sec)	Initial level (cm)	final level (cm)	Breach depth (cm)	Breaching rate cm/sec
3	60	210	150	90	32	58	0.39
4	60	210	150	88	35	53	0.35
5	30	180	150	90	36	54	0.36
6	30	180	150	89	34	55	0.37
15	60	210	150	90	37	53	0.35
17	120	210	90	90	34	56	0.62
18	60	150	90	90	44	46	0.51
19	150	240	90	86	34	52	0.58

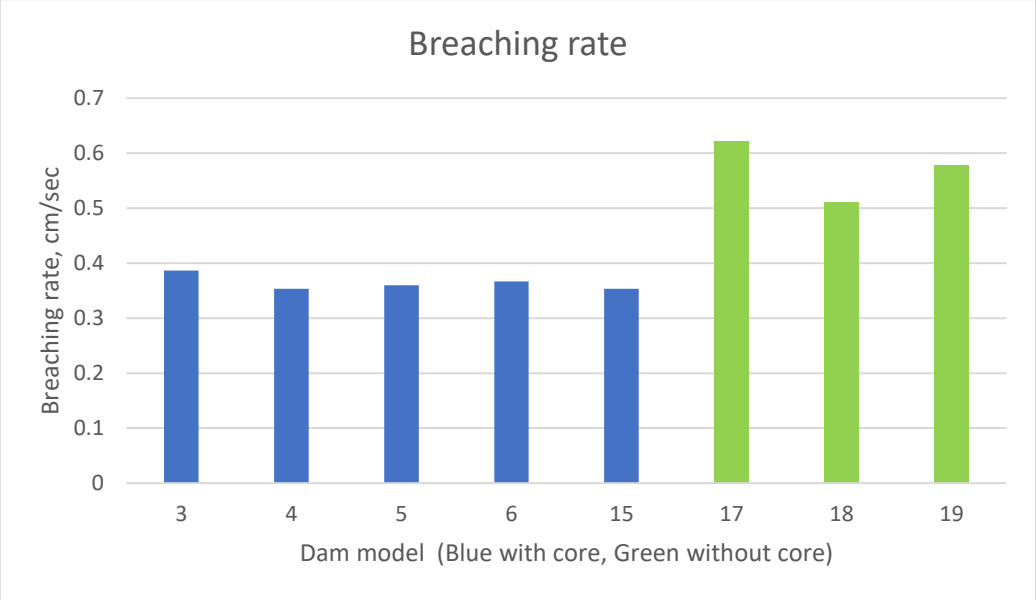

Figure 5.1: Breaching rate for dam with core and without core

Similarly, breaching rate at 40 cm downstream of the core is also observed to see how it differs in different dam location. The same calculation procedure is followed as previously, and the Table 5.8 and chart in the Figure 5.2 are presented below. The output result for breaching rate is just opposite than from the previous case which is due to the downstream position in this case. The breaching rate for the dam without core has lower values than with the core one and consistent values for each dam type is observed which again supports the test results and reliability of the physical models conducted.

Table 5.8: Comparision of breaching rate at 40 cm downstream of core

Dam model	Breach initiation time (sec)	Maximum breach time (sec)	Time interval (sec)	Initial level (cm)	final level (cm)	Breach depth (cm)	Breaching rate cm/sec
3	0	150	150	90	19	71	0.47
4	30	180	150	90	22	68	0.45
5	30	180	150	90	14	76	0.51
6	0	150	150	90	19	71	0.47
15	30	180	150	90	13	77	0.51
17	90	240	150	90	29	61	0.41
18	30	150	120	90	44	46	0.38
19	60	210	150	84	37	47	0.31

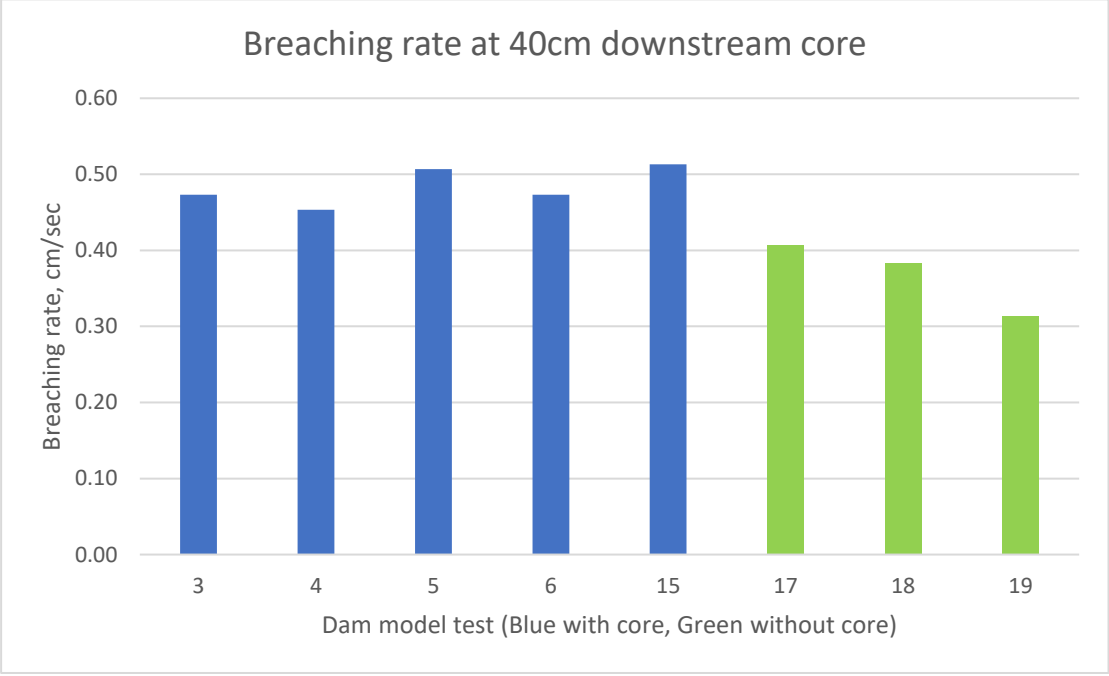

Figure 5.2: Breach rate at 40 cm downstream core

Another noticeable finding is that all the above-mentioned models have pilot channel on it at left side of the crest with a dimension of top width 20 cm, bottom width 10 cm and height 10 cm which runs along flow direction. The purpose of this channel was to start the breaching on that side so that the breach progress could be captured well on cameras and observed during the testing period. All the tests went as planned and full breaching happened around

the pilot channel which proves that the part of the dam where it gets overtopped first will eventually develops into the full breach opening. Figure 5.3 illustrates the same explanation as the first figure in the left shows the initial dam condition before testing and right side picture demonstrates how the pilot channel develops into the full breach opening with other end left undisturbed.

Figure 5.3: Left side- Dam model before breaching with pilot channel on the top Right side-Dam model after breach progress around pilot channel

5.3 Limitations of the setup

In general there exists some common limitations on experimental studies of physical model due to limited availability of space, time, fund and other technical issues which are difficult to address everything at a time. In this study, breaching process and its development over the time for rockfill dam with core and without core was performed. The limiting factors in this case are found to be the size of the flume setup, reservoir capacity, core material, construction methodology etc. Some of the major limitations are briefly explained below:

- The width of the flume is 1 meter throughout which limits the length of the dam across flow direction. When the breaching happens, it cannot extend much towards the left where the pilot channel is built due to the limited space availability which restrict the model to fully extend and limits it to gain its natural form of breach opening. In this study, it has been assumed that the model is symmetrical with reference to the glass wall at left side in the direction of water flow.

- The rubber membrane is used as a core material which is a larger single piece which when goes under the breaching process creates some disturbance to the natural flow over the breach surface creating addition spillway effect.

- The upstream reservoir of dam model is of small storage capacity which is a falling head reservoir during breach and does not represent the real state scenario as the reservoir size in real cases are way bigger when compared with the dam size.

- As more tests are carried out, fine particles in the construction material are constantly washed away and latter tests have more coarser particles losing some portion of fine material.

6 Concluding summary and recommendation

This section is about the conclusion drawn from the physical models conducted in the lab and parametric models employed for eight different models of rockfill dams which are discussed in the previous sections. At the end some constructive feedback for the future tests and recommendations for the inprovements of the physical models are given which are based on the experience gained and feedback in this period of study.

6.1 Concluding summary

The breaching process and parameters of rockfill dams greatly vary depending upon the dam configuration, dam type, material properties, building methodology and protection measures of the dam body. This is a complex combination of different mechanisms to failure which includes horizontal and vertical erosion, different flow regimes, both the sub-critical and supercritical flow condition, upstream and downstream boundary condition, and failure mode. Each dam has a capability to act a unique model when there is a slight modification in the design, material used and construction methodology which was seen in the result of the models discussed earlier. Hence, it is of paramount importance that the possible risks of dam hazards are well evaluated with regards to failure and downstream areas be assessed to minimize the possible effects of catastrophe by dam failure. In Norway, recent decades see more demand of new regulations for planning, construction, and operation of dams for the safety reason which has been a major issue for downstream areas since long ago. All these planning would require proper investigation and good understanding of different dam models and their behavior in extreme load condition. This study helps further investigation in the field of dam safety and improves the dam design, construction, and operation technology.

Total of eight different tests were conducted for this study of dam where three of them were without core and remaining with the central core. Both dam types were incorporated with a pilot channel and material used was same except the rubber membrane core at center. Supply of inflow in upstream reservoir was also made alike to see the change in behavior for same scenarios. The major difference observed between the two dam types are erosion rate, breach initiation time, throughflow and overtopping mode, leakage through the dam and failure time. Use of different software like SFM Agisoft, GIS software, R programming script made the analysis work simple and enhance the quality of data handling.

From the physical models carried out, it came to know that dams without core suffers more with the throughflow and higher chances of partial failure before it reaches overtopping failure. However, in most of the model tests, the failure was combination of both the throughflow and overtopping. At first, throughflow causes small sliding in the downstream slope of dam while overtopping gives significant erosion and quick breach resulting to a complete failure. Also, pilot channel facilitates dam to be overtopped first and help to erode and breach through that section. The rate of erosion at center of a dam is higher for a dam without central core and vice versa. When the erosion starts from the pilot channel progressing to the full breach opening, the breach section observed was of steep side slopes which later became stable with further down slides of material giving the breach opening a trapezoidal shape. Moreover, both the dam (with core and without core type) run under smooth breaching process and no sudden collapse were observed. Both types had similar range of outflow discharge, however, dams with core experience some lagging in erosion and breaching when referenced to breach initiation time. The embankment dams have higher degree of uncertainty as small deviation in the materials and dam configuration would show different breach behavior. Hence, it is always too early to come into conclusion by looking into few tests of any type of dam model tests.

Parametric models satisfactorily provide good estimation of breaching parameters, however, some of them are less predictable to some parameters. This signifies that every test model should be employed number of different parametric models so that no wrong interpretation is made to any of these evaluations. Also, it is highly recommended to examine the assumption made to any parametric models before implication as this would greatly affect the result, if did not match the same criteria to the tested dam model. Zhang et al. (2009) for peak discharge, D. C. Froehlich (1995a) for failure time and again Zhang et al. (2009) for breach opening are amongst the best parametric models to estimate the breaching parameters. Empiric equations are powerful due to their simplicity since they do not require any computer simulations or physical models to be implemented. The simplicity, however, may also be its weakness, as breach parameter prediction uncertainty has been observed to be quite large for these models.

6.2 Recommendation

This study helps to better understand the embankment dam, their behavior, failure mechanism, breaching process and possible risk and hazard associated with a dam failure. The scope and investigation can be further expanded with a quality research work with some improvisation in current setup and methodology.

- The model setup is 1:10 scale which obviously is a good representation of a real field dam but still there exists some scaling effects which could be minimized by testing in a bigger dam to see more realistic behavior of failure mechanism and breach processes.
- The width of the flume setup is 1 meter which restrict natural expansion of breach opening and limits the width which can be improved with higher width setup so that breach opening can extend to the fullest. This gives more realistic data as the model

performs in a natural way. To minimize the possible errors, this study assumes mirror reflection which adds extra 1 meter width of existing flume to the left side referencing the glass wall.

- The rubber membrane as a central core is a large single sheet membrane which in the middle of the test obstruct the natural flow of water over the breach opening. So, a proper alternative of rubber membrane as a central core improves the breaching process and prevent spillway effect of rubber membrane seen currently.
- The size of the reservoir is very small comparing to the dam size which has become a falling head reservoir, and this may not represent a real scenario. Relatively larger size upstream reservoir setup is more realistic and can give good result.
- Further analysis of dam failure in numerical modelling gives additional data set for comparison and verification which adds reliability in this type of study. Also, numerical analysis is flexible for input data where material input, design and flow data can be altered to see the change in behavior in short period which saves time and cost.

References

Agisoft. (2018). Tutorial (Beginner level): 3D Model Reconstruction with Agisoft PhotoScan 1.1. 6, 1–7.

Alonso, E. E., & Cardoso, R. (2010). Behavior of materials for earth and rockfill dams: Perspective from unsaturated soil mechanics. Frontiers of Architecture and Civil Engineering in China, 4(1), 1–39. https://doi.org/10.1007/s11709-010-0013-6

Breaching, A. T. C. on D. (2011). Earthen Embankment Breaching. Journal of Hydraulic Engineering, 137(12), 1549–1564. https://doi.org/10.1061/(ASCE)HY.1943-7900.0000498

Clague, J. J., & Evans, S. G. (2000). A review of catastrophic drainage of moraine-dammed lakes in British Columbia. Quaternary Science Reviews, 19(17–18), 1763–1783. https://doi.org/10.1016/S0277-3791(00)00090-1

Froehlich, D. (2016). Empirical model of embankment dam breaching Fluvial hydraulics View project DRIP-Dam Rehabilitation and Improvement Project View project. https://doi.org/10.1201/9781315644479-285

Froehlich, D. C. (1995a). Peak Outflow from Breached Embankment Dam. Journal of Water Resources Planning and Management, 121(1), 90–97. https://doi.org/10.1061/(ASCE)0733-9496(1995)121:1(90)

Froehlich, D. C. (2016). Predicting Peak Discharge from Gradually Breached Embankment Dam. Journal of Hydrologic Engineering, 21(11), 04016041. https://doi.org/10.1061/(ASCE)HE.1943-5584.0001424

Froehlich, D. C. (1995b). Embankment dam breach parameters revisited. International Water Resources Engineering Conference - Proceedings, 1, 887–891.

Froehlich, D. C., & Asce, M. (2008). Embankment Dam Breach Parameters and Their Uncertainties. Journal of Hydraulic Engineering, 134(12), 1708–1721. https://doi.org/10.1061/(ASCE)0733-9429(2008)134:12(1708)

ICOLD. (2011). Definition of a Large Dam. International Commission on Large Dams. https://www.icold-cigb.org/GB/dams/definition_of_a_large_dam.asp

Jandora, J., Říha, J., & Vysoké učení technické v Brně. (2008). The failure of embankment dams due to overtopping.

Kiplesund, G. H., Ravindra, G. H. R., Rokstad, M. M., & Sigtryggsdóttir, F. G. (2021). Effects of toe configuration on throughflow properties of rockfill dams. Journal of Applied Water Engineering and Research, 9(4), 277–292. https://doi.org/10.1080/23249676.2021.1884615/SUPPL_FILE/TJAW_A_1884615_SM4576.MP4

MacDonald, T. C., & Langridge-Monopolis, J. (1984). Breaching Charateristics of Dam Failures. Journal of Hydraulic Engineering, 110(5), 567–586.

https://doi.org/10.1061/(ASCE)0733-9429(1984)110:5(567)

Marche, C. (2005). Embankment dam overtopping and collapse: an innovative approach to predict the breach outflow hydrograph. Transactions on The Built Environment, 84. www.witpress.com,

Morris, M., West, M., & Hassan, M. (2018). A guide to breach prediction. Dams and Reservoirs, 28(4), 150–152. https://doi.org/10.1680/jdare.18.00031

Ratnayaka, D. D., Brandt, M. J., & Johnson, K. M. (2009). Dams, Reservoirs and River Intakes. Water Supply, 149–193. https://doi.org/10.1016/B978-0-7506-6843-9.00013-5

Říha, J. (2006). Improvements in reservoir construction, operation and maintenance.

Schmocker, L. (2011). Hydraulics of dike breaching. PhD Thesis, 12–19. https://doi.org/10.3929/ethz-a-010025751

Senarathna, N. D. H. A. (2021). Effect of downstream erosion protection on the breaching of rockfill dams. June.

Shervais, K., & Dietrich, J. (2016). Structure from Motion (SfM) Photogrammetry Data Exploration and Processing Manual. Unavco, 1–28.

Veileder for fyllingsdammer. (2012).

Wahl, T. L. (2004). Uncertainty of Predictions of Embankment Dam Breach Parameters. Journal of Hydraulic Engineering, 130(5), 389–397. https://doi.org/10.1061/(ASCE)0733-9429(2004)130:5(389)

Walder, J. S., & O'Connor, J. E. (1997). Methods for predicting peak discharge of floods caused by failure of natural and constructed earthen dams. Water Resources Research, 33(10), 2337–2348. https://doi.org/10.1029/97WR01616

Xu, Y., Zhang, L. M., & Asce, M. (2009). Breaching Parameters for Earth and Rockfill Dams. Journal of Geotechnical and Geoenvironmental Engineering, 135(12), 1957–1970. https://doi.org/10.1061/(ASCE)GT.1943-5606.0000162

Zhang, L. M., Xu, Y., & Jia, J. S. (2009). Analysis of earth dam failures: A database approach. Georisk: Assessment and Management of Risk for Engineered Systems and Geohazards, 3(3), 184–189. https://doi.org/10.1080/17499510902831759

Zhong, Q., Wu, W., Chen, S., & Wang, M. (2016). Comparison of simplified physically based dam breach models. Natural Hazards, 84(2), 1385–1418. https://doi.org/10.1007/S11069-016-2492-9/TABLES/18

Appendix A – Breach formation

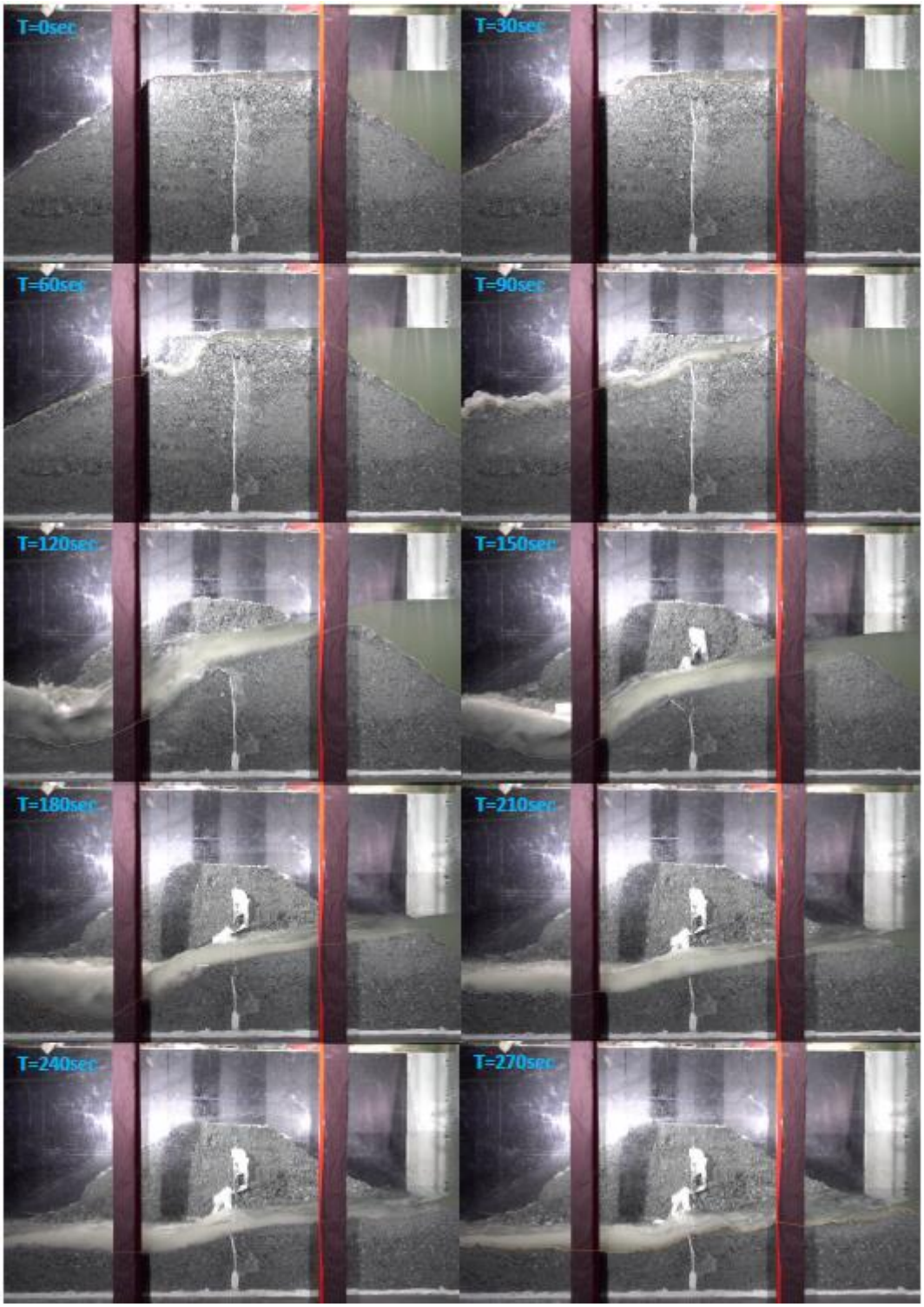

Appendix A 1: Temporal evolution of breach formation, Model 3

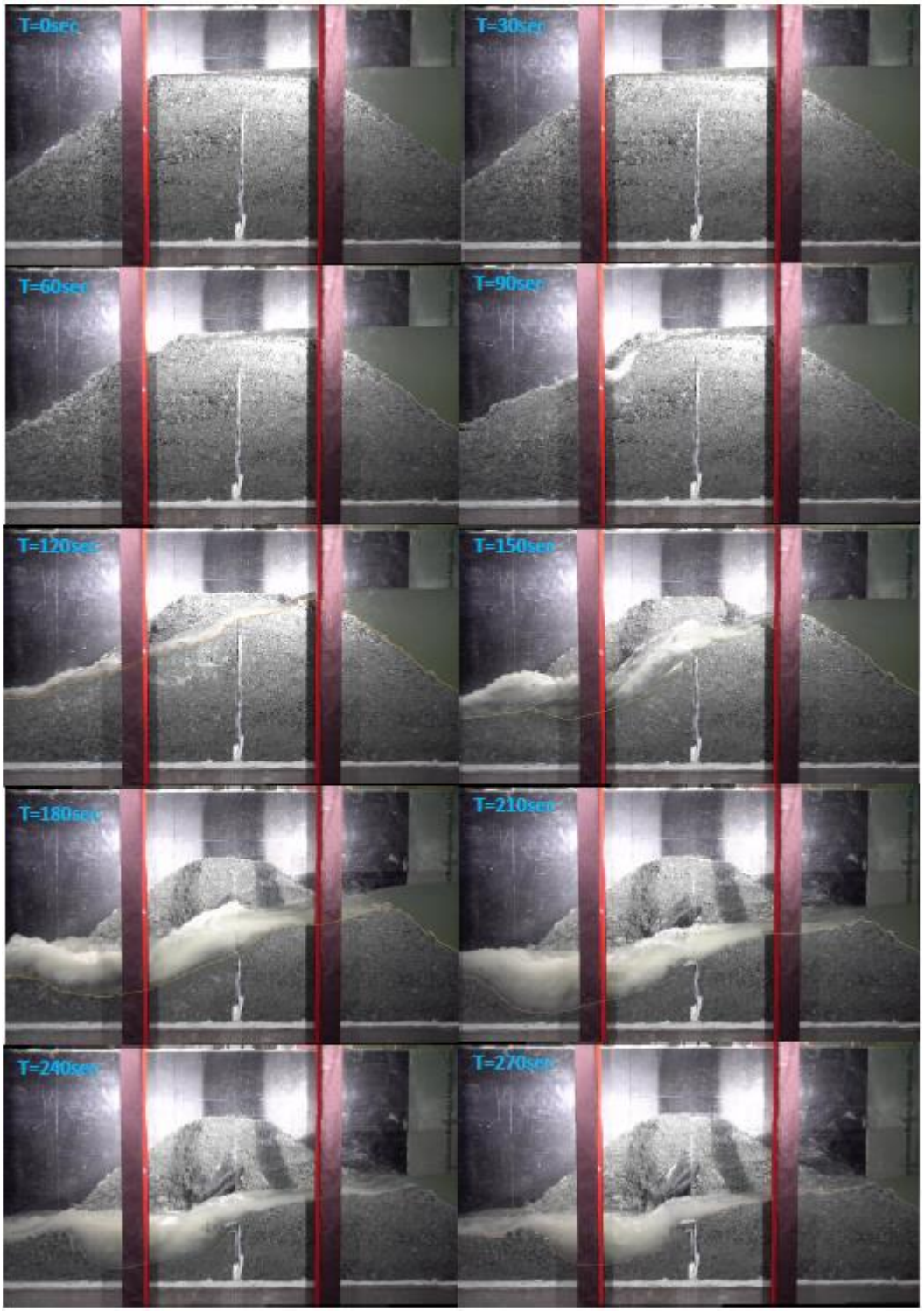

Appendix A 2: Temporal evolution of breach formation, Model 4

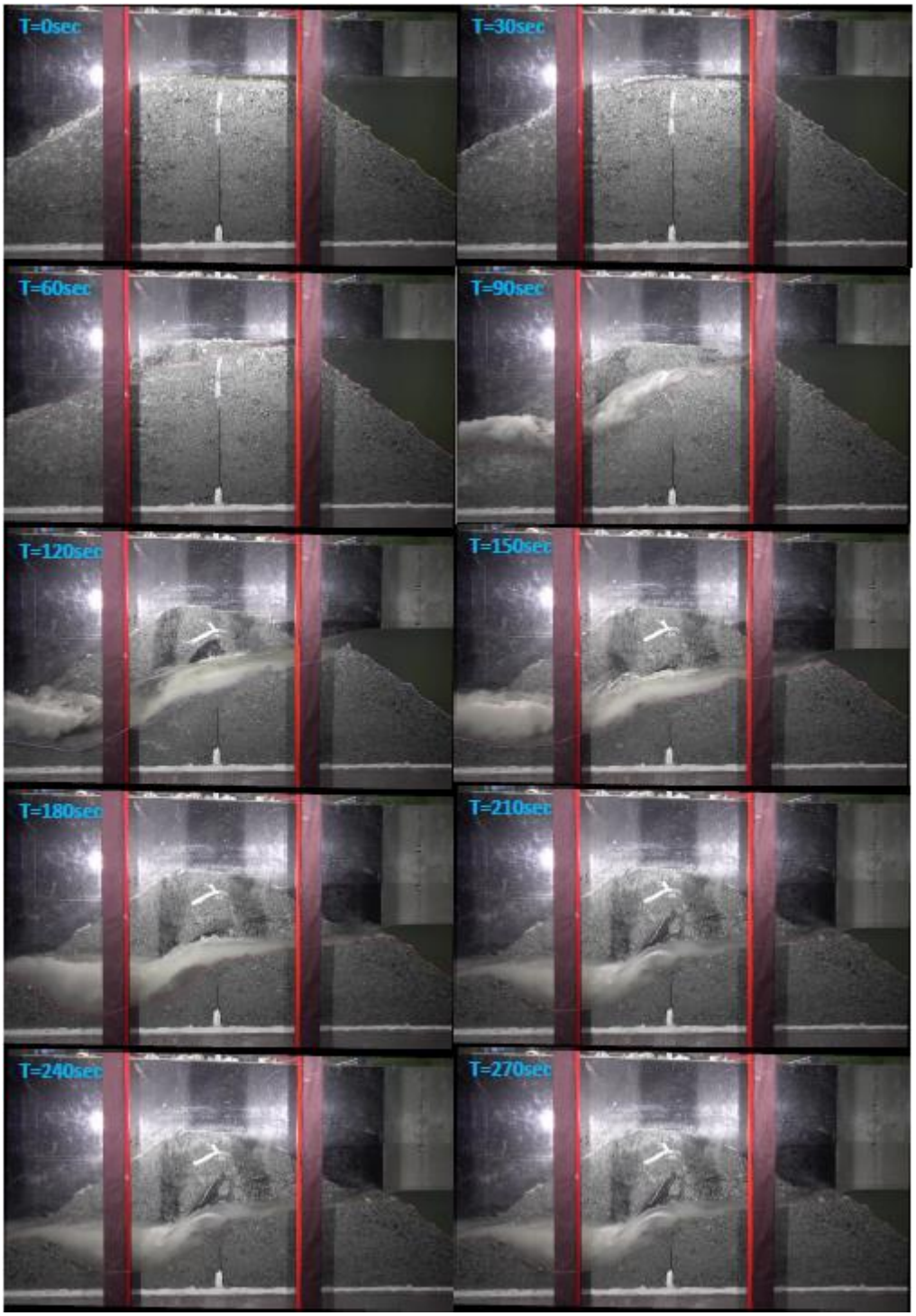

Appendix A 3: Temporal evolution of breach formation, Model 5

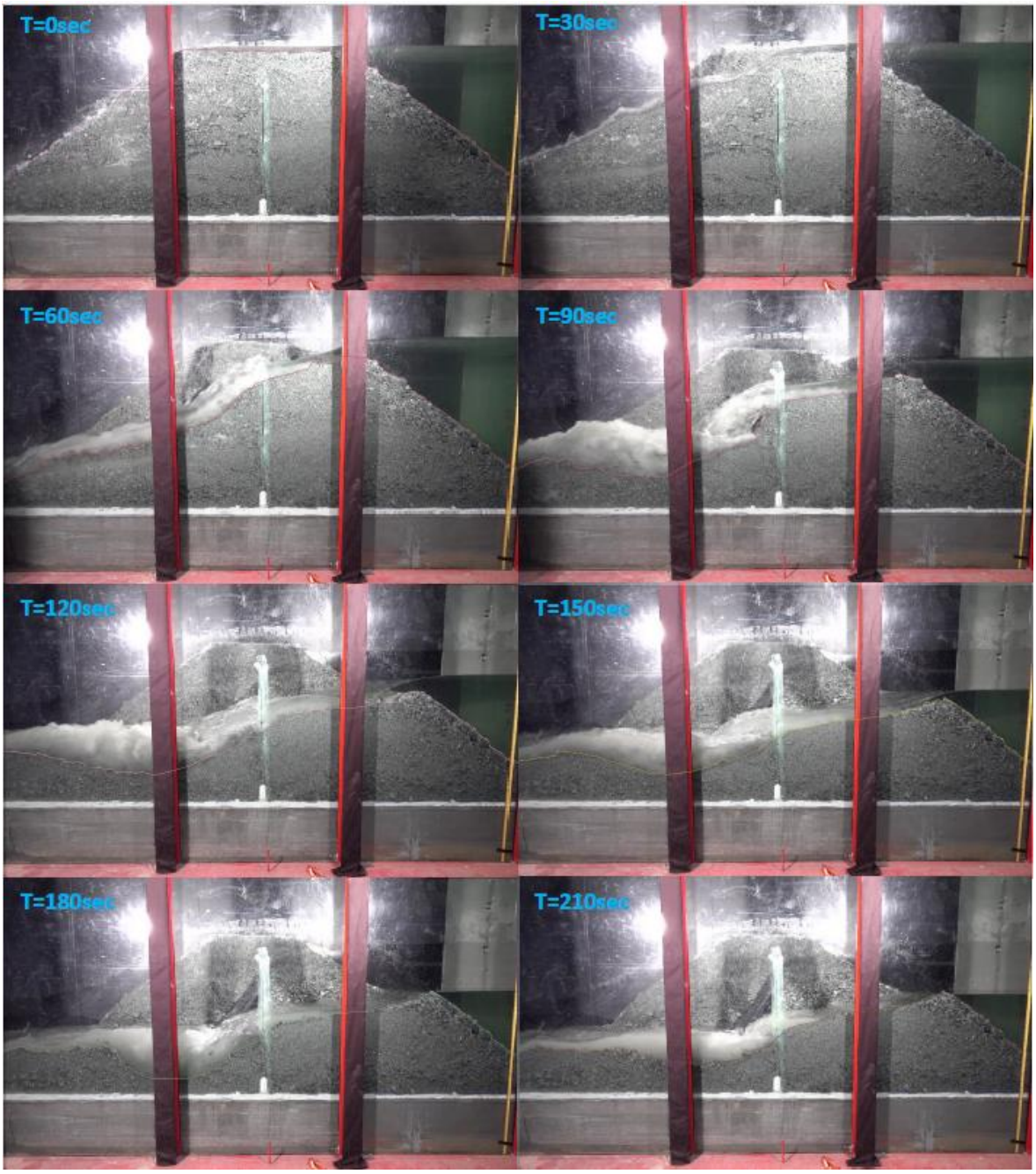

Appendix A 4: Temporal evolution of breach formation, Model 6

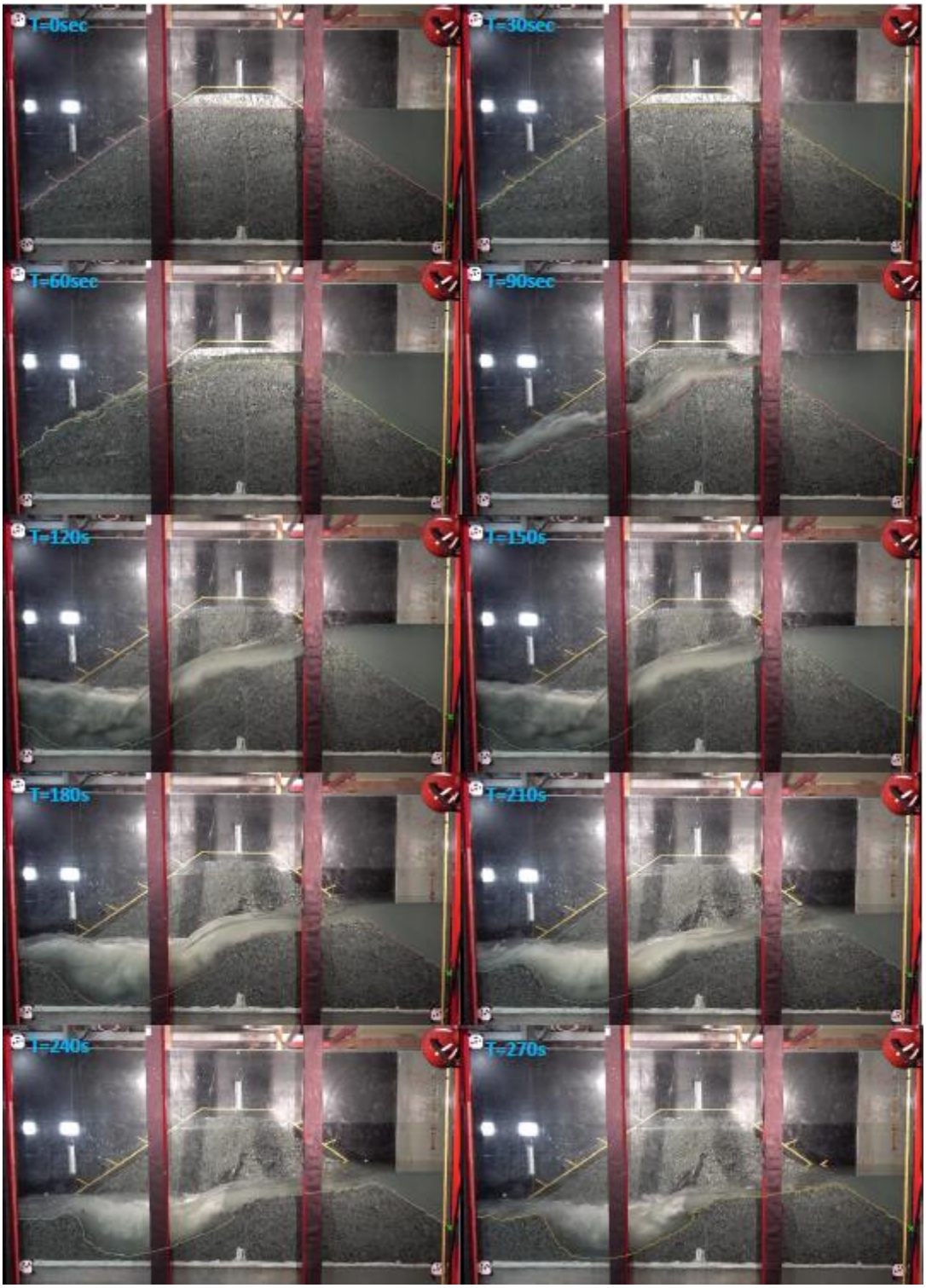

Appendix A 5: Temporal evolution of breach formation, Model 15

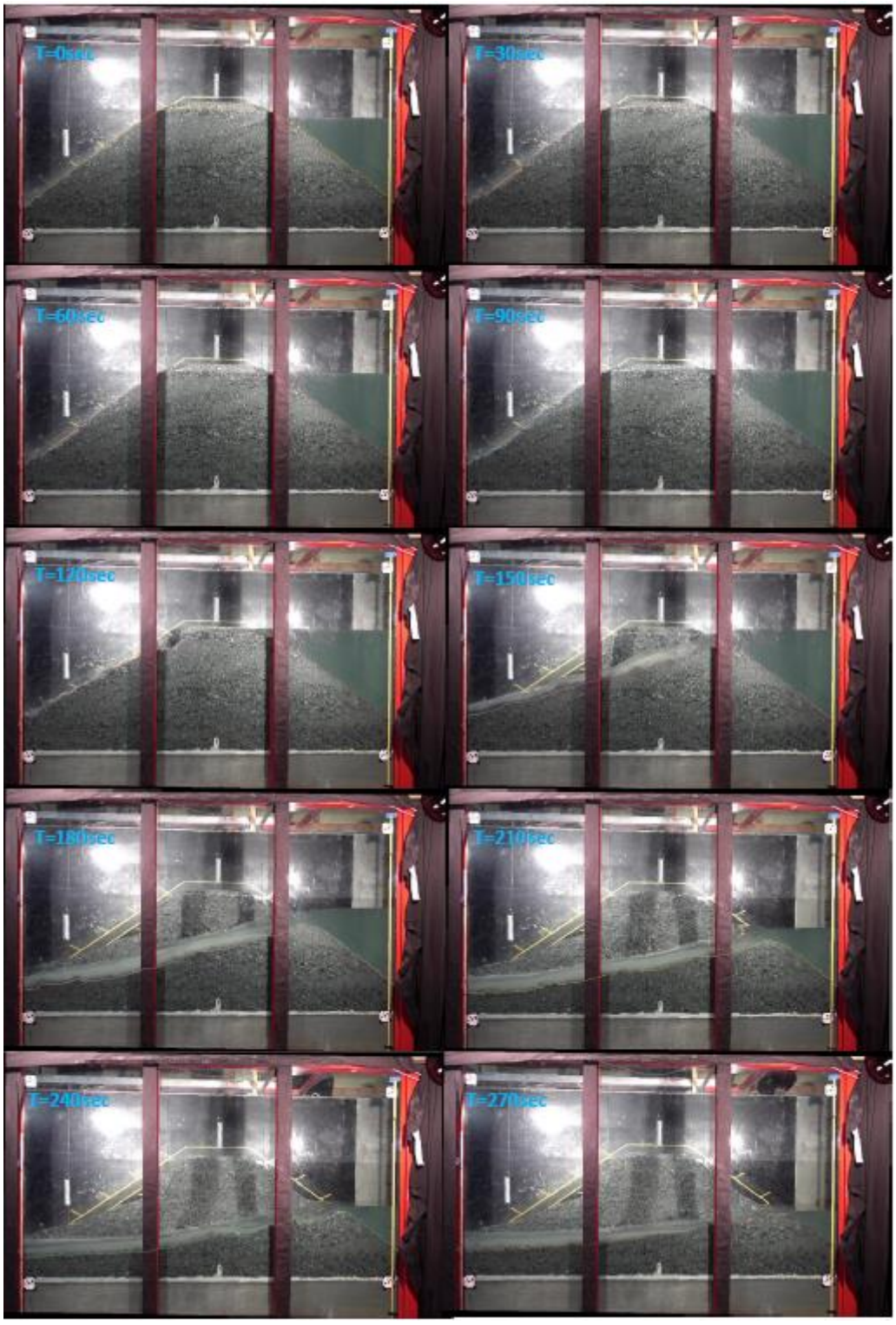

Appendix A 6: Temporal evolution of breach formation, Model 17

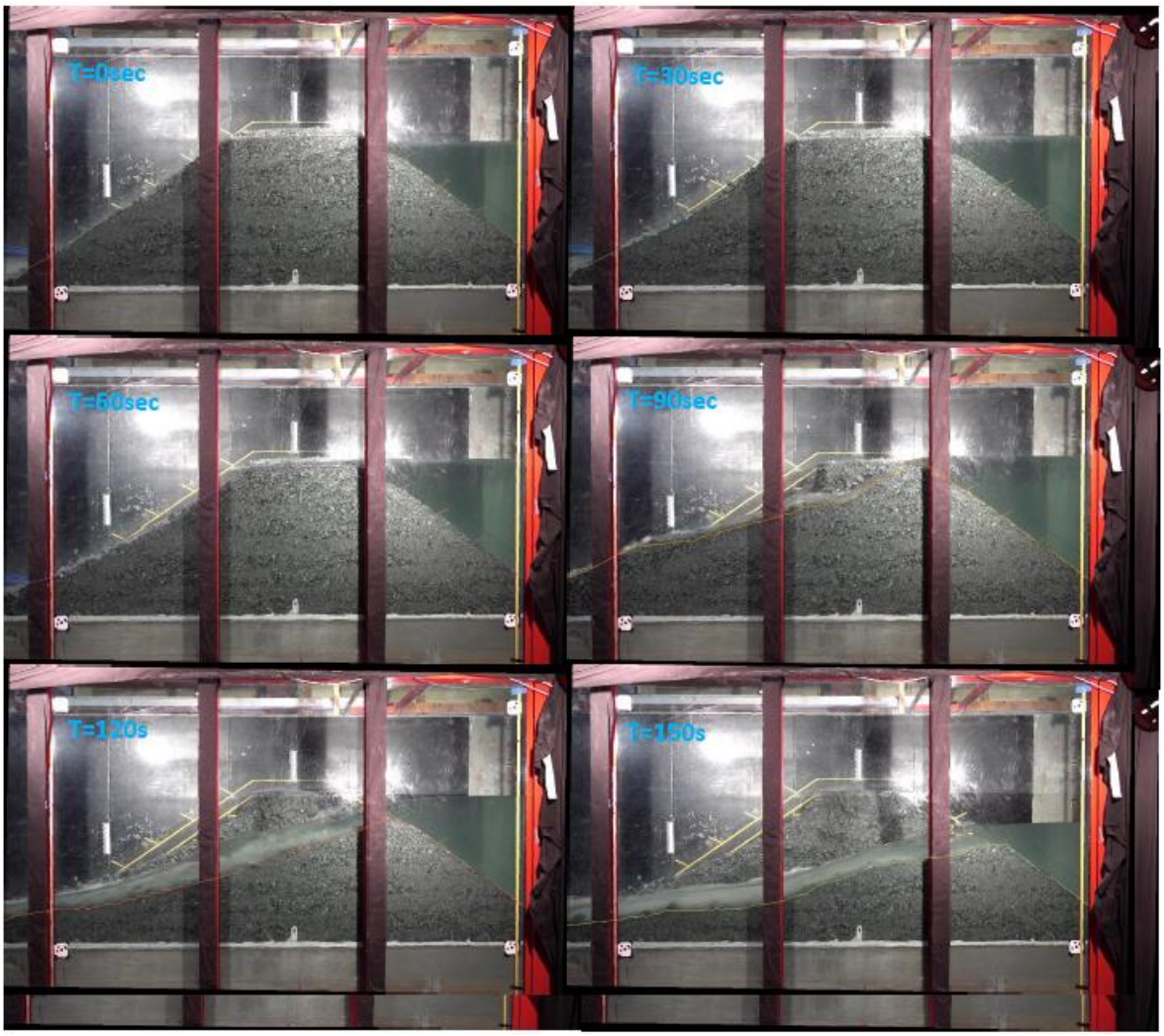

Appendix A 7: Temporal evolution of breach formation, Model 18

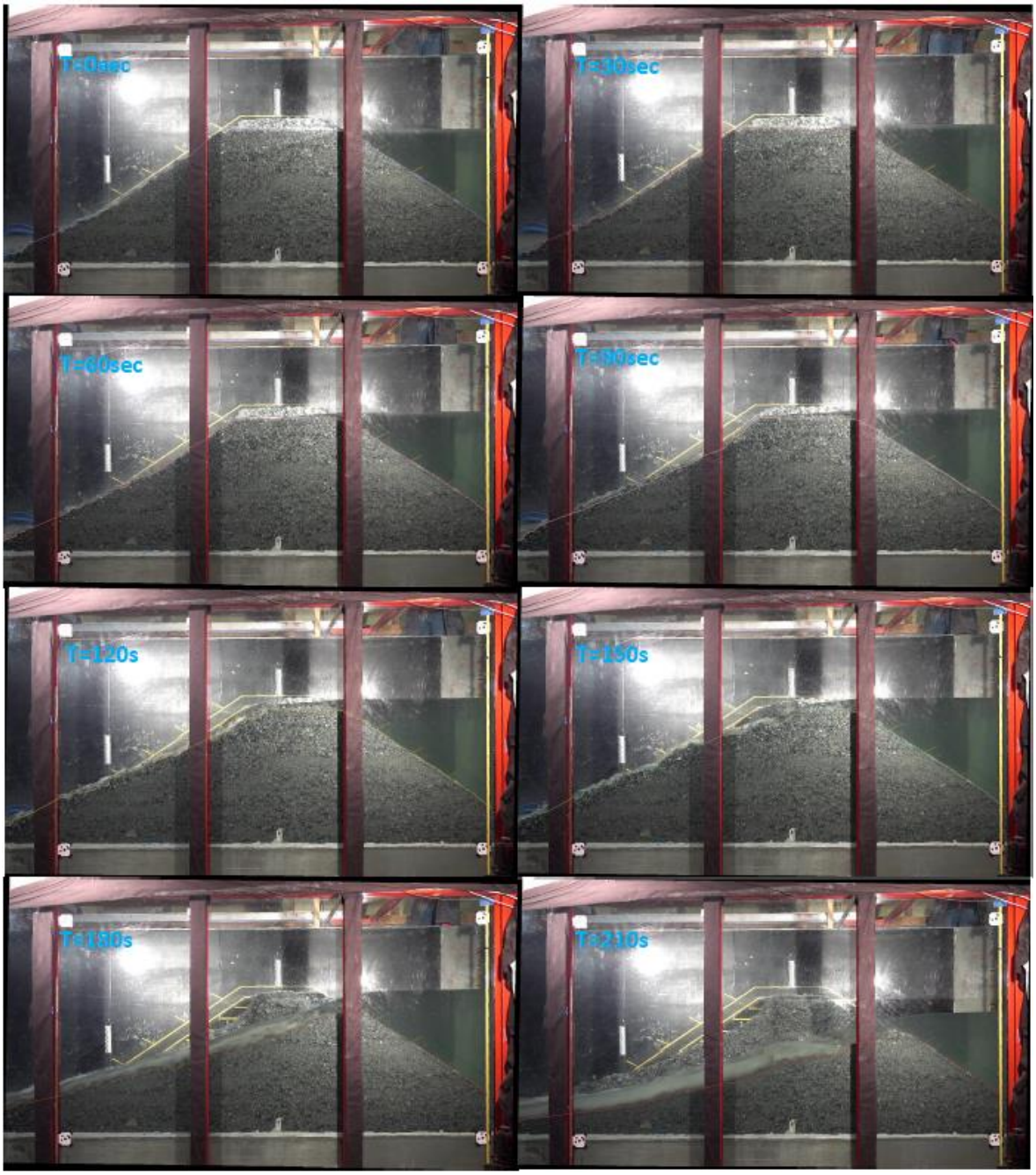

Appendix A 8: Temporal evolution of breach formation, Model 19

Appendix B – Side view tracking

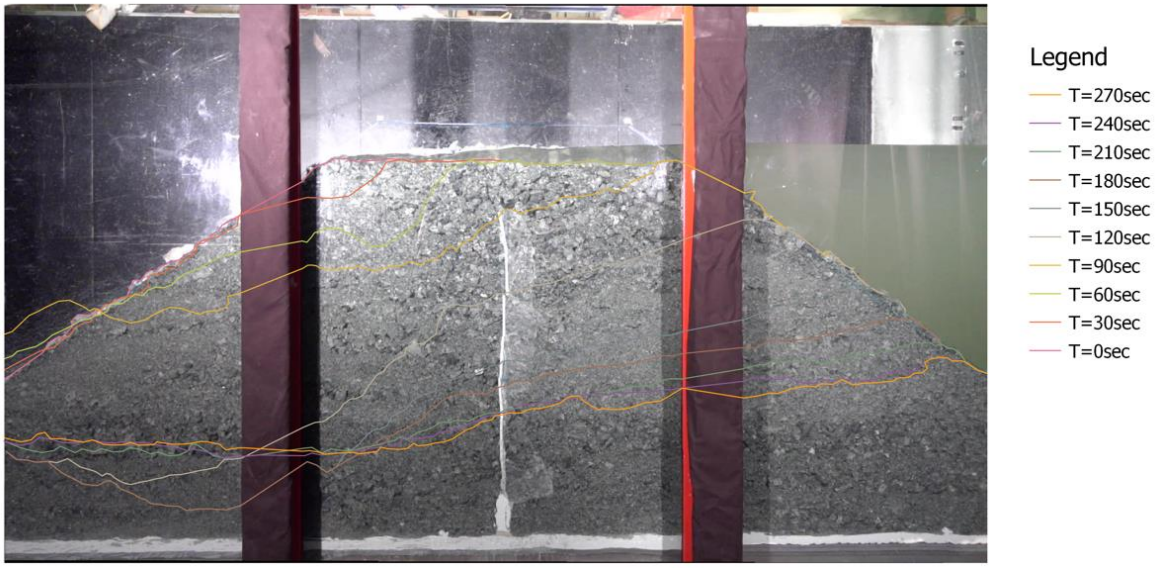

Appendix B 1: Side view tracking, Model 3

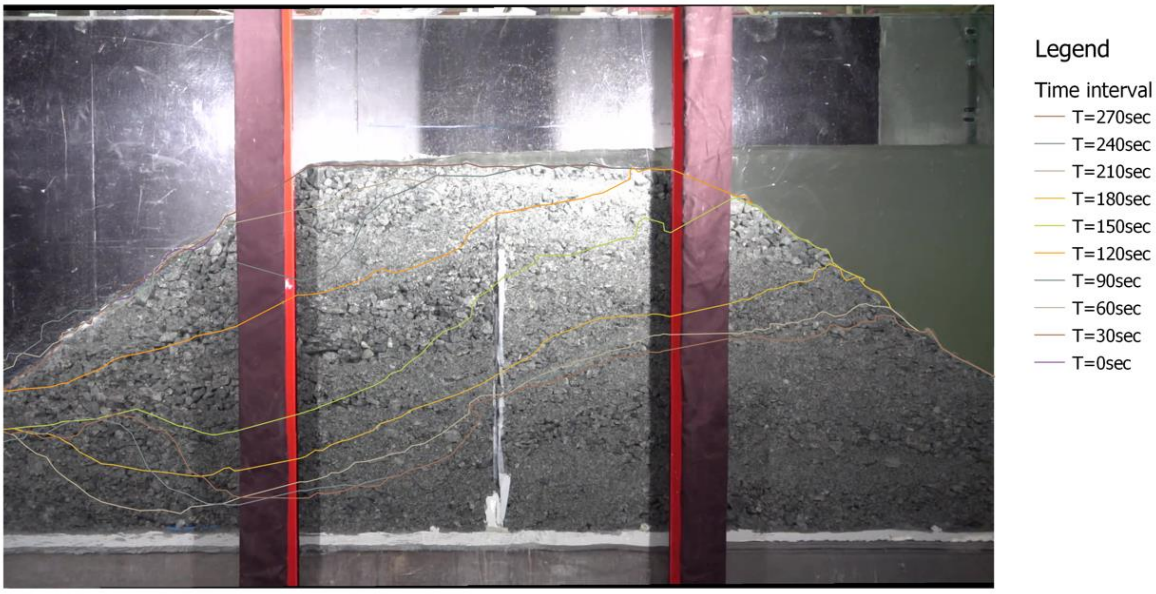

Appendix B 2: Side view tracking, Model 4

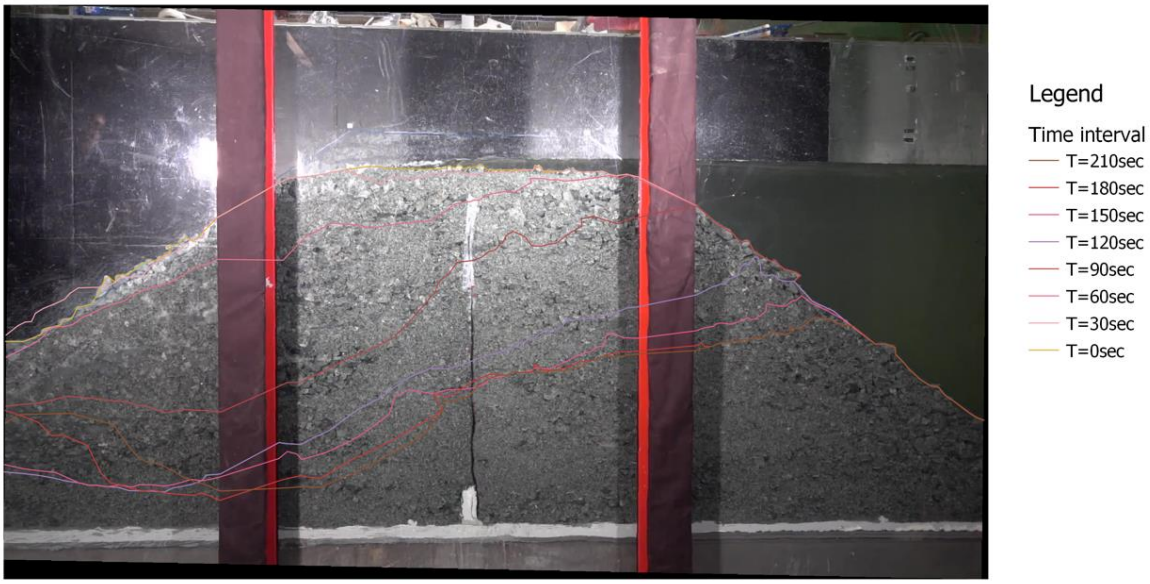

Appendix B 3: Side view tracking, Model 5

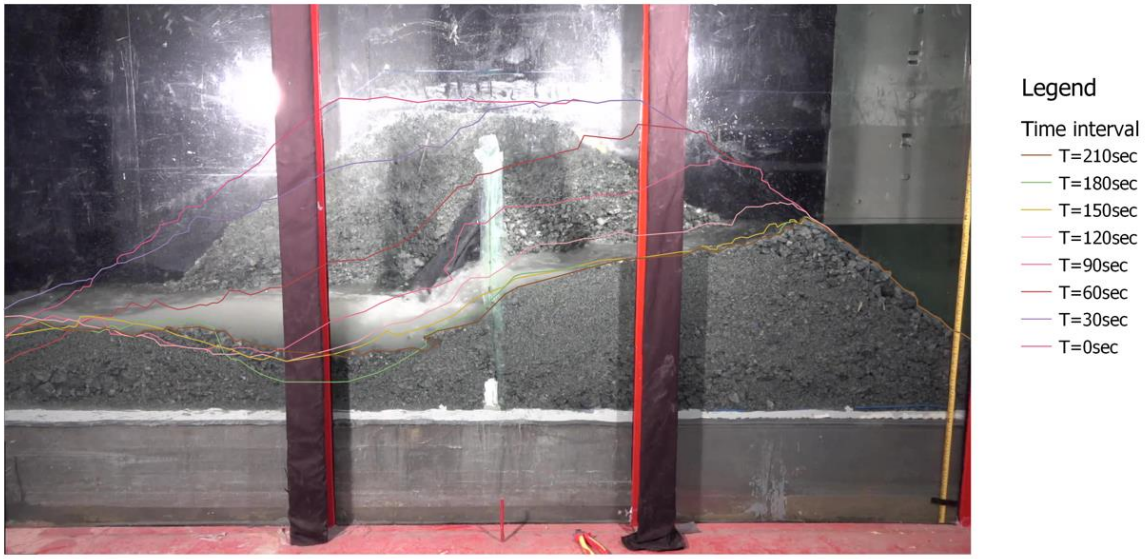

Appendix B 4: Side view tracking, Model 7

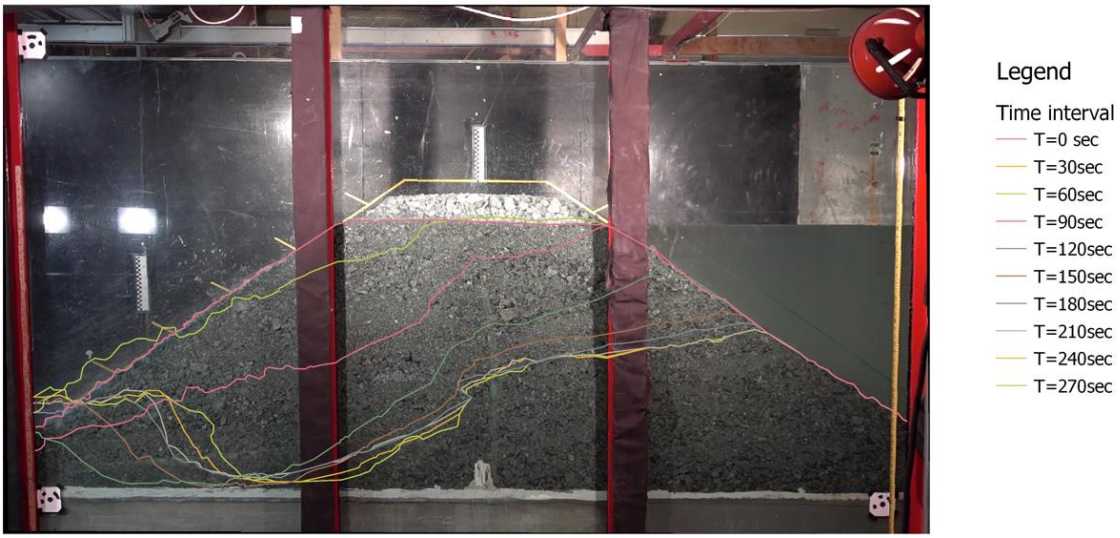

Appendix B 5: Side view tracking, Model 15

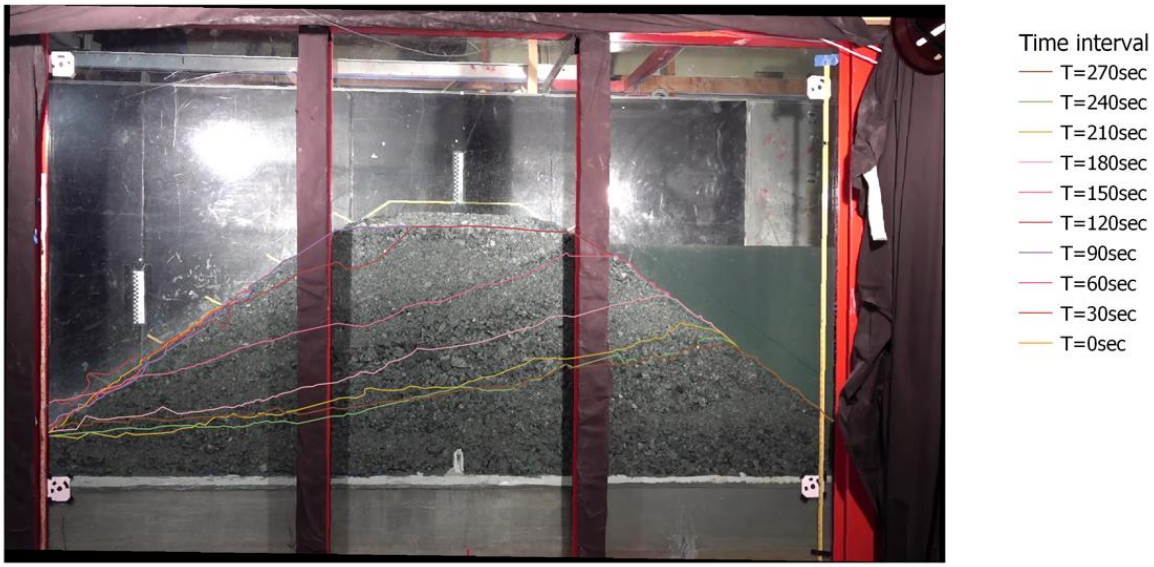

Appendix B 6: Side view tracking, Model 17

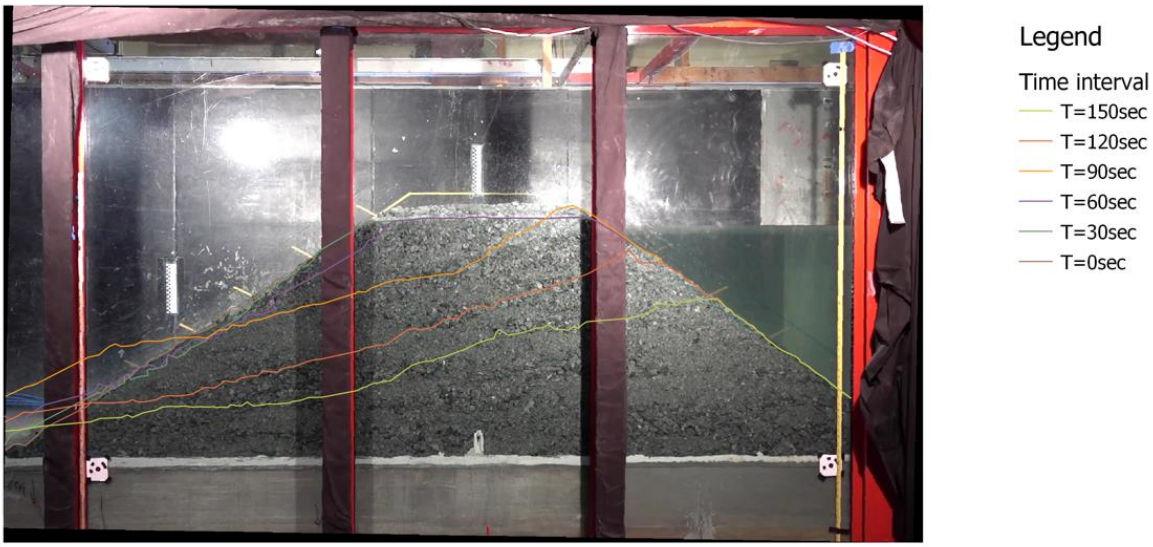

Appendix B 7: Side view tracking, Model 18

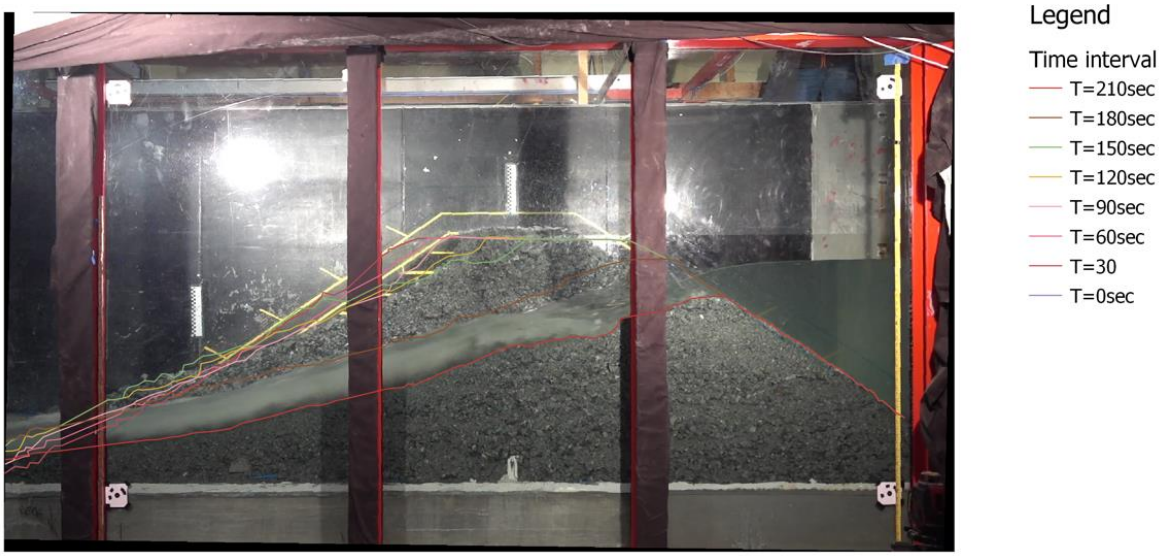

Appendix B 8: Side view tracking, Model 19

Appendix C – Structure from motion

Appendix C 1: Before test 3D modelling of model 15 in Agisoft software

Appendix C 2: After test 3D modelling of model 15 in Agisoft software

Appendix C 3: Before test 3D modelling of model 17

Appendix C 4: After test 3D modelling of model 17

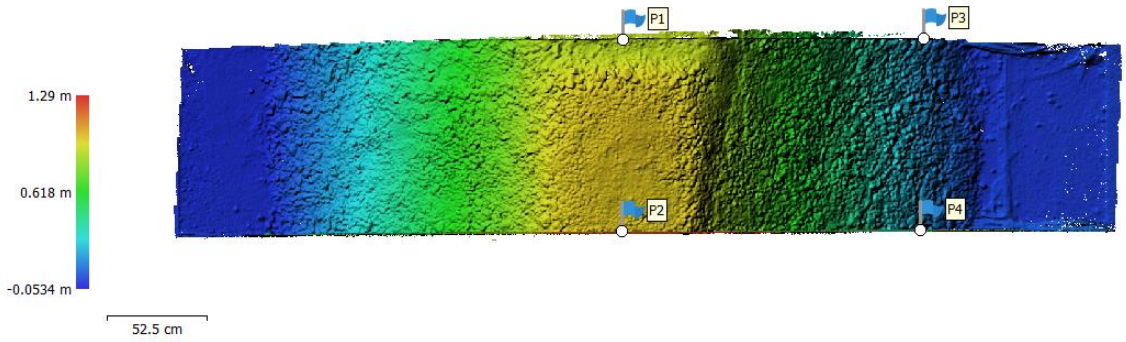

Appendix C 5: DEM before test of model 15 (upstream: left end)

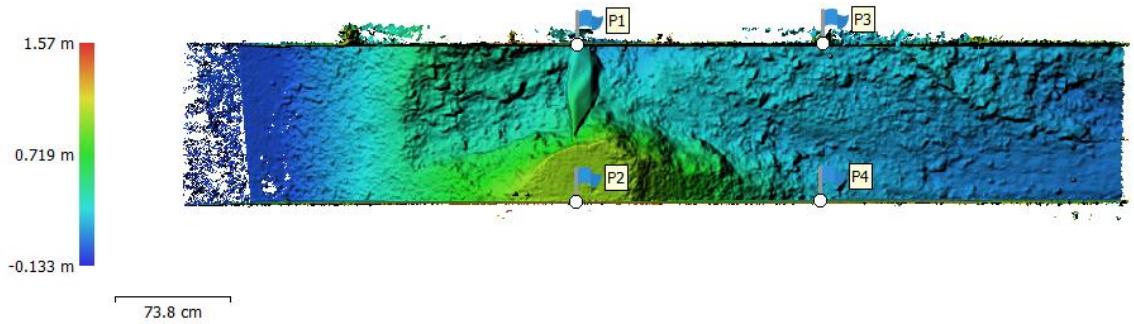

Appendix C 6: DEM after test of model 15 (upstream: left end)

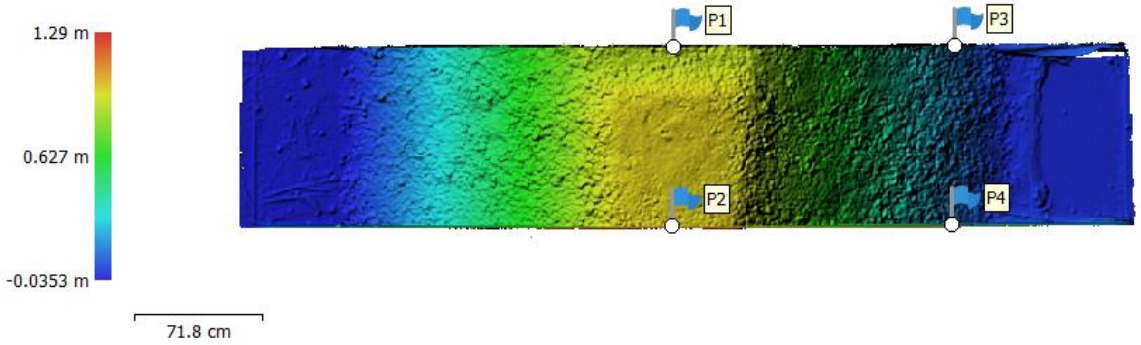

Appendix C 7: DEM before test of model 17 (upstream: left end)

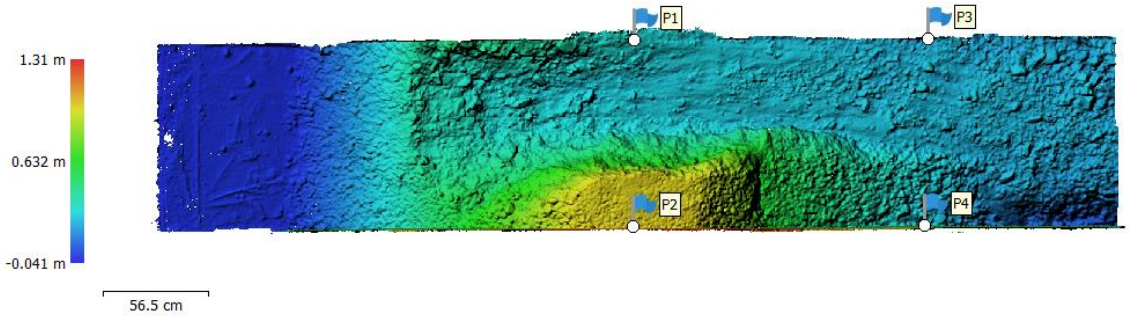

Appendix C 8: DEM after test of model 17 (upstream: left end)

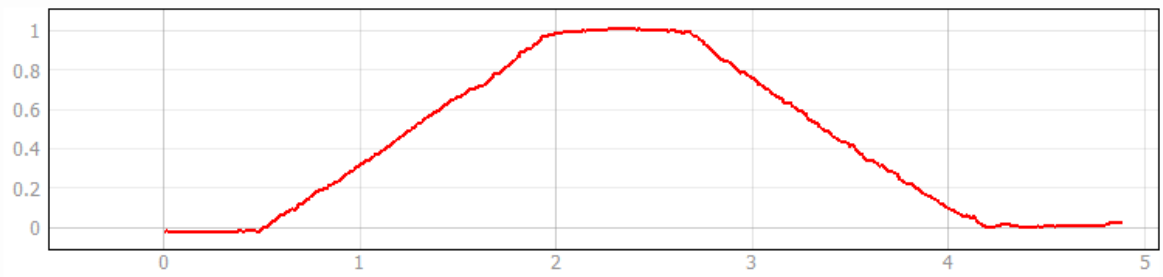

Appendix C 9: Longitudinal profile of model 15 dam before test at center (upstream: left end)

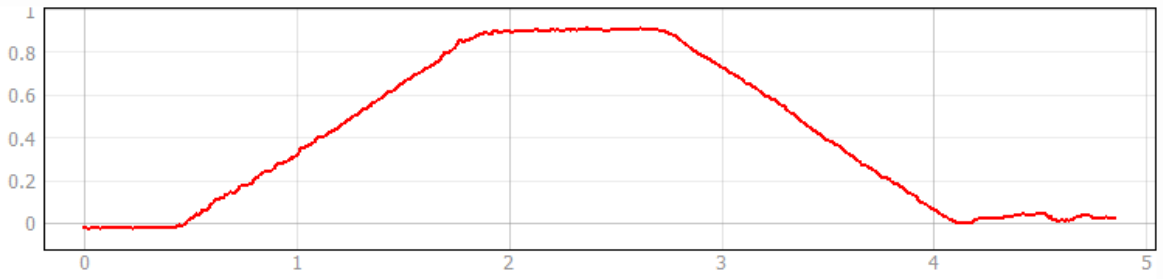

Appendix C 10: Longitudinal profile of model 15 dam before test at left end (upstream: left end)

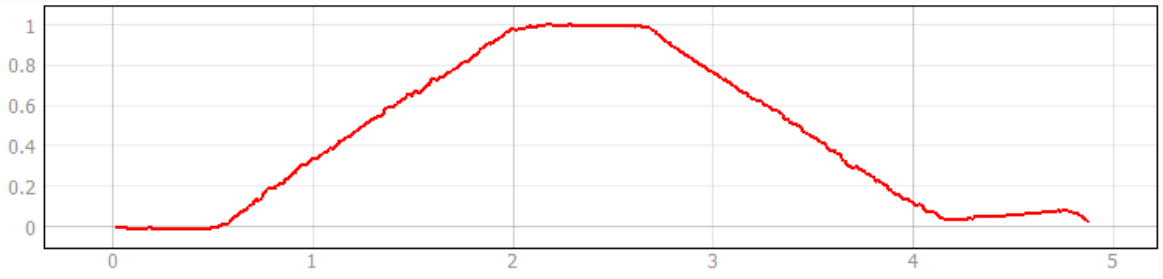

Appendix C 11: Longitudinal profile of model 15 dam before test at right end (upstream: left end)

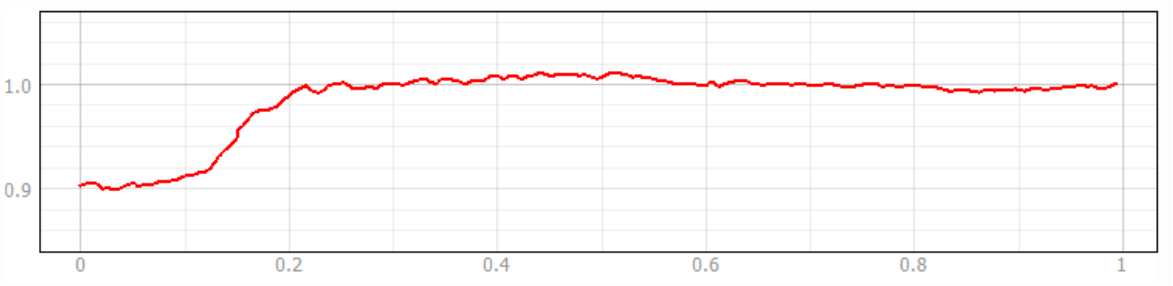

Appendix C 12: Cross-section at center of model 15 before test

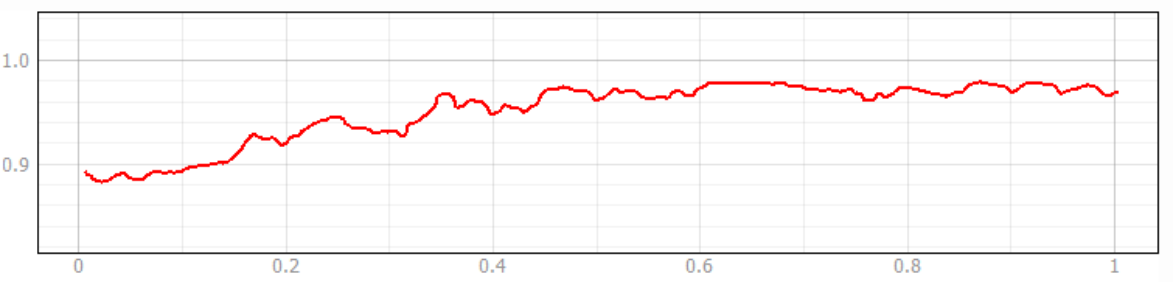

Appendix C 13: Cross-section at 40 cm upstream of model 15 before test

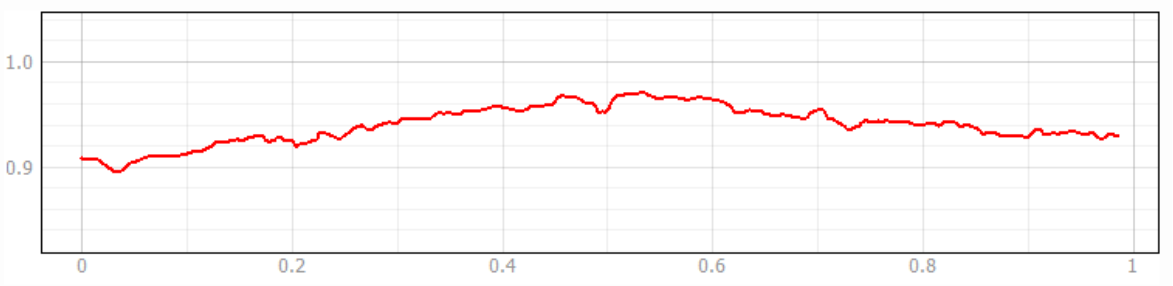

Appendix C 14: Cross-section at 40 cm downstream of model 15 before test

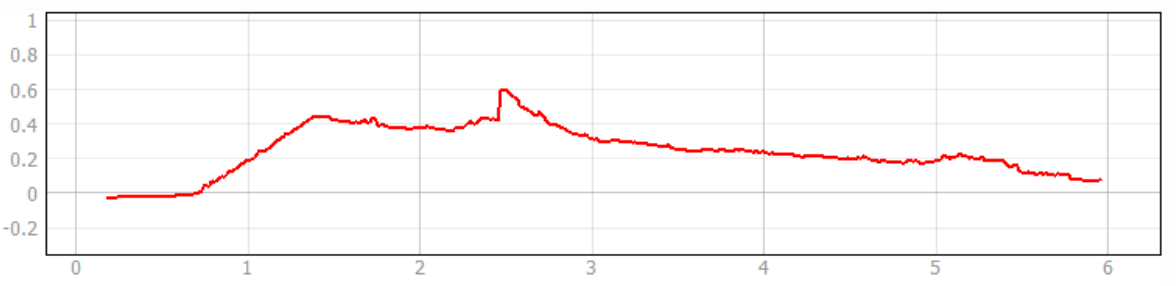

Appendix C 15: Longitudinal profile at center of model 15 after test (upstream: left end)

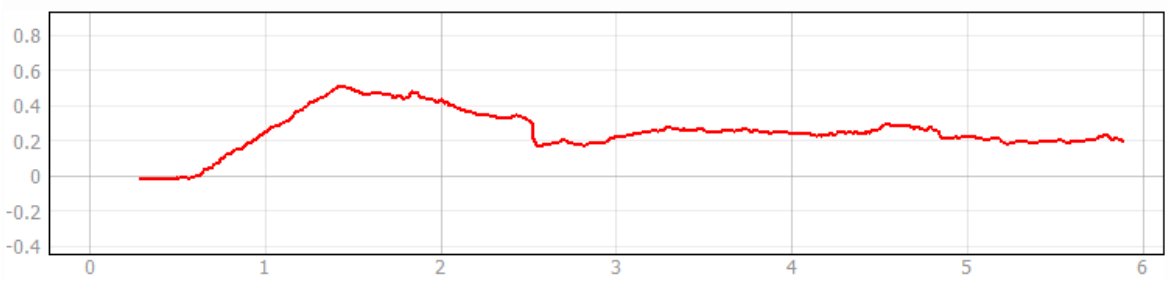

Appendix C 16: Longitudinal profile at left end of model 15 after test (upstream: left end)

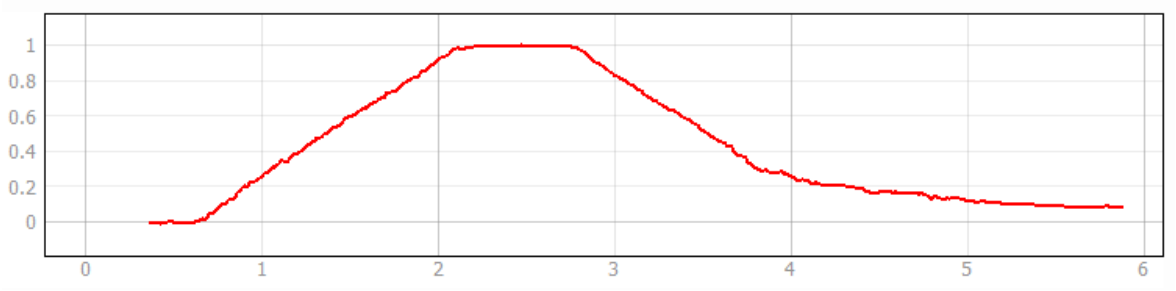

Appendix C 17: Longitudinal profile at right end of model 15 after test (upstream: left end)

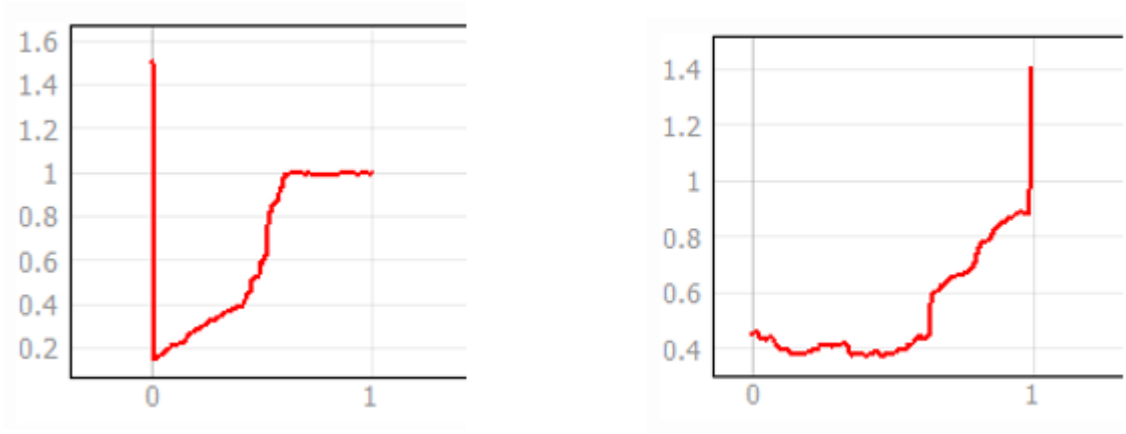

Appendix C 18: Cross-section at center (left figure) and 40 cm upstream (right figure) after test of model 15

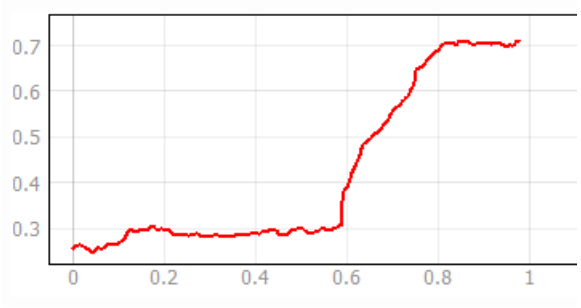

Appendix C 19: Cross-section at 40 cm downstream of model 15 after test

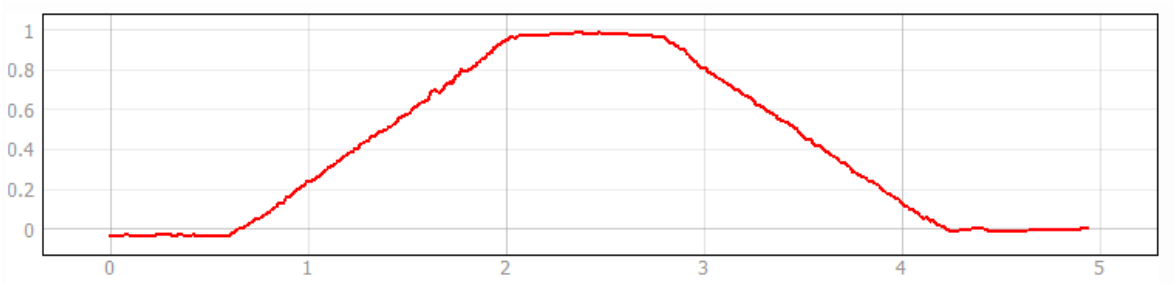

Appendix C 20: Longitudinal profile at center of model 17 before the test (upstream: left end)

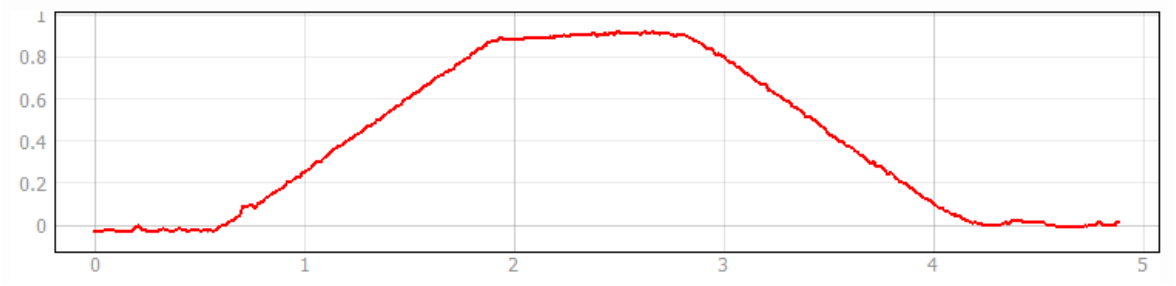

Appendix C 21: Longitudinal profile at left end of model 17 before the test (upstream: left end)

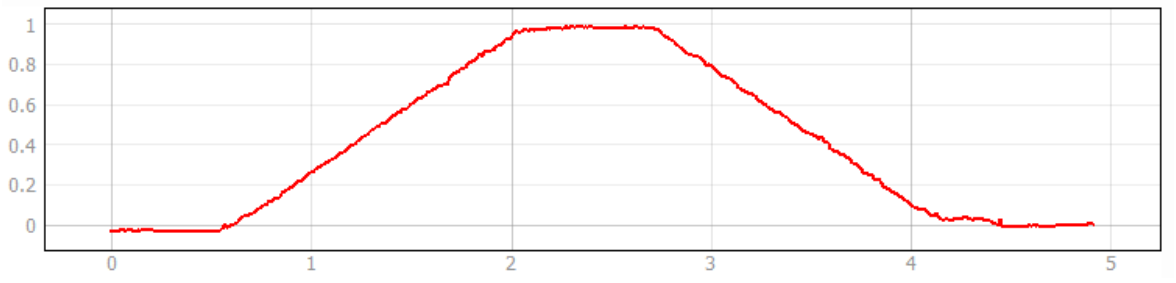

Appendix C 22: Longitudinal profile at right end of model 17 before the test (upstream: left end)

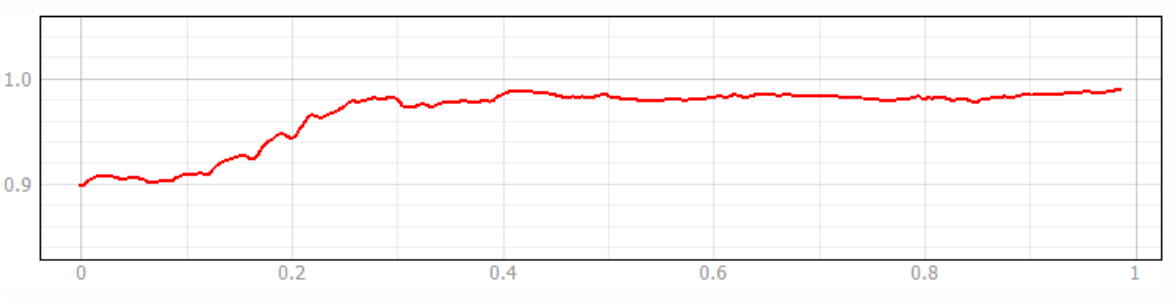

Appendix C 23: Cross-section at center of model 17 before the test

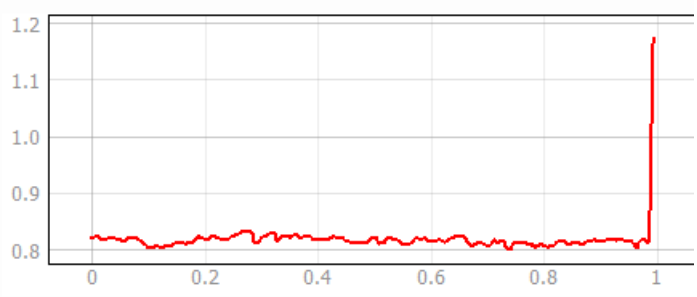

Appendix C 24: Cross-section at 40 cm upstream of model 17 before the test

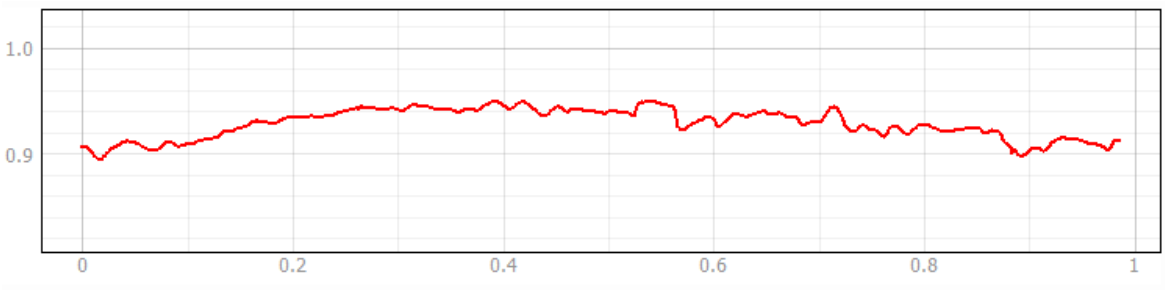

Appendix C 25: Cross-section at 40 cm downstream of model 17 before the test

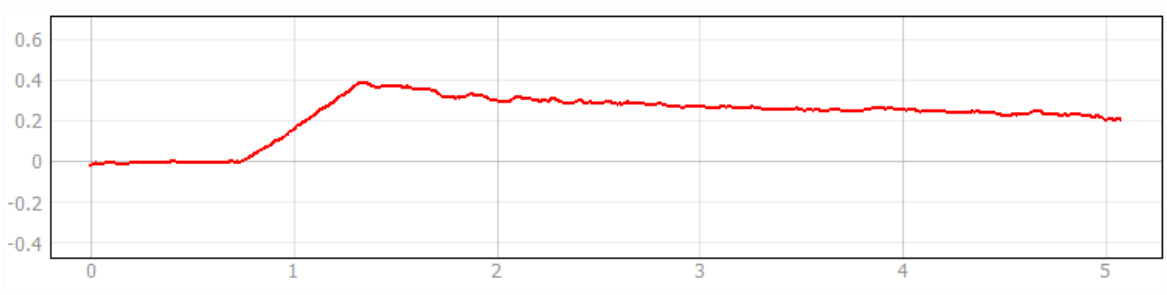

Appendix C 26: Longitudinal profile at center of model 17 after the test (upstream: left end)

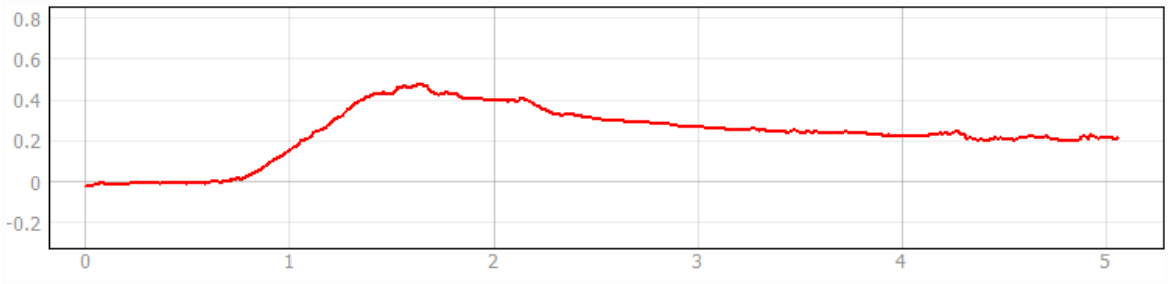

Appendix C 27: Longitudinal profile at left end of model 17 after the test (upstream: left end)

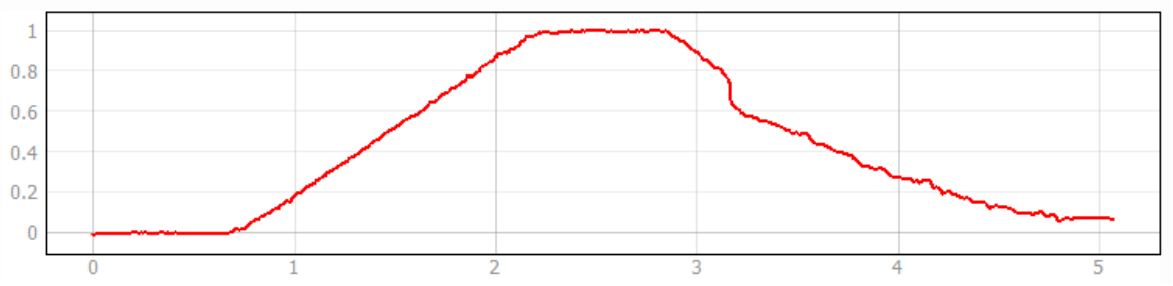

Appendix C 28: Longitudinal profile at right end of model 17 after the test (upstream: left end)

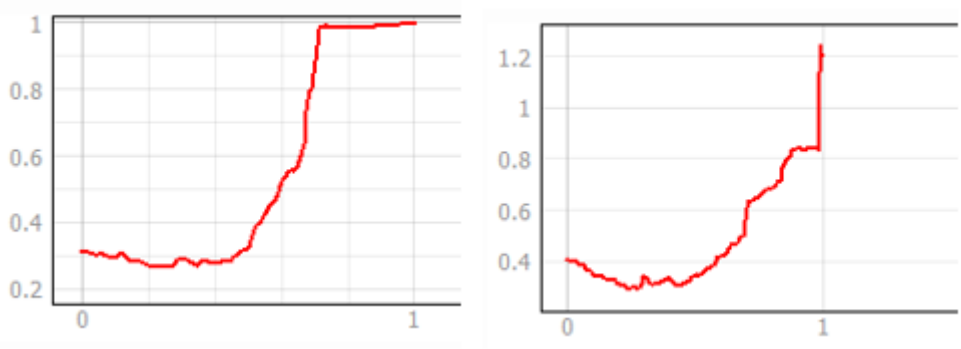

Appendix C 29: Cross-section at center (Left figure) and 40 cm upstream (right figure) after the test of model 17

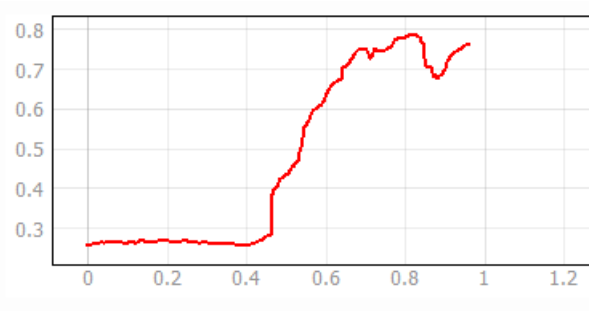

Appendix C 30: Cross-section at 40 cm downstream of model 17 after the test

Appendix D – Breach progress

Appendix D table 1: Breach progress at center and 40 cm downstream of model 3

Time	At center	40 cm ds
0	90	90
30	90	83
60	90	76
90	79	66
120	60	31
150	44	19
180	38	18
210	32	23
240	32	22
270	31	22

The chart is plotted below for the given data of breach progress of model 3.

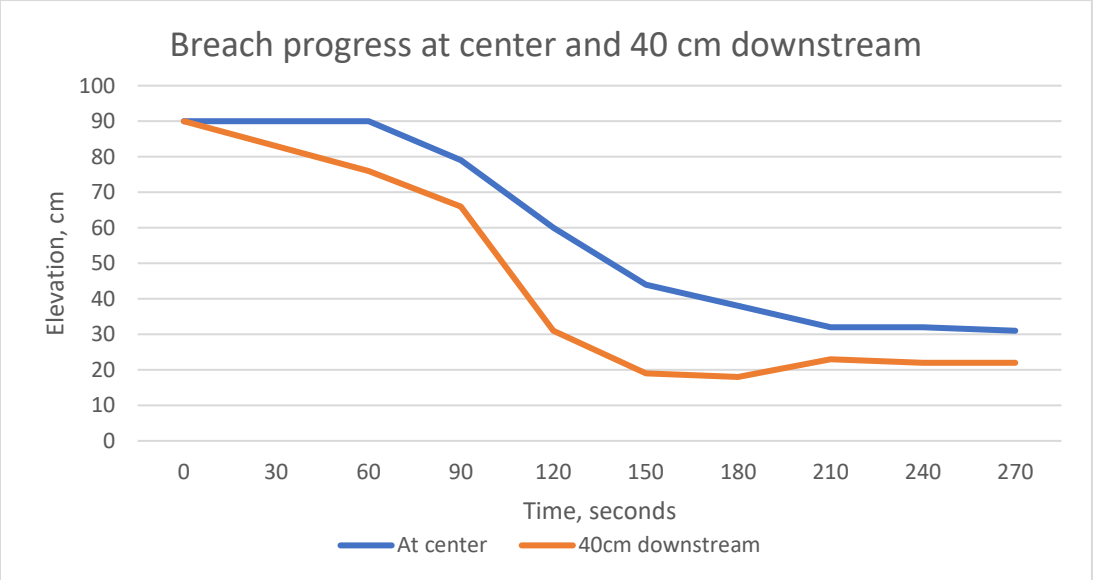

Appendix D figure 1: Breach progress of model 3

Appendix D table 2: Breach progress at center and 40 cm downstream of model 4

Time	At center	40 cm ds
0	90	90
30	90	90
60	88	81
90	88	65
120	78	60
150	61	33
180	39	22
210	35	15
240	34	12
270	33	10

The chart is plotted below for the given data of breach progress of model 4.

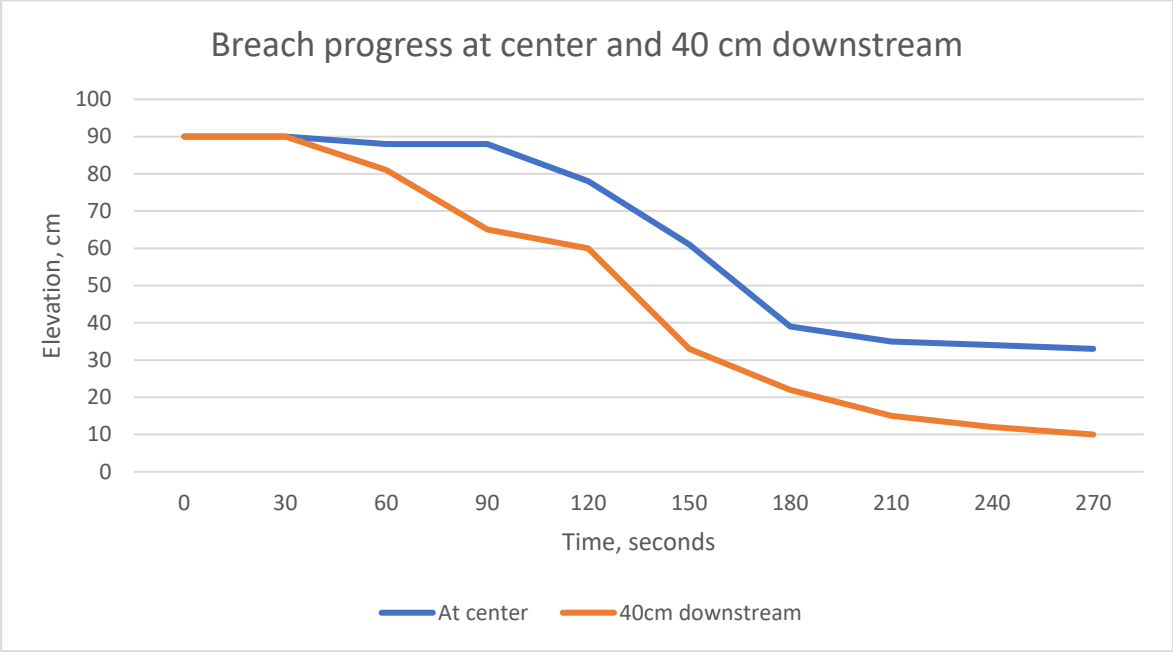

Appendix D figure 2: Breach progress of model 4

Appendix D table 3: Breach progress at center and 40 cm downstream of model 5

Time	At center	40 cm ds
0	90	90
30	90	90
60	83	74
90	68	38
120	42	23
150	36	18
180	36	14
210	34	11

The chart is plotted below for the given data of breach progress of model 5.

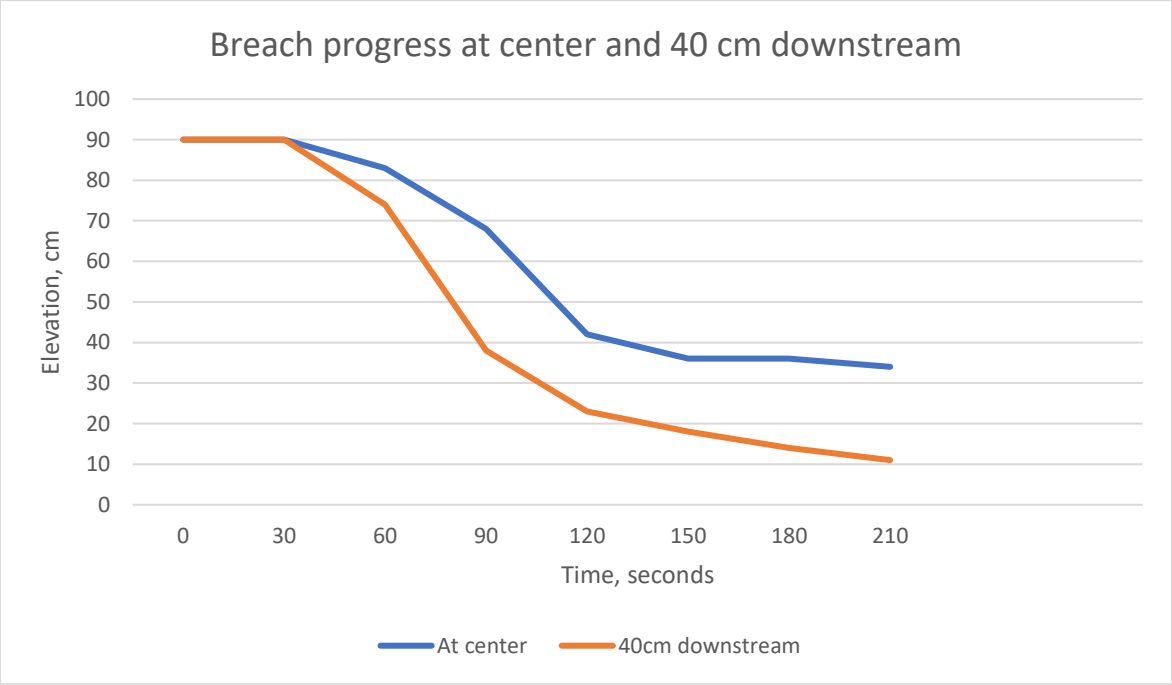

Appendix D figure 3: Breach progress of model 5

Appendix D table 4: Breach progress at center and 40 cm downstream of model 6

Time	At center	40 cm ds
0	90	90
30	89	74
60	71	45
90	58	30
120	41	21
150	36	19
180	34	10
210	32	19

The chart is plotted below for the given data of breach progress of model 6.

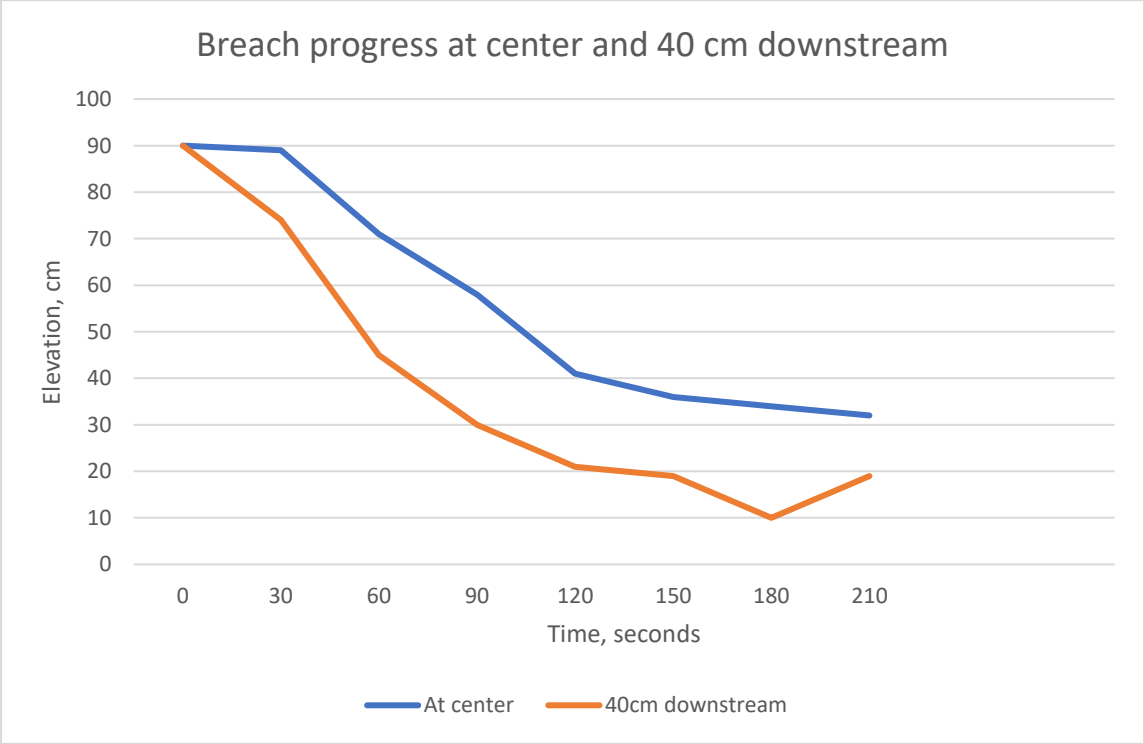

Appendix D figure 4: Breach progress of model 6

Appendix D table 5: Breach progress at center and 40 cm downstream of model 15

Time	At center	40 cm ds
0	90	90
30	90	90
60	90	77
90	79	47
120	54	22
150	44	14
180	39	13
210	37	13
240	37	9
270	36	6

The chart is plotted below for the given data of breach progress of model 15.

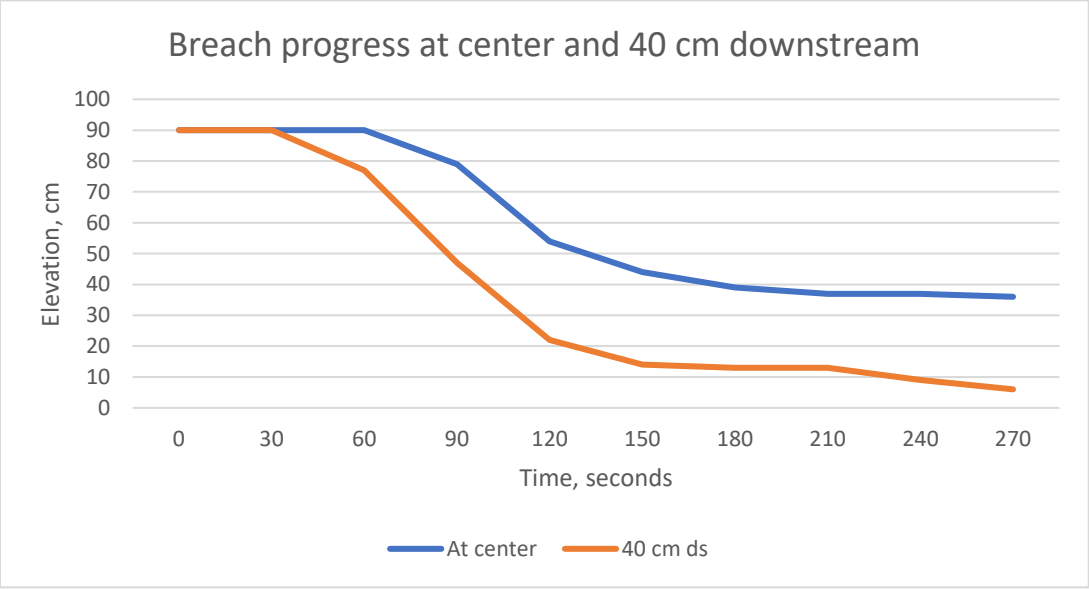

Appendix D figure 5: Breach progress of model 15

Appendix D table 6: Breach progress at center and 40 cm downstream of model 17

Time	At center	40 cm ds
0	90	90
30	90	90
60	90	90
90	90	90
120	90	77
150	68	57
180	49	37
210	34	30
240	33	24
270	32	26

The chart is plotted below for the given data of breach progress of model 17.

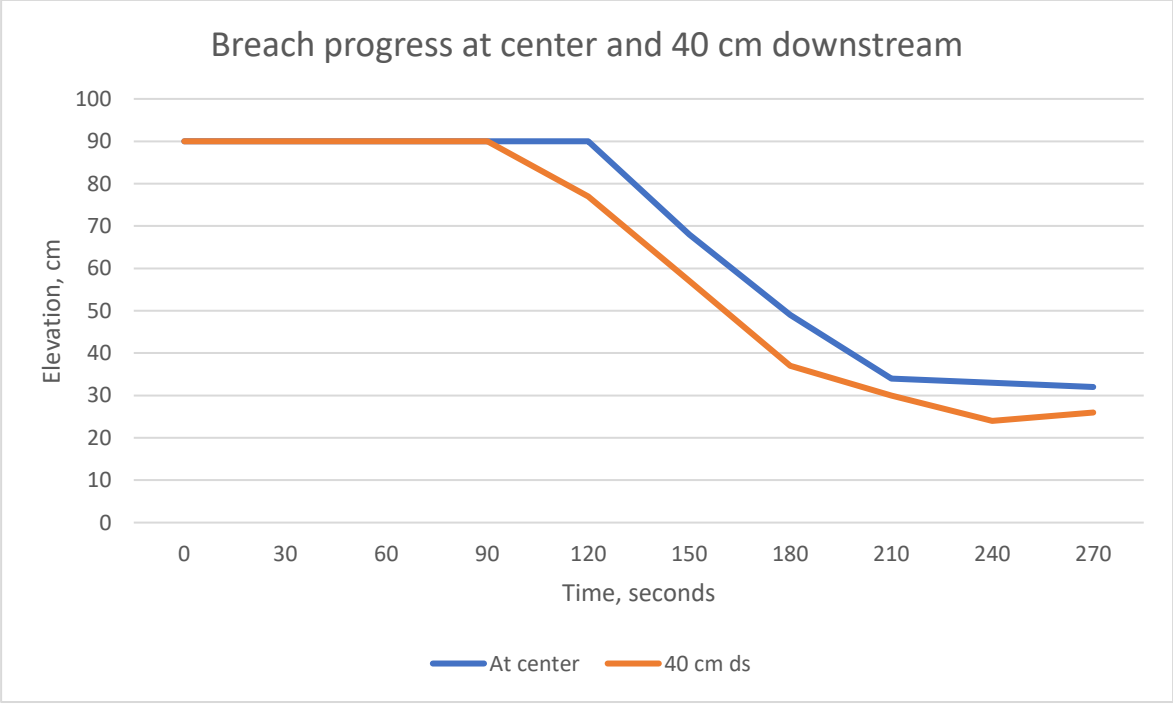

Appendix D figure 6: Breach progress of model 17

Appendix D table 7: Breach progress at center and 40 cm downstream of model 18

Time	At center	40 cm ds
0	90	90
30	90	90
60	90	84
90	76	66
120	58	43
150	44	29

The chart is plotted below for the given data of breach progress of model 18.

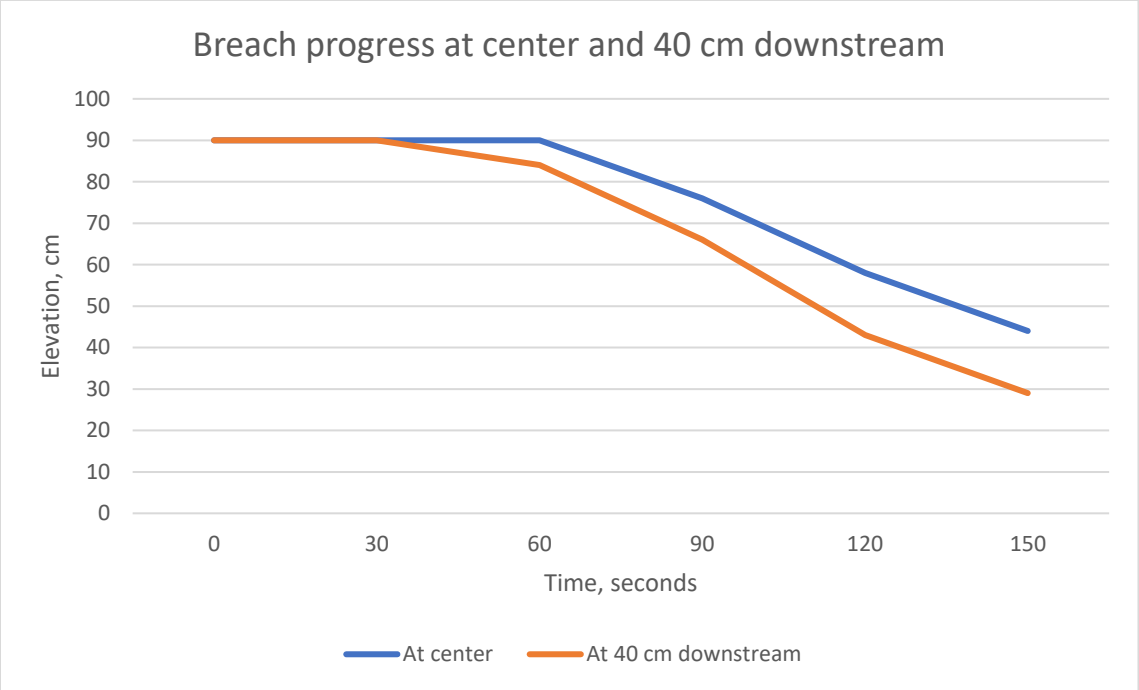

Appendix D figure 7: Breach progress of model 18

Appendix D table 8: Breach progress at center and 40 cm downstream of model 19

Time	At center	40 cm ds
0	90	90
30	90	90
60	90	84
90	90	78
120	90	74
150	86	74
180	67	54
210	51	37

The chart is plotted below for the given data of breach progress of model 19.

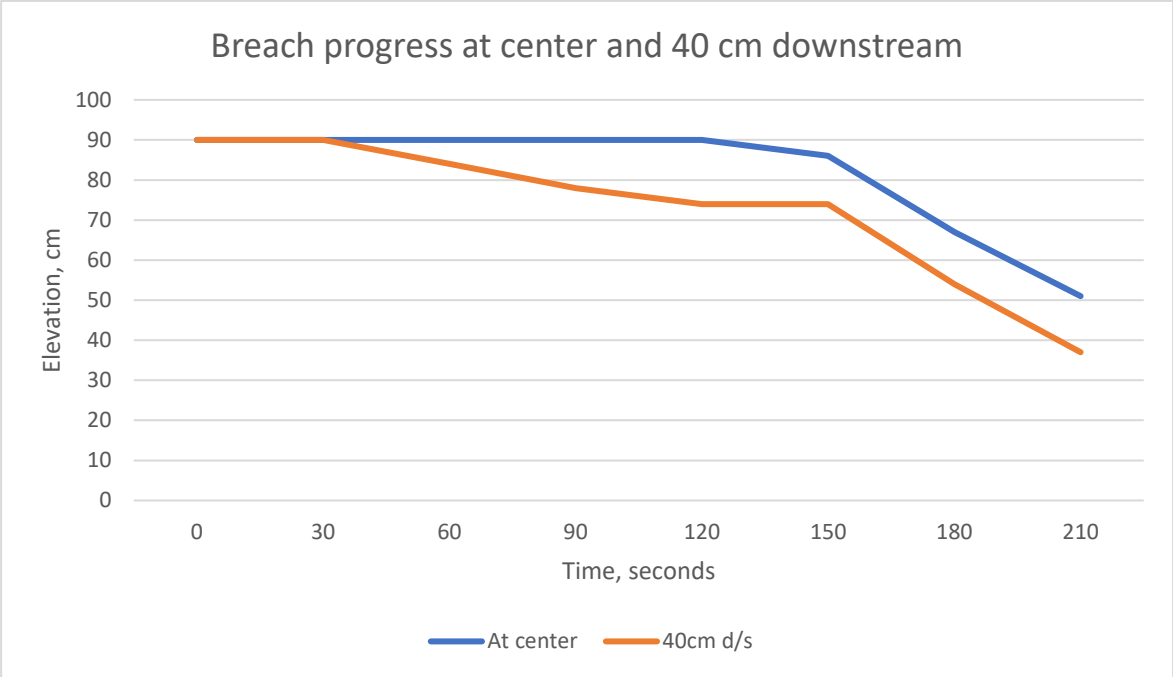

Appendix D figure 8: Breach progress of model 19

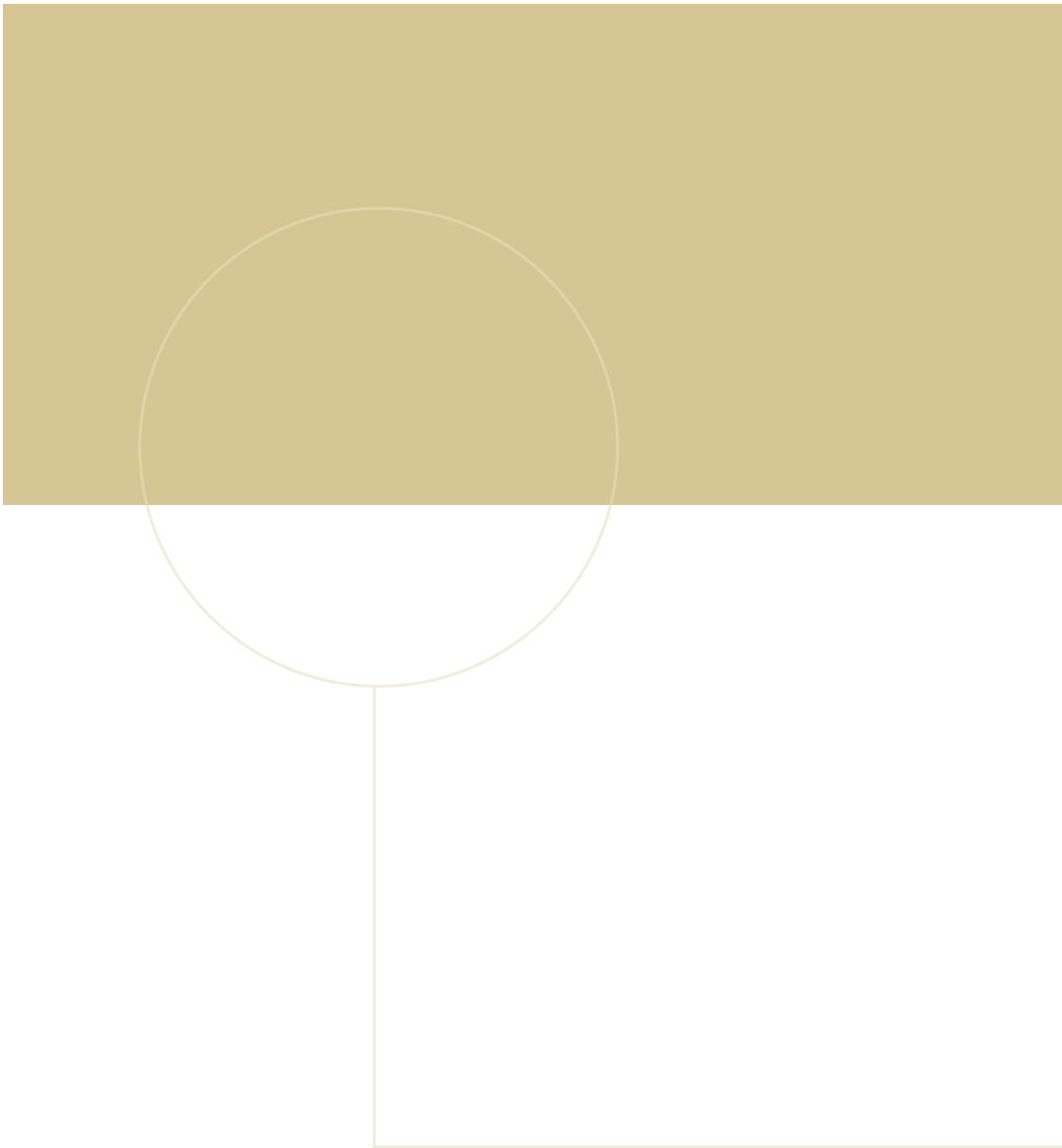

NTNU

Norwegian University of
Science and Technology